Effects of Floating Solar Platforms on the Hydrodynamics and the Ecosystem of a Coastal Sea

Master programme: Climate Physics, Utrecht Univercity

Thodoris Karpouzoglou: 6074073

Supervisors:

Johan van der Molen (NIOZ) Huib de Swart (UU) Brigitte Vlaswinkel (OOE)

Oceans of Energy

29th January 2019

Abstract

The effects of floating photovoltaic (PV) installations on the hydrodynamics and the ecodynamics of a coastal sea as the North Sea are analysed, with a coupled physical-biogeochemical 1D column model (GOTM-ERSEM-BFM). The model is calibrated and validated with the use of Smartbuoy observations from three locations in the North Sea. The equations of the model are altered as to include four different effects (ef) of the PV installations, namely: ef1) decreased light conditions due to the shadowing effect of the platforms, ef2) reduced wind stress due to the limitation of the free surface of the water column, ef3) introduction of an additional surface stress experienced by currents, due to friction induced by the platforms, ef4) reduced wave height due to the presence of the platforms. The 1D model is capable of reproducing the main seasonal patterns of ecosystem variables such as chlorophyll a, with performance comparable to a 3D model. Moreover, it proves to be more efficient in open-sea locations where horizontal advection is of less importance. Regarding the individual effects, ef1 is the dominant one. However, some ecosystems may reveal resilience to ef1 for small percentages of coverage. The effect of ef2 on the hydrodynamics and the ecosystem is small in locations with strong tidal currents. This effect can be very important for stratified locations due to its impact on the top mixed layer and thus on primary production. The ef3 can be important for the ecosystem of locations with strong currents. This is evident for small percentages of coverage where ef3 leads to a minimum of suspended sediment near the surface (and maximum of irradiance). The ef4 reduces strongly the concentration of suspended sediment in the water column. However, the reduction occurs mainly at lower depths and out of the photic zone, leading to no significant changes in the light availability of the ecosystem. Overall, the shadowing effect (ef1) of the platforms on the ecosystem is the most important. However, for the case of well mixed locations with high concentration of suspended sediment near the surface, ef1 is partly compensated by the effect of reduced turbidity that follows the other three effects. This is more prominent for small percentages of coverage where ef3 is of comparable importance to ef1, resulting in no significant overall impact of the PV installations on the marine ecosystem. Concluding, well mixed locations with high currents and large concentration of suspended sediment near the surface are more favorable to the installation of a solar power plant. However, this statement is restricted by the assumption that the power plant will not occupy more than 20% of the 1D domain.

Acknowledgements

Many thanks to my supervisors Dr. Huib de Swart, Dr. Johan van der Molen and Dr. Brigitte Vlaswinkel for their methodical guidance, patience, persistence and the valuable time that they spend for this project. Many thanks are in order to Piet Ruardij for his valuable help and to Oceans of Energy for offering me an internship.

Contents

1 Introduction

The last decades have been characterized by an increase in global energy demand and an acceleration of climate change (Nejata et al. [2015] ; IPCC [2018]). For this reason, it is essential to evaluate alternative sources of clean energy. Due to the scarcity of available land, the construction of offshore renewable energy installations has already received ample attention in the Netherlands, especially for the case of wind turbines. However, other technologies are becoming available. Apart from the extraction of energy from waves and tides, the construction of offshore solar parks gathers more and more attention and is an option that needs to be further examined. Their benefits (compared to terrestrial based installations) arise from the increasing commercial value of land and the expected increased yield of the offshore installations. The latter occurs due to the cooling effect of water (Sahu et al. [2016]). Even though an intervention with photovoltaic (PV) installations in an offshore environment contributes to the mitigation of climate change, research is needed on the potential impacts of large scale solar farms on the marine ecosystem. The present work is a collaboration between Utrecht University (UU), the Royal Netherlands Institute for Sea Research (NIOZ, Texel) and Oceans of Energy (OOE). OOE is a company operating on the domain of offshore solar energy, aiming to implement the first offshore solar park for commercial use. This study investigates the potential effects of large-scale PV installations on the hydrodynamics and ecosystem of coastal seas. In this report, the focus is on the North Sea.

Figure 1: *Image of an inshore floating solar park at Huainan, China.*
https://interestingengineering.com/china-powered-worlds-largest-floating-solar-power-plant

The North Sea is a relatively shallow marginal sea (average depth 74 m) of the Atlantic Ocean (figure 2a). It is located between western Europe and the United Kingdom and covers an area of about 570.000 km^2 (Otto et al. [1990] ; Nauw et al. [2015]). The hydrodynamics of the North Sea are mainly controlled by the influence of three forcing agents, namely the tidal forcing, wind forcing and buoyancy. The effect of tides on the hydrodynamics of the region is the most significant. Tidal waves, propagating along the east coast of the Atlantic Ocean, force tidal waves in the North Sea which in turn propagate cyclonically. The most dominant tidal component is the semi-diurnal lunar tide (M2: period of 12h25m) with tidal range of 0-10 m and current amplitude of 0-2 m/s (figure 2b). Moreover, a clear spring-neap variation (period

of 14d) is observed due to the interaction of M2 with the semi-diurnal solar tide (S2) (Nauw et al. [2015]). The nonlinear tidal dynamics result in residual tidal currents (order of cm/s) towards the direction of the tidal wave propagation (cyclonically). The cyclonic orientation of this residual circulation results in a northward flow along the Dutch coast (see figure 16a of the appendix). The interaction of the tidal currents with the bottom generates turbulence in the water column. Turbulence results in effective vertical mixing of horizontal momentum and of tracers such as temperature, suspended sediment (SSC), phytoplankton and nutrients. Subsequently, the ecosystem characteristics are strongly affected by tides, as the latter result among others in higher concentrations of SSC near the surface (see figure 16b of the appendix) and thus lower light levels in the water column. The tidal currents result in horizontal advection of the above mentioned tracers as well. However, this effect on the ecodynamics is of minor importance compared to the one of vertical mixing.

The wind field over the North Sea consists mainly of north-westerlies and south-westerlies (see figure 16e of the appendix) with typical values of wind speed, at 10 m above sea level, varying between 7 and 10 m/s (Coelingh et al. [1996])(see figure 16c of the appendix). Wind generates both sea waves (period of several seconds) and wind-driven currents (period of several days or longer and velocity of several cm/s). The varying wind characteristics in time and space result in variable wave heights and current characteristics. Overall, wave height increases towards the northern North Sea due to the increasing depth of the water column (Weisse and Gunther [2007]) (see figure 16d of the appendix). In the shallower Southern Bight, waves are smaller. However, they can reach up to 9 m with a return period of 10 yr (van der Molen and de Swart [2001]). Waves breaking at the surface or waves interacting with the bottom also generate turbulence in the water column and thus vertical mixing of SSC, phytoplankton, nutrients etc. The effect of wave induced horizontal advection (stokes drift, wave induced currents) is of smaller significance.

The density gradient between waters of oceanic and shelf origin and the buoyancy input by rivers also drive a residual cyclonic circulation (Blaas and de Swart [2002] ; (Hill et al. [2008])). Moreover, the buoyancy input by rivers and the heating at the surface adds to the possibility of local density stratification. On the other hand, turbulence tends to create a well-mixed water column. Those opposing effects result in differences in the vertical structure of one location to another. For the shallower regions of the Southern Bight, where the vertical mixing due to waves and currents is strong, the water column remains well mixed during the whole year (Sundermann and Pohlmann [2011] ; Pickering et al. [2012]). Concurrently, deeper locations that stratify during summer can be found further to the north (Pingree et al. [1978]). The occurrence of stratification is crucial for the marine ecosystem. It prevents vertical exchange between horizontal layers and affects the flow of suspended sediment, nutrients and phytoplankton towards the surface. Moreover, the timing of stratification relates with that of the spring bloom (Sverdrup [1953]).

Coastal and shelf seas supply 80% of the world's wild-captured seafood. As a marginal sea of the European continental shelf, the North Sea holds a key role on the food supply of north-western Europe (Watson et al. [2016]). Phytoplankton is the base of the marine food web in the North Sea. Among the different phytoplankton species, diatoms and different taxa of the family of flagellates are considered as the most important for the region (Reid et al. [2016]). Diatoms are the prevailing algal group of the North Sea, especially during the spring bloom. As any other phytoplankton species, diatoms consume light and nutrients and they are subject to grazing from zooplankton and filter feeders. Diatoms consume silicate and create a silicate shell around them. This results in a higher sinking velocity for diatoms compared to the other species.

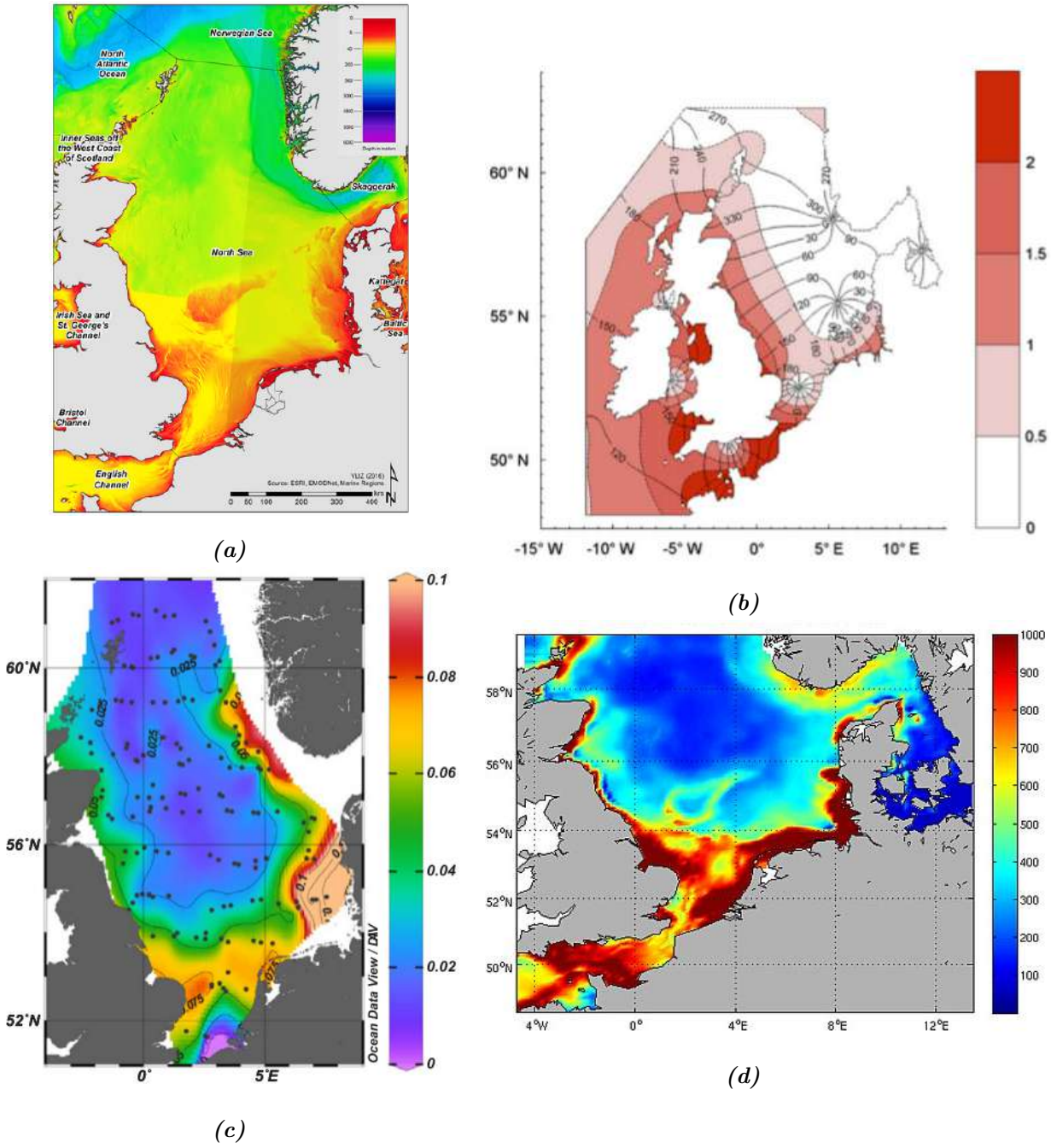

Figure 2: *a: Bathimetry map of the North Sea from EMODNet Bathimetry (http://www.emodnet-bathymetry.eu/). b: Chart for the M2 tidal constituent based on model simulation. Colored contour patches give amplitude (m), solid lines with values indicate phase (Pickering et al. [2012]). c: Spatial distribution of depth-averaged terrestrial dissolved organic matter. This should serve as an indication of nutrient concentration. The unit is normalised fluorescence intensity (Painter et al. [2018]). d: Modeled (GETM-ERSEM) net primary production (depth-averaged). Average for the Period: 03-Jan-1989-31-Dec-1989. https://www.nioz.nl/en/about/cos/ecosystem-modelling/model-results-north-sea/north-sea-aggregated/net-primary-production*

Flagellates are characterized by the possession of one or more flagella which are long hair-like appendages that act as organelles of motion and feeding. In the North Sea they succeed

diatoms as the main algal group, with higher concentrations during the second half of the year (Reid et al. [2016]). Primary production is the production of organic from inorganic material. The productivity of a marine ecosystem depends, among others, on the availability of nutrients. As previously mentioned, the North Sea receives fresh waters from several large European rivers. The enrichment of those waters with anthropogenic nutrients results in increased nutrient concentration at the near shore regions (figure 2c) and thus increased productivity (figure 2d). Occasionally, this leads to eutrophication related problems (Painter et al. [2018]).

The characteristics of the North sea (e.g currents, waves, density stratification, mixing, suspended sediment (SSC) and phytoplankton concentration), are expected to be altered under the presence of large scale PV-installations. The latter may have four expected effects on the hydro and eco-dynamics. The first effect **(ef1)** is the decreased light conditions due to the shadowing effect of the platforms while the second effect **(ef2)** is the reduced wind stress due to the limitation of the free surface of the water column. The third effect **(ef3)** relates to the introduction of an additional surface stress experienced by currents, due to friction induced by the platforms. The last effect **(ef4)** is the reduced wave height due to the presence of the platforms. The quantification of the sustainability of an environment has been a topic of intense discussion (Tett et al. [2007]). Here, the effects of the PV installations on the sustainability of the marine ecosystem is quantified by the changes of the total amount of primary production within the water column. This is because primary production is controlled by the availability of light and nutrients. Thus, it is a variable that is expected to be sensitive to increased PV coverage as the latter affects among others the levels of light within the water column.

As large scale wind farms have already been implemented in the North Sea, their effect on the hydrodynamics and marine ecosystem have received ample attention in the past years. The literature describes a wide spectrum of different effects (IMSA [2011] ; de León et al. [2011] ; van der Molen et al. [2014]). Among those are the effects of reduced wind speed and its effect on the hydro/eco dynamics, the increased noise levels and their obstructions to animals (van der Molen et al. [2014]), the changes in the wave field (braking and reflecting/refractive effects at the monopiles) (de León et al. [2011]) and the effect on the biodiversity caused by the epifauna and epiflora that settle on the structures (IMSA [2011]). In contrast to wind-turbines, solar parks demand a large area of sea surface to be covered with solar panels, resulting in a direct effect on the irradiance of the domain. Thus, the main effects of the PV-installations are not expected to be similar to the ones of the wind turbines.

Until now, floating PVs have been implemented mostly in inshore aquatic environments. Hence, the effects of the platforms on the ecosystem have been discussed mainly for this type of environments (Santafe et al. [2014] ; Sahu et al. [2016] ; da Silva and Branco [2018]). Most of the studies agree that the PVs decrease the evaporation from the reservoir and increase water quality through a reduction of algal growth, due to the shadowing effect of the platforms. However, no further analysis is presented on the topic. The effects of other types of floating structure on aquatic environments have been analyzed in more detail. In one of them Nakamura and Mueller [2008] examined the performance of artificial floating islands (AFIs) as a restoration tool for eutrophicated aquatic environments. AFIs are vegetated floating platforms used in lakes, ponds and water reservoirs, for the limitation of algal growth. Their shade and the nutrient uptake from their vegetation result in a decrease of phytoplankton. The main results of the study are summarized in figure 3. Here, the decrease of chlorophyll a for increased coverage with AFIs is presented for an experimental test cell with surface: 24 m^2 and depth: 2 m (see figure 17b of the appendix). In order to distinguish the effect of shading from the effect of nutrient uptake

by vegetation, chlorophyll a was measured under the effect of AFIs and non-vegetated floating platforms (plywood). The differences were small indicating that the shading effect was the dominant one (see figure 17a of the appendix).

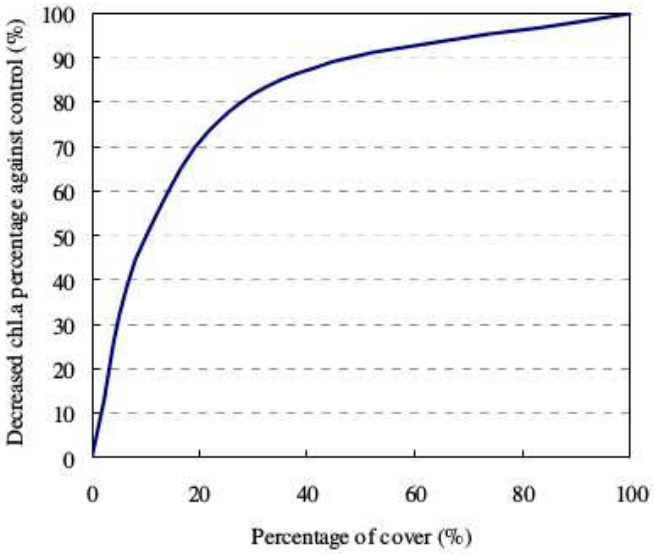

Figure 3: *Percentage of artificial floating island (AFI) coverage versus decrease of chlorophyll a (%) against control condition (case of no coverage). The results refer to an experimental test cell with surface:* 24 m^2 *and depth:* 2 *m Nakamura and Mueller [2008]*

The strong differences between offshore and inshore environments (salt, high waves, tides, different phytoplankton species) indicate that the effects of the PVs on marine ecosystems is different and needs to be studied separately. The main effects of floating PVs on an inshore environment are related to the reduction of incoming solar radiation (ef1). In the case of offshore installations other effects are expected to be important. In an offshore marine environment the strong winds, strong tidal currents and high waves result in increased vertical mixing and thus increased SSC. The increased SSC results in a stronger light attenuation with depth and thus it poses limitations on primary production (Wetsteyn and Kromkamp [1994]). Therefore, the effects of ef2, ef3 and ef4 that follow the presence of PVs could result in less SSC and higher water. This could counteract the impacts of reduced incoming solar radiation (ef1).

In this study a modeling approach is used due to the absence of field observations. To develop the implementation of solar PV panels and to enable a first exploration of the large parameter space, a 1D vertical column approach is used. The selection of a 1D vertical model implies restrictions on the realistic representation of the water column and the ecosystem. In real marine environments the advection of variables such as temperature, suspended sediment, salinity and chlorophyll a is of significant importance for the ecodynamics. Thus, to address the problem in a realistic way a 3D numerical model is needed. However, a 3D model is computationally expensive and time-consuming and thus not adequate for the time-limited first exploratory study discussed here. Taking into consideration the limitations of the present approach, this project aims to provide a first overview of the potential impacts of floating PV installations on the hydrodynamics and the ecosystem of the North Sea and provide useful insights into the role of the different effects (ef1, ef2, ef3, ef4).

According to the abovementioned considerations, the specific research questions (RQ) that are addressed here are the following.

RQ1) What is the skill of a 1D vertical column model to reproduce observed data of ecological variables (chlorophyll a, nutrients) for different locations of the North Sea?

RQ2) What is the overall effect of the PV installations on the hydrography and ecosystem at different locations in the North Sea and what is the relative importance of the individual effects? Under which circumstances can it be argued that the effects ef2, ef3 and ef4 could compensate the impact of ef1 on the ecosystem?

RQ3) Which location characteristics would be favorable for the implementation of PV power plants in terms of ecosystem response?

The structure of the report is as follows. In section 2.1 a description is given for the basic aspects of the model selected for this study (GOTM-ERSEM-BFM). In section 2.2 the modifications made on the equations of the model in order to implement the PV-installations are presented. In section 2.3 a description of the output variables is given together with some background theory. The observed data (SmartBouy) used for the model's calibration, a description of the sampling regions and the methods of calibration/validation are presented in sections 2.4, 2.5 and 2.6, respectively. The design of the experiments for this study is discussed in section 2.7. In section 3 the results of the experiments related to RQ1 and RQ2 are presented. In section 4 RQ3 is discussed together with other important remarks and suggestions for further work. Finally, section 5 contains the main conclusions of the study.

2 Material and methods

2.1 Model description

For the purpose of this work the coupled physical-biogeochemical model GOTM-ERSEM-BFM (version: July 2016) is used. The **G**eneral **O**cean **T**urbulence **M**odel (GOTM) is a one-dimensional water column model that includes the most important hydrodynamic and thermodynamic processes related to vertical mixing in natural waters. The model is based on the Reynolds averaged Navier Stokes equations and on the Reynolds-averaged transport equations of temperature and salinity, under the Boussinesq and the hydrostatic approximations (Burchard et al. [2006]). In this application of GOTM salinity is considered as constant and thus it is not discussed further. GOTM comprises modules for the mean flow and the turbulence sub-models. The mean flow sub-model calculates the quasi-steady components (average over the turbulence time scale), while the turbulent sub-model calculates the eddy viscosity and diffusivity which are used from the calculation of the vertical turbulent fluxes (eddy viscosity principle) (Burchard et al. [1999]). GOTM contains an additional module that provides the mean flow model with information on the air-sea interactions. The strength of GOTM lies on the fact that it allows for different combinations of momentum and tracer equations and a choice between different turbulence parameterizations and boundary conditions (Burchard et al. [1999] ; Umlauf et al. [2005]). For this study, the model is forced with time series of air temperature, humidity, cloud cover and wind velocities at 10 m from the ECMWF ERA40 data set (http://apps.ecmwf.int/datasets/data/era40-daily/levtype=sfc/). Moreover, it is forced with time series of depth-averaged tidal velocities which are extracted from the harmonic analysis of

the 3D GETM model (van der Molen et al. [2017]).

Coupled with GOTM, an ecosystem model (ERSEM-BFM) is used for the calculation of the ecological variables. The **E**uropean **R**egional **S**eas **E**cosystem **M**odel - **B**iogeochemical **F**lux **M**odel(ERSEM-BFM) (version used: July 2016) is a development of the model ERSEM III (Baretta et al. [1995]). It is a pelagic-benthic ecosystem model describing the biogeochemical fluxes in the lower trophic levels of the marine food web (phytoplankters, zooplankters, bacteria, benthic agents). The model simulates the cycles of carbon, nitrogen, phosphorus, silicate and oxygen, allowing for variable internal nutrient ratios within the different groups. The model applies a functional group approach and it contains six pelagic phytoplankton groups (diatoms, flagellates, picophytoplankton, resuspended benthic diatoms, dinoflagellates and phaeocystis), four zooplankton groups and five benthic faunal groups (four macro-fauna and one meio-fauna groups) (van der Molen et al. [2017]). The current version of ERSEM-BFM contains a suspended particulate matter (SPM) resuspension method that feeds into simulations of under-water light climate and primary production. The model calculates the resuspension of sediment and couples the resuspension of detritus with it. The SPM is resuspended and vertically mixed in response to combined wave and current conditions. Within the SPM model a simple JONSWAP equilibrium wave model is used for the calculation of the significant wave height, period and direction (van der Molen et al. [2017]). As in this study ERSEM-BFM is coupled with a 1D hydrodynamic model, it is running in a 1D configuration.

The wave sub-model is a module of ERSEM-BFM. As in the current configuration there is no feedback from ERSEM-BFM to GOTM, the latter do not take in to acount the effect of waves on turbulence and neither on the resuspension of sediment. For SSC in GOTM, it is taken in to account through the consideration of different Jerlov water types (N.G.Jerlov [1976]). In figure 4, a general schematic representation of GOTOM-ERSEM-BFM is presented. Subsequently, the parts of the model (GOTM-ERSEM-BFM) that are important for this study are discussed separately and the equations are presented.

2.1.1 GOTM mean flow sub-model

Equation of velocity

Assuming no advection of momentum (GOTM considers zero horizontal gradients for all variables), zero vertical velocities and incompressibility for the fluid, the zonal and meridional components of the momentum equation read

$$\partial_t u - \partial_z\Big((\nu_t + \nu)\partial_z u\Big) = -g\,\partial_x\zeta + fv \tag{1}$$

$$\partial_t v - \partial_z\Big((\nu_t + \nu)\partial_z v\Big) = -g\,\partial_y\zeta - fu. \tag{2}$$

Here, u and v are the steady components of zonal and meridional velocities. The constant $\nu = 1.3 \times 10^{-6}$ $\mathrm{m^2 s^{-1}}$ is the molecular viscosity, ν_t is the vertical eddy viscosity which is calculate by the turbulence model, ζ is the sea surface elevation, f the Coriolis parameter and $g = 9.81$ $\mathrm{ms^{-2}}$ the gravitational acceleration. The first terms of the right hand side of equations 1 and 2, are the horizontal gradients of the sea surface elevation. Those terms cannot be calculated from a 1D model (note that in this version the model considers a fixed surface at $\zeta = 0$), thus they need to be defined from time series of observed values. In the current

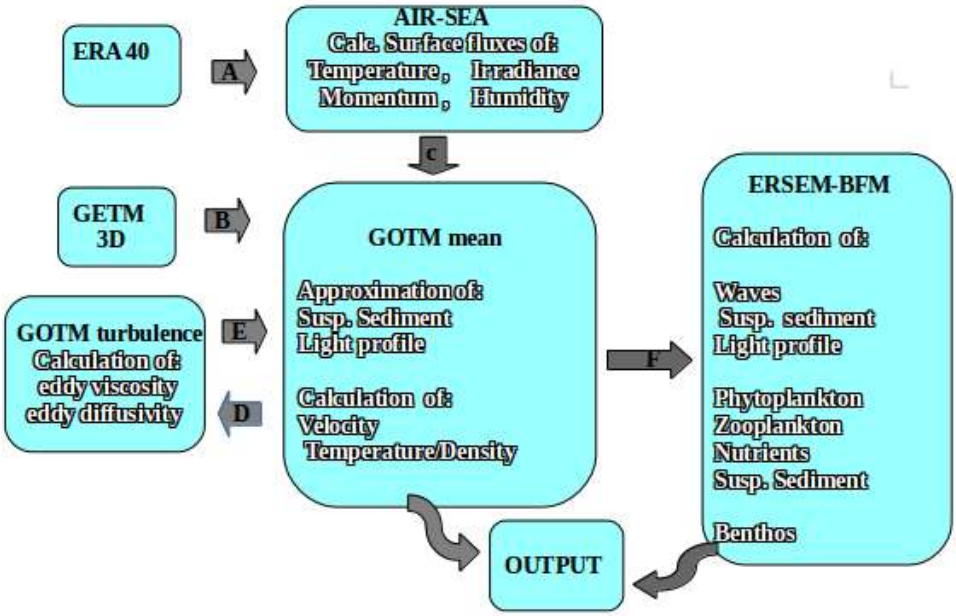

Figure 4: *Rough representation of the main functions of GOTM-ERSEM-BFM. The arrows represent the flow of information between the different parts of the coupled model. A: Information on wind, irradiance, temperature and humidity of air, B: depth-averaged tidal velocities, C: Information on wind stress, irradiance, temperature and humidity at sea surface. D: Parameters needed for the calculation of turbulent properties (e.g. shear frequency), E: eddy viscosity and diffusivity, F: Parameters needed for the calculation of ecological variables (and sediment) (e.g. velocity at the bottom, temperature, density, heat diffusivity ets..)*

application those values are given by the depth-averaged values of tidal velocities, from the M2 and S2 harmonic constituents calculated from GETM 3D (van der Molen et al. [2017]). The derivation of the surface slopes from modeled current velocities and its efficiency are discussed in Burchard [1999]. The boundary conditions at the surface and bottom for the two components of the velocity are

$$(\nu_t + \nu)\,\partial_z u\big|_{z=0} = \frac{\tau_x^s}{\rho_0} \quad , \quad u\big|_{z=-H+z_0^b} = 0 \tag{3}$$

$$(\nu_t + \nu)\,\partial_z v\big|_{z=0} = \frac{\tau_y^s}{\rho_0} \quad , \quad u\big|_{z=-H+z_0^b} = 0 \tag{4}$$

with τ_x^s and τ_y^s the zonal and meridional components of stress due to wind at the surface, ρ_0 a constant reference density, H the depth of the water column and z_0^b the roughness lengths at the bottom given by

$$z_0^b = 0.1\frac{\nu}{u_*^b} + 0.03 h_0^b \tag{5}$$

with $h_0^b = 0.05$ m the height of the roughness elements at bottom and u_*^b the frictional velocity at the bottom given by

$$u_*^b = \left(\nu_t \sqrt{(\partial_z u)^2 + (\partial_z v)^2}\big|_{z=-H+z_0^b}\right)^{1/2}. \tag{6}$$

The no slip condition of equations 3 and 4 (right) for the bottom might appear non-standard for high resolution modeling of turbulent flows. The law of quadratic bottom friction is introduced

on numerical level in the model. This is done to account for the fact that the model calculates the bottom velocity not exactly at the bottom, but in the middle of the bottom layer (Burchard et al. [1999]).

Equation of temperature

Temperature is one of the tracers considered in GOTM. Salinity is considered as constant for the current application of the model. Thus, only the vertical gradient of temperature determines stratification. The Reynolds averaged equation of temperature, after assuming no horizontal advection and zero vertical velocities is

$$\partial_t T - \partial_z\big((\nu'_t + \nu')\,\partial_z T\big) = \frac{\partial_z I}{\rho_o C_p} \tag{7}$$

where T is the steady component of temperature, $\nu' = 1.4 \times 10^{-7}$ $(\mathrm{m^2 s^{-1}})$ is the molecular diffusivity and ν'_t is the eddy diffusivity which is calculated by the turbulent sub-model. The right hand side of the equation represents the absorption of short wave radiation which is considered as an inner source of heat, while $C_p = 3980$ $\mathrm{J\,kg^{-1}\,K^{-1}}$ stands for the specific heat capacity of sea water and I (Wm^{-2}) for the energy flux which is parameterized according to Paulson and Simpson [1977].

Following Kondo [1975] and Rosati and Miyakoda [1988], the boundary condition of temperature at the surface is parameterized as

$$(\nu'_t + \nu')\,\partial_z T\big|_{z=0} = \frac{-Q_E - Q_H - Q_B}{C_p \rho_0} \tag{8}$$

where Q_B is the long wave radiation and Q_E and Q_H the latent and sensible heat fluxes respectively. For the bottom zero flux conditions are considered as

$$\partial_z T\big|_{z=-H} = 0. \tag{9}$$

2.1.2 GOTM turbulence sub-model

In the turbulence sub-model of GOTM, the $k-\epsilon$ closure assumption has been used. The model is based on the relation of Kolomogorov & Prandtl for the calculation of eddy viscosity (ν_t) and eddy diffusivity (ν'_t)(Burchard et al. [1999])

$$\nu_t = c_\mu \sqrt{k} L \quad , \quad \nu'_t = c'_\mu \sqrt{k} L. \tag{10}$$

Here k is the turbulent kinetic energy per mass $(m^2 s^{-2})$, c_μ and c'_μ are the stability functions which are calculated according to Galperin et al. [1988] and L is the turbulent length scale given by

$$L = (c^0_\mu)^3 \,\frac{k^{3/2}}{\epsilon}. \tag{11}$$

In this expression $c^0_\mu = 0.5562$ is a constant and ϵ $(m^2 s^{-3})$ is the turbulent energy dissipation rate. The variables of k and ϵ are the two prognostically calculated turbulence parameters needed for the computation of ν_t and ν'_t (Burchard et al. [2000]). The transport equations for k and ϵ

can be derived from the Navier Stokes equations after some simplifying model assumptions. In one dimension the equations for k and ϵ read

$$\partial_t k - \partial_z(\nu_t \partial_z k) = P + B - \epsilon \tag{12}$$

$$\partial_t \epsilon - \partial_z(\frac{\nu_t}{\sigma_\epsilon}\partial_z \epsilon) = \frac{\epsilon}{k}(c_{\epsilon 1}P + c_{\epsilon 3}B - c_{\epsilon 2}\epsilon). \tag{13}$$

Here $\sigma_\epsilon = 1.08$, $c_{\epsilon 1} = 1.44$, $c_{\epsilon 2} = 1.92$ and $c_{\epsilon 3} = \begin{cases} -0.4 & (B<0) \\ 1 & (B\geq 0) \end{cases}$ are constants, while P and B are the shear and buoyancy production terms of turbulence and they are given by

$$P = \nu_t S^2 \quad , \quad B = -\nu'_t N^2 \tag{14}$$

with $S = \sqrt{(\partial_z u)^2 + (\partial_z v)^2}$ the shear frequency and $N = \sqrt{-\frac{g}{\rho_0}\partial_z \rho}$ the Brunt-Väisälä frequency, to be calculated from the mean flow model. GOTM provides multiple selections for the boundary conditions of k and ϵ. In this version Neumann boundary conditions are selected. Those read

$$\nu_t \partial_z k\big|_{z=0} = 0 \quad , \quad \nu_t \partial_z k\big|_{z=-H} = 0 \tag{15}$$

$$\partial_{\tilde{z}} \epsilon\big|_{\tilde{z}=0} = -(c^o_\mu)^3 \frac{k^{3/2}}{\kappa(\tilde{z} + z_o)^2} \quad \text{with} \quad \tilde{z} = |z| \tag{16}$$

$$\partial_{\tilde{z}} \epsilon\big|_{\tilde{z}=0} = -(c^o_\mu)^3 \frac{k^{3/2}}{\kappa(\tilde{z} + z_o)^2} \quad \text{with} \quad \tilde{z} = H - |z|. \tag{17}$$

On equation 15 the boundary conditions of k are given for the surface and bottom and on equations 16 and 17 the boundary conditions of ϵ for surface and bottom, respectively. The parameter $\tilde{z}$ is the distance from the surface and bottom, respectively.

2.1.3 ERSEM-BFM main equation

For ERSEM-BFM, the prognostic equation solved for the pelagic variables (different phytoplankters, zooplankters, nutrients, detritus, SSC, oxygen, ets..) is given by

$$\partial_t c + w\partial_z c - \partial_z(\nu'_t \partial_z c) = S + D \tag{18}$$

Here c denotes the concentration of the different variables, w their sinking velocity, ν'_t the eddy diffusivity and S and D the sources and sink terms of the different variables. The boundary conditions are different for each ecosystem variable and are generally given by fluxes at the surface and at the bottom of the domain. For phytoplankton, S represents gross primary production (PP) and D the losses through excretion, respiration, predation by zooplankton and mortality in the form of lysis. More detailed calculations are included in Geider et al. [1997] and Vichi et al. [2006]).

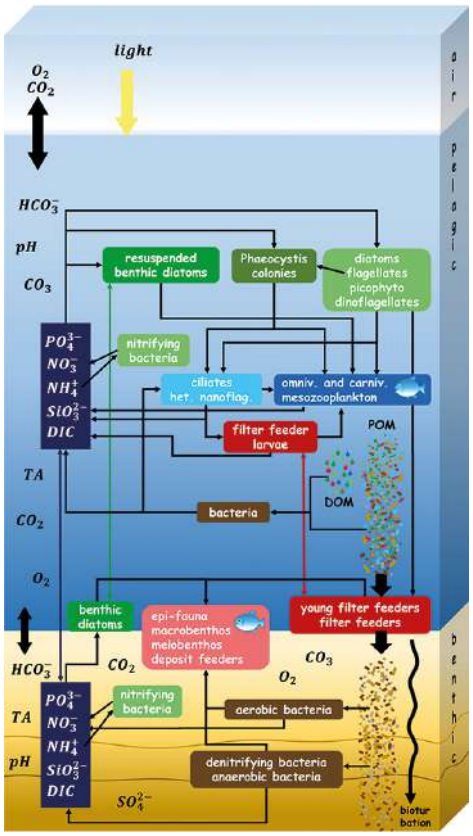

Figure 5: *"Schematic representation of nutrient and carbon flows in the biogeochemical model ERSEM-BFM, including DOM (Dissolved Organic Matter), POM (Particulate Organic Matter) and DIC (Dissolved Inorganic Carbon). TA stands for Total Alkalinity. The fish symbol indicates mortality due to fish predation, which is included in the model as cannibalism to ensure a biomass-based response (more prey biomass means increased predation). The sea bed consists of 3 layers: the oxic layer, the denitrification layer and the anoxic layer, which are separated by the oxygen penetration depth and the sulfide horizon depth, respectively". Caption and figure from: https://www.nioz.nl/en/expertise/waddencentre/data-tools/modelling/end-2-end*

2.1.4 ERSEM-BFM wave sub-model

The current version of ERSEM-BFM is supplied with a wave sub-model of which the output is used for the calculations of sediment resuspension. The wave sub-model is based on a JONSWAP equilibrium wave model and calculates the significant wave-height, period and direction of the waves as a response to the wind forcing (van der Molen et al. [2016]). Then the resulting wave orbital velocities at the bottom add to the suspension of sediment. Concerning the wave sub-model, firstly it considers a maximum duration of three hours ($t_d = 10.800$s) for the interaction between wind and sea (duration limited wave height) and includes limitations for the wave height for depths shallower than 10 m. Then and according to the Sverdrup-Munk-Bretschneider method the significant wave height (H_s) follows from

$$H_s = \min(H_{s,full}, H_{s,lim}) \tag{19}$$

where $H_{s,full}$ is the unlimited (fetch and duration) wave height and it is given by

$$H_{s,full} = 0.243\frac{U^2}{g} \tag{20}$$

while $H_{s,lim}$ stands for the duration limited wave height given by

$$H_{s,lim} = 0.0016\sqrt{F_*}\frac{U^2}{g}. \tag{21}$$

In this expression $U = 0.7\,(U_{10})^{1.2}$ is the adjusted wind speed (empirical relation) (van der Molen et al. [2014]) with U_{10} the wind velocity at 10 m above the sea level and F_* is the dimensionless

fetch given by

$$F_* = \frac{gF}{U^2} \tag{22}$$

where F is the fetch defined as the distance over which wind blows above the sea surface and is given from $F = U_{10}t_d$. The wave peak period is calculated as

$$T_p = \min(T_{p,full}, T_{p,lim}) \tag{23}$$

where $T_{p,full}$ and $T_{p,lim}$ are the unlimited and fetch limited peak periods respectively. Those are obtained from

$$T_{p,full} = 8.14\frac{U}{g} \quad , \quad T_{p,lim} = 0.286F_*^{0.33}\frac{U}{g}. \tag{24}$$

2.2 Model adaptation

Here, the modifications that have been done in the equations of the model are presented. The modifications aim to the investigation of the impact of the PV-installations on the hydrodynamics and ecodynamics, through the introduction of four individual effects that can be treated separately. As mentioned, the four individual effects are: **ef1:** decreased light conditions due to the shadowing effect of the platforms, **ef2:** reduced wind stress due to the limitation of the free surface of the water column, **ef3:** introduction of an additional surface stress experienced by currents, due to friction induced by the platforms, **ef4:** reduced wave height due to the presence of the platforms.

The PVs will be mounted on floating platforms that will extend 0.2 m below and 0.3 m above the sea surface. However, for simplicity the vertical extent of the installations is not taken into account. Moreover, the mean height of the roughness elements of the platforms are considered as equal to the one considered for the sea bed ($h_0^{pv} = 0,05$ m). The adapted version of the model needs to allow for no coverage, full coverage and partial coverage of the domain. Thus, a new variable (*cover*) that varies between zero and one, is introduced. The implementation of *cover* in the model is done in a way as to allow for separate investigation of the individual effects (ef1, ef2, ef3, ef4). This is done with the use of switch-on switch-off variables for the individual effects (α_1, α_2, α_3, $\alpha_4 \in \{0, 1\}$). Then increased coverage can result in decreased light, or decreased wind stress, or increased stress due to friction induced by the platforms, or decreased wave height, or all the above together. The effect of coverage is implemented through a linear dependence of certain variables on *cover*. This is a strong hypothesis as it assumes no non-linear interactions between the covered and the uncovered part of a domain. Such interactions, if present, cannot be quantified with this model approach. However, it is stressed that the overall aim of this work is to allow for a first investigation of how the state of the model will change under different scenarios of coverage with PV-installations.

2.2.1 Irradiance

According to the above, the surface value of irradiance in the domain (see equation 7) under the influence of the platforms (I_o') is modeled as

$$I_o' = (1 - cover\,\alpha_1)I_o \quad , \quad \alpha_1 \in \{0, 1\}. \tag{25}$$

2.2.2 Wind stress

In the same spirit, the wind stress (see equations 3, 4 left), follows the decrease of the free surface of the domain. The reduced wind stress components ${\tau'}^s_x$, ${\tau'}^s_y$ due to the presence of the PV-installations are

$$ {\tau'}^s_x = (1 - cover\,\alpha_2)\tau^s_x \quad , \quad {\tau'}^s_y = (1 - cover\,\alpha_2)\tau^s_y \tag{26} $$

$$ \alpha_2 \in \{0, 1\}. $$

2.2.3 Stress due to friction induced by the platforms

To account for the friction experienced by the currents due to the PVs, the stresses ${\tau'}^s_{x,pv}$ and ${\tau'}^s_{y,pv}$ are introduced to the surface boundary conditions of equations 3 and 4. Then the equations read

$$ (\nu_t + \nu)\partial_z u\big|_{(z=0)} = \frac{{\tau'}^s_x + {\tau'}^s_{x,pv}}{\rho_0} \quad , \quad (\nu_t + \nu)\partial_z v\big|_{(z=0)} = \frac{{\tau'}^s_y + {\tau'}^s_{y,pv}}{\rho_0}. \tag{27} $$

With the use of the logarithmic law of the wall and taking into account the effect of coverage the new stresses read

$$ {\tau'}^s_{x,pv} = -\,r_s u_s \sqrt{u_s^2 + v_s^2}\, cover\,\alpha_3 \quad , \quad {\tau'}^s_{y,pv} = -\,r_s v_s \sqrt{u_s^2 + v_s^2}\, cover\,\alpha_3 \tag{28} $$

$$ \alpha_3 \in \{0, 1\}. $$

Here, u_s and v_s are the velocities at the middle of the top layer of the model and r_s the surface drag coefficient given by

$$ u_s = \frac{u^{s,x}_*}{\sqrt{r_s}} \quad , \quad v_s = \frac{u^{s,y}_*}{\sqrt{r_s}} \quad , \quad r_s = \left(\frac{\kappa}{\ln\!\left(\frac{z_0^{pv} + h_{top}/2}{z_0^{pv}} \right)} \right)^2 \tag{29} $$

with κ the Von Karman constant, h_{top} the thickness of the top layer, $u^{s,x}_* = \sqrt{\nu_t \partial_z u\big|_{z=0}}$ and $v^{s,x}_* = \sqrt{\nu_t \partial_z v\big|_{z=0}}$, the zonal and meridional components of surface frictional velocity and z_0^{pv} the surface roughness length for the covered part of the domain to be defined as

$$ z_0^{pv} = 0.1\frac{\nu}{u^s_*} + 0.03 h_0^{pv}. \tag{30} $$

Here, the parameter $h_0^{pv} = 0,05$ m is the mean height of the roughness elements at the bottom of the platform and $u^s_* = \left(\nu_t \sqrt{(\partial_z u)^2 + (\partial_z v)^2}|_{z=0}\right)^{1/2}$ is the frictional velocity at the surface due to the installations. Note that in equation 29 for $h_{top} \to 0$, the values of u_s and v_s are approaching 0. As in the case of bottom friction the physical meaning of equations 27 (with α_2, $\alpha_3 = 1$ from equations 26 and 28) is the no slip condition for the surface velocity of a fully covered domain.

2.2.4 Wave height

The reduction of the wave height due to the presence of the PVs is implemented with a linear reduction of the dimensionless fetch (equation 22) with increasing coverage. This reads

$$F'_* = F_*(1 - cover\,\alpha_4) \quad , \quad \alpha_4 \in \{0, 1\}. \tag{31}$$

The above method should not be considered as an attempt to describe realistically the decrease of wave height due to the PV installations. For the case of an offshore solar farm near the coast the waves should mostly be advected into the region and not generated within it. Thus, the reduction of wave height should mostly be related with braking/reflecting effects on the platforms. However, the simplistic nature of a 1D column model using a JONSWAP equilibrium model for the implementation of waves, combined with the absence of observed data to test a theoretical model for the wave damping on the PVs, oppose restrictions. Even if not realistic, a reduction of the fetch with increasing coverage is consistent with the assumption of zero horizontal gradients of a 1D model. The assumption of zero horizontal gradients requires that the water column of the experiment, should be surrounded by identical water columns. Consequently, those water columns would have the same amount of coverage and thus the fetch for the waves arriving at the domain would depend on the amount of coverage.

2.3 Output of the model

A model study provides access to a great amount of output variables. In this report only those that have been considered as more relevant for the study are presented. The variables have been selected in order to provide a wide overview of the ways that the PVs effect the water column. Namely they are: irradiance, temperature, depth-averaged current velocity, bottom current velocity, top mixed layer depth, significant wave height, eddy diffusivity, suspended sediment, diatom concentration, flagellates concentration and net-primary production.

- The concentration of suspended sediment (SSC) (mg/m^3) is calculated from equation 18. It is presented as it relates with the water quality and the light availability of the domain. The importance of SSC for the extinction of light can be approximated by the ratio

$$\frac{\epsilon_o}{\epsilon_{ss}\,SSC} \tag{32}$$

  where ϵ_o is the background extinction of light and ϵ_{ss} is the extinction coefficient due to suspended sediment.

- Irradiance (I) (mE/m^2/s) is indicating the light availability in the water column. The unit is milliEinstein per square meter per second and indicates the flux of photons. The vertical profile of I is affected by SSC. Thus, the change of irradiance with *cover* should reveal, apart from the effect of shadow (ef1), the effect of the PVs on turbidity (ef2,ef3,ef4).

- Temperature (T) (C^o) responds to the changes of I. Moreover, it should relate with an indirect effect on primary production as the latter is favored by high temperatures.

- The significant wave height (H_s) (m) (see section 2.1.4) responds to ef4 and is presented due to its importance for sediment resuspension.

- Depth-averaged current velocity (U) (m/s) (see section 2.1.1) responds mainly to ef2 and ef3 of the platforms. Additionally, the value of velocity at the bottom is given due to its importance for the resuspension of sediment.

- Top mixed layer (TML) is the layer below the surface that have been homogenized by turbulence. With $TMLd$ the depth of this layer is noted. In terms of ecology, the formation of the TML is closely related with the timing of the spring bloom (Sverdrup [1953]). Additionally, it results in limited exchange of tracers (temperature, sediment, nutrient, phytoplankton, ets..) between the surface and the deeper layers, affecting this way their vertical distribution. According to Hunter and Simpsons [1974] the formation of a TML requires

$$\frac{g\alpha}{\rho\epsilon_k rc}\frac{I_o H}{U_b^3} \geq 8/3\pi \tag{33}$$

  where α is the linear expansion coefficient, c the specific heat, ρ_o a reference density, r the drag coefficient of the quadratic friction law, ϵ_k is the fraction of the kinetic energy transformed to potential energy at the bottom, g is gravitational acceleration, H the depth of the water column, U_b the bottom velocity and I_o the irradiance at surface. Thus, the effects of the PVs on two latter mentioned variables are expected to affect the timing of stratification.

- Eddy diffusivity $(\nu'_t)(m^2/s)$ is presented due to its importance for the vertical transport (through diffusion) of SSC (see equation 18).

- Among the phytoplankton species only diatoms (c_d) and flagellates (c_f) (mg/m^3) are presented as they are the two dominant species and they indicate different functional groups.

- Finally, primary production $(PP)(mgm^{-2}day^{-1})$ (see section 2.1.3) is considered as an indication of the sustainability of the marine environment and thus presented.

2.4 Smartbuoy data

In order to calibrate the model and to address RQ1 a comparison of the model results with observations is needed. For this reason data from the Smartbuoy observational system are used. Smartbuoys are deployed by the Center for Environmental Fisheries and Aquaculture Science (Cefas) and they are moored, automated, multi-parameter recording platforms which are used to collect marine environmental data. The data are collected from a network of selected locations within UK and Dutch waters. They consist of high resolution time series, at 1 m below the surface, of salinity, temperature, turbidity, oxygen saturation (fraction of saturated oxygen relative to total amount), chlorophyll fluorescence and nitrate and silicate concentration. Later analysis of collected and preserved water samples is done for nutrient and phytoplankton species. The data are open access and they can be found along with more information at https://www.cefas.co.uk/publications-data/smartbuoys/.

2.5 Locations of experiment

In order to study locations with different environmental conditions the following Smartbuoy stations were selected: Oyster Grounds (longitude: 54.41°, latitude: 4.02°), Noordwijk10 (from now on Noordwijk) (longitude: 52.301°, latitude: 4.303°) and West Gabbard (longitude: 51.9895°, latitude: 2.08983°) (figure 6).

Figure 6: *Map with the Smartbuoy stations in the North Sea. With the red dots the stations of Oyster Grounds (OG), West Gabbard (WG) and Noordwijk (NW) are indicated. http://wavenet.cefas.co.uk/Smartbuoy/Map*

The selection of the above stations aims to allow for an investigation of the possible responses of the hydrodynamics and ecodynamics of the North Sea to the floating PVs. The station of Oyster Grounds is located at 45 m depth and is characterized by a yearly-averaged depth-averaged current amplitude of ~ 0.15 m/s (results from M2, S2 harmonic constituents extracted from a harmonic analysis of GETM 3D see van der Molen et al. [2016]). The winter near-surface values (1m depth) for suspended sediment are ~ 0.04 kg m^{-3}, for nitrate ~ 5 $(mmol/m^3)$, for silicate ~ 5 $(mmol/m^3)$ and for chlorophyll a ~ 5 $(mmol/m^3)$ (Smartbuoy observations). Moreover, the location stratifies every summer between April and October (~ 210 days/year) due to increased irradiance (Tijssen and Wetsteyn [1984]). The station of Noordwijk is located at 18 m depth with yearly-averaged depth-averaged current amplitude of ~ 0.3 m/s. The winter near-surface values (1m depth) for nitrate are ~ 60 $(mmol/m^3)$, for silicate ~ 30 $(mmol/m^3)$ and for chlorophyll a ~ 25 $(mmol/m^3)$. The location remains well mixed over the year and it is selected due to its vicinity with the experimental location of OOE (Scheveningen). The station of West Gabbard is located at 32 m depth with yearly-averaged depth-averaged current amplitude of ~ 0.55 m/s. The winter near-surface values (1m depth) for suspended sediment are ~ 0.15 kg m^{-3}, for nitrate ~ 12 $(mmol/m^3)$, for silicate ~ 8 $(mmol/m^3)$ and for chlorophyll a ~ 25 $(mmol/m^3)$. As Noordwijk, West Gabbard remains well mixed over the year. Subsequently, The location of Oyster Grounds is representative of the poor in nutrients, open-sea regions with low current velocities and seasonal stratification. The locations of West Gabbard and Noordwijk are representative of the nutrient enriched, shallow near coast regions, with high current velocities that remain well mixed during the whole year.

2.6 Model calibration/validation

The calibration period was selected according to the availability of observed data (Oyster Grounds, West Gabbard: 2006-2008, Noordwijk: 2001-2002). Due to the small duration of the sampling period for the locations of Oyster Grounds and Noordwijk a validation of the model was only possible for West Gabbard, which was validated for the period of 2002-2006.

The calibration of the model was done in terms of minimization of the value of the root mean square error (RMS) and maximization of the value of correlation (corr) between the modeled and observed timeseries. This was defined as the best fit. The values of RMS and corr are given by

$$RMS = \sqrt{\frac{\sum_{i=1}^{N}(a_{m,i} - a_{o,i})^2}{N}} \quad , \quad corr = \frac{\sum_{i=1}^{N}\left[(a_{m,i} - \overline{a_m})(a_{o,i} - \overline{a_o})\right]}{N\sigma_{am}\sigma_{ao}} \tag{34}$$

where N indicates the length of the time series, $a_{m,i}$ and $a_{o,i}$ indicate the modeled and observed values at a certain time t_i, $\overline{a_m}$ and $\overline{a_o}$ the expected value of the time series and σ_{am} and σ_{ao} their standard deviations. The calibration was done for the variables of chlorophyll a, nitrate and silicate. The initial concentrations of nitrate ($N3n_o$), silicate ($N5s_o$), phosphate ($N1p_o$) and detritus ($Q6c_o$) were considered as tuning parameters as they determine how much nutrient is initially available. The values of porosity of bed (pporo), suspended sediment extinction coefficient (pepsESS) and salinity (sal) were defined by site specific constants.

2.7 Design of experiment

In order to address RQ1 the model results have been compared with the observations of the Smartbuoys with the procedure described in section 2.6. Then the values of root mean square error (RMS) and correlation (corr) of the best fit have been compared with the existing literature for the variable of chlorophyll a.

In order to address RQ2 runs of the calibrated model have been conducted for the period 1972-2008. The different effects of the platforms (ef1, ef2, ef3, ef4) on hydrodynamics and ecodynamics were treated separately and conclusively (overall effect) as well. For each effect model runs have been conducted for different values of *cover* and for the three locations. The first 27 years were considered as spin-up and thus not taken into account. The sensitivity on coverage of the time-depth averaged values of the output variables (see section 2.3) was evaluated for the different effects and the different locations. For this reason the relative change of the variables (R_A) with coverage was calculated as

$$R_A = \frac{\overline{A_{(t,z,cover)}}\big|_{cover=i}}{\overline{A_{(t,z,cover)}}\big|_{cover=0}} \tag{35}$$

where A is any of the output variables, the nominator and denominator stand for the time and depth-averages for each coverage scenario (*cover*= 0.1, 0.2, 0.3, 0.4, 0.5, 0.6, 0.7, 0.8, 0.9) and the reference case, respectively. Moreover, the depth-averaged yearly time series (averaged over 1998-2008) and the vertical profiles (averaged over 1998-2008) of the selected variables have been compared between different values of coverage and the results are presented in the appendix.

Finally,to address RQ3, the main points of the results for the three locations are discussed.

3 Results

3.1 Model skill assessment

A first analysis of the model (GOTM-ERSEM-BFM) outputs revealed unrealistic values for phaeocystis concentrations and thus phaeocystis was excluded from the calculations. After the exclusion, the values of the tuning parameters ($N3n_o$, $N5s_o$, $N1p_o$, $Q6c_o$) given in table 1

resulted in the best fit between model and observations (see section 2.6). In table 1, the values of the site-spesific constants used in the model set-up are given as well. The comparison between the calibrated model runs and the Smartbuoy observations are presented for selected variables of the three locations in figures 7 and 8. The comparison is given for the surface values (1 m below surface) of chlorophyll (figure 7, panels a,b,c), silicate (figure 7, panels d,e,f) and nitrate (figure 8, panels a,b,c). This is because the procedure of calibration was mainly aiming at a model-observations agreement for those variables. The concentration of suspended sediment was missing from the Noordwijk data set. Instead, the comparison between model and observations for the sea surface temperature is presented (figure 8, panels d,e,f).

For surface temperature (figure 8 panels d,e,f) the correlation (corr) was higher than 0.9 and the root mean square error (RMS) less than $1.5\,C^0$ for all locations. For silicate (figure 7 panels d,e,f) and nitrate (figure 8 panels a,b,c) the statistics were better for the locations of Oyster Ground and West Gabbard ($RMS < 3.6$ mmol/m^3, $corr > 0.7$ mmol/m^3). The lower skill of the model for the location of Noordwijk is partly explained by the importance of phaeocystis for the region. The comparison between model and observations for the variable of chlorophyll a (figure 7, panels a,b,c) indicate the skill of the model to resolve primary production. For the location of Oyster Grounds, where phaeocystis is not important, the model is capable of reproducing the main seasonal patterns of chlorophyll a. However, this results in an overestimation of the spring bloom. The values for RMS and corr are 1.22 mg/m^3 and 0.36, respectively. van der Molen et al. [2016] compared the same Smartbuoy observations for the location of Oyster Grounds with the results of GETM-ERSEM-BFM (3D) obtaining lower value of correlations and higher value of root mean square error. The above indicates that the advection of chlorophyll a is likely not important for the location, resulting in good performance of a 1D models which allows for local calibration. For the locations of West Gabbard and Noordwijk the model results in a large underestimation of chlorophyll a. This is partly attributed to the absence of phaeocystis from the model's calculations. However, the model is still capable of reproducing the main seasonal patterns.

Table 1: *Final set-up for model's tuning parameters and site-specific constants*

	Oyster Grounds	Noordwijk	West Gabbard
$N3n_o$ (mol/m^3)	6	21	21
$N5s_o$ (mol/m^3)	5	40	7.5
$N1p_o$ (mol/m^3)	0.15	1.2	0.15
$Q6c_o$ (mol/m^3)	1.5 10^5	6 10^5	1.8 10^5
pporo0	0.423	0.45	0.45
pepsESS (1/m)	0.11 10^-3	0.055 10^-3	0.055 10^-3
sal (psu)	35	30	35

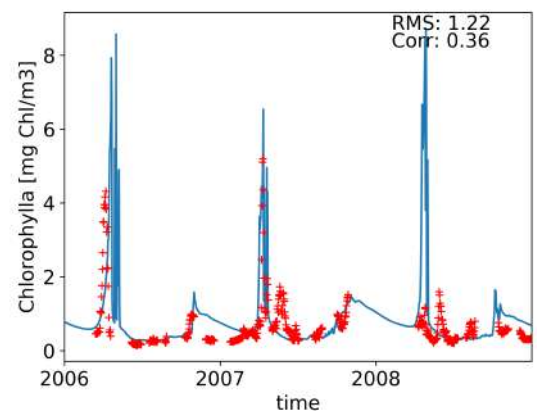

(a) Oyster Grounds

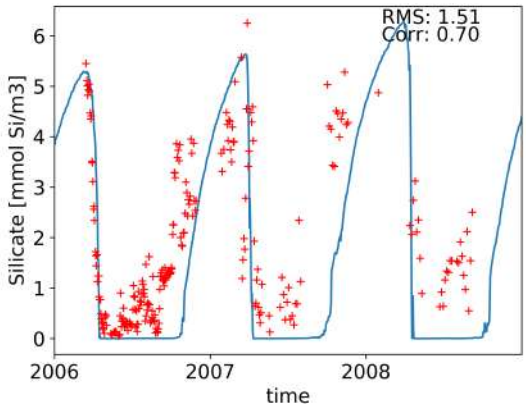

(d) Oyster Grounds

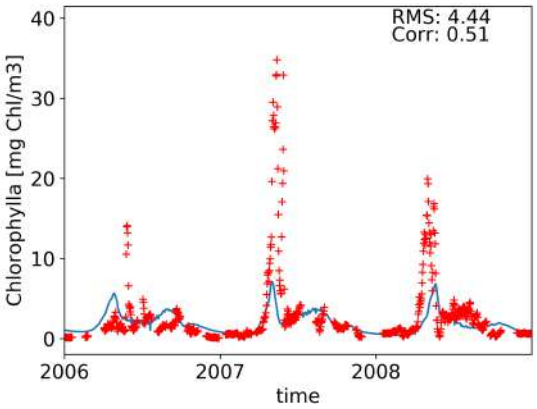

(b) West Gabbard

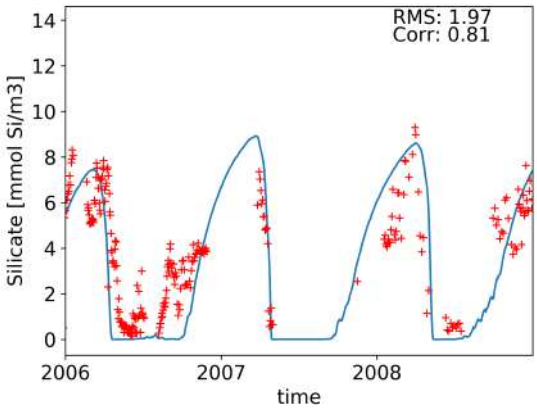

(e) West Gabbard

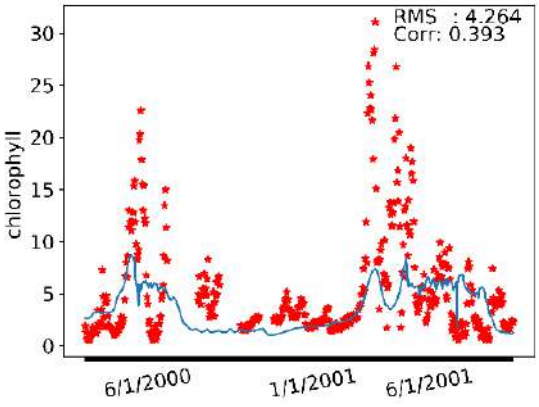

(c) Noordwijk

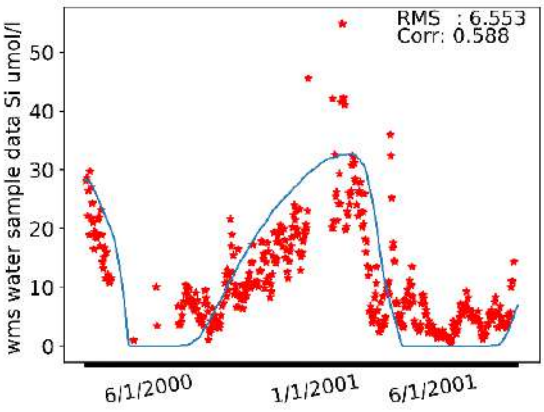

(f) Noordwijk

Figure 7: *Assessment of the model performance for the three locations trough comparison with observations from the Smartbuoys. The variables of chlorophyll a (panels a,b,c) and silicate (panels d,e,f) are presented. With RMS, the root mean square error (units same as in the y-axis of the panel) and with corr, the correlation between the curves are denoted.*

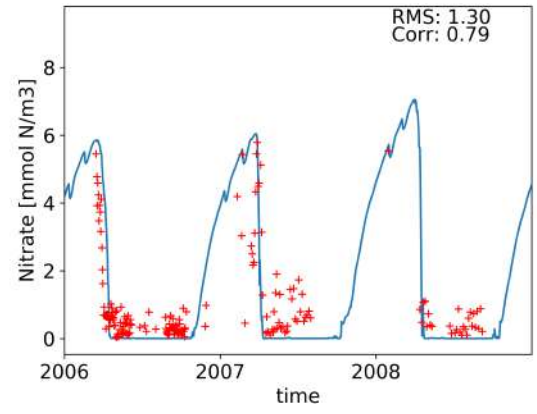

(a) Oyster Grounds

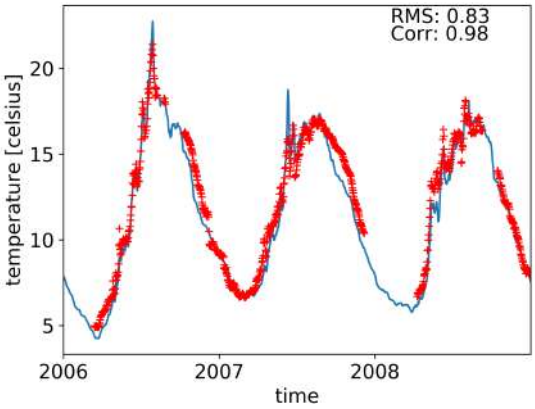

(d) Oyster Grounds

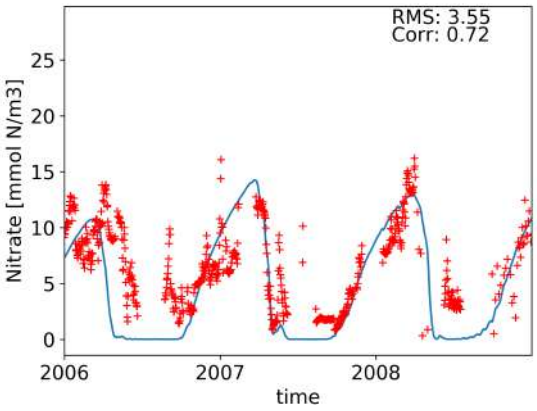

(b) West Gabbard

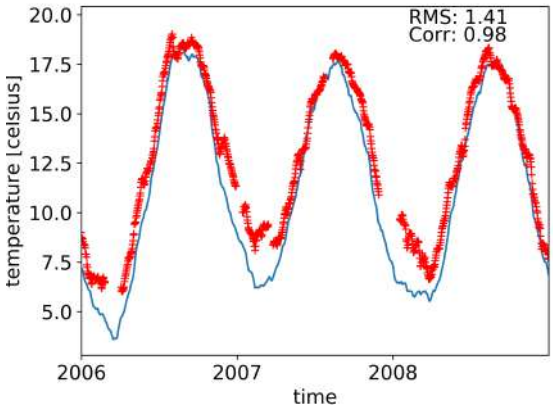

(e) West Gabbard

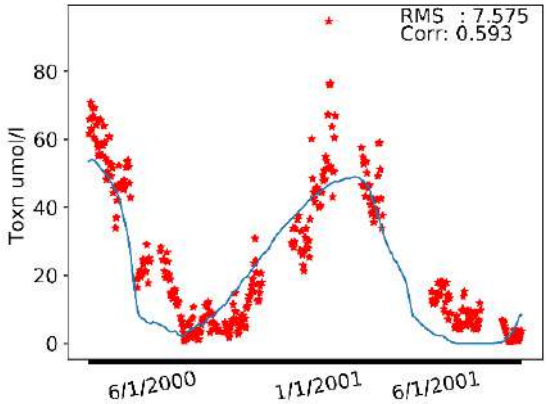

(c) Noordwijk

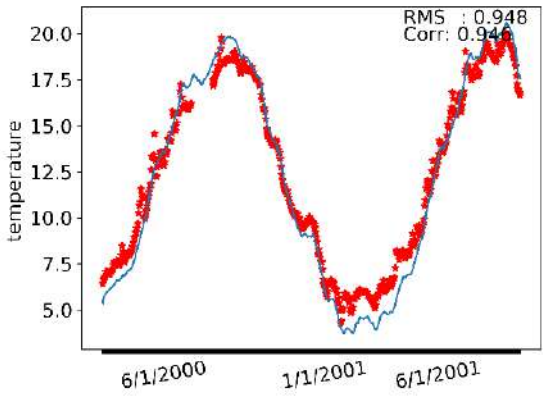

(f) Noordwijk

Figure 8: *Assessment of the model performance for the three locations trough comparison with observations from the Smartbuoys. The surface values of nitrate (panels a,b,c) and temperature (panels d,e,f) are presented. With RMS, the root mean square error (units same as in the y-axis of the panel) and with corr, the correlation between the curves are denoted.*

For West Gabbard, the values for RMS and corr are 4.44 mg/m^3 and 0.51, respectively. Again, a comparison with the performance of GETM-ERSEM-BFM (3D) (van der Molen et al.

[2016]) for the location indicates that the 1D model is performing well for the region, as it resulted in comparable values of *corr* and RMS with the 3D model. For the location of Noordwijk the statistics are worst ($corr = 0.393$, $RMS = 4.264$ mg/m^3). A validation was possible only for the location of West Gabbard. Here, the model was validated for the period 2002-2006, resulting in the values of $corr = 0.52$ and $RMS = 3.30$ mg/m^3.

3.2 Sensitivity of model to coverage

In this section the sensitivity of the model to coverage is addressed. Figures 9, 10, 11 and 12 reveal the response of the output variables (see section 2.3) to *cover*. The sensitivity is studied for each individual (ef1, ef2, ef3, ef4) and the overall effect. On the vertical axis the relative change ratio of each variable, as defined in equation 35, is presented. The approach does not provide information on the absolute values of the variables. Thus, the time and depth-averaged values of each variable for the three locations are given for the reference case (table 2). Additionally, the approach does not reveal the time and depth distribution of the variables. However, the reader may refer to the appendix for information on the yearly time series and the time averaged vertical profiles.

Table 2: *Time-depth averaged reference (cover = 0) values of the output variables for the three locations.*

	Oyster Grounds	Noordwijk	West Gabbard
I (mE/m^{2}s)	63	49	37
T (C^o)	10.1	11.8	11.2
U (m/s)	0.15	0.33	0.55
U_b (m/s)	0.1	0.19	0.33
$TMLd$ (m)	10.9	0.1	0.12
SSC (mg/m^3)	2150	9250	10500
H_s (m)	1.4	0.78	1.4
ν'_t (m^2/s)	2.1 10^{-2}	1.8 10^{-2}	4.6 10^{-2}
c_d (mg/cm^3)	58	132	61
c_f (mg/cm^3)	3.65	15	9.5
PP (mg/m^{2}day)	349	515	310

3.2.1 Oyster Grounds

In figure 9a the effect of the platforms on the depth-averaged current velocity U is presented for the location of Oyster Grounds. Effects ef2 and ef3 result in a decrease of the velocities. The response of U_b (figure 9b) is different. The bottom velocity decreases due to ef2, while ef3 may result even to a small increase for large values of *cover*. This is related with a suppression of the flow towards larger depth that follows ef3 of the PV installations (see figure 22a of appendix). Figure 9g shows the response of irradiance I. The effect of shadow (ef1) is the most prominent, resulting in nearly linear reduction of irradiance with increasing coverage. The changes due to

ef2, ef3 and ef4 are negligible. For suspended sediment concentration (SSC), figure 9c shows a strong decrease with decreasing wave height (ef4) (figure 9d). Effect ef1 results in an increase of SSC. This is due to the later stratification of the water column (see figure 18d of the appendix) that follows the decreased value of I (see equation 33). As the presence of the top mixed layer limits the concentration of suspended sediment near the surface, the reduced duration of stratification that follows ef1 induces an increase of the yearly averaged suspended sediment near the surface (see figure 18c of the appendix). The ef2 affects SSC through the decreased values of ${\nu'}_t$ (figure 9e), U_b and $TMLd$ (figure 9f). Smaller values of ${\nu'}_t$ result in less (upward) diffusion of SSC (equation 18) and thus increased settling rate. Smaller values of U_b result in less resuspension of SSC. However, decreased $TMLd$ results in an increase of SSC near the surface (for the stratification period) (see figure 20c and d of the appendix). Those factors have counteracting effects, resulting in small changes for the time-depth averaged values of SSC under ef2. Overall the coverage with PV installations leads to a decrease of suspended sediment. However, as mentioned this has no significant effects on irradiance. This can be explained by the value of the fraction of equation 32 which for typical values of SSC for the location of Oyster Grounds is ~ 1.55 (larger than unit). This indicates that light extinction due to suspended sediment is not important comparing to the background extinction for the location. Regarding temperature (figure 9h) it decreases mostly due to ef1. However, ef2 has a prominent effect as well. The earlier stratification that follows the reduction of wind stress results in an earlier and under colder conditions isolation of the bottom waters from the surface (see figure 20b and d of the appendix). This leads to lower values of the time-depth averaged temperature of the water column.

The relative change of diatom concentration with increasing coverage is given by figure 10a. The figure reveals a strong reduction of diatoms due to ef1. Moreover, the shift of their spring bloom towards the summer months is mentioned for ef1 (see figure 19a of the appendix). The ef2 results in a decrease of diatom concentration as well. This could follow the decreased temperature of the water column or a reduced availability of nutrients, however those are untested assumptions. Under ef2 the spring bloom of diatoms follows the earlier stratification of the region and occurs earlier in the year (see figure 21a of the appendix). For ef4 the diatom concentration is increasing, probably as a response to the reduction of suspended sediment, while for ef3 no significant changes are observed. Regarding the concentration of flagellates (figure 10b, it increases strongly due to ef1 and ef2. The different response of flagellates and diatoms to ef1 could be understood in terms of competition between species. As diatoms have the largest volume to surface ratio among the phytoplankton species, they need more light and nutrients in order to survive. Thus, diatoms are the first to be affected by the scarcity of light that follows a coverage of a fraction of the surface with PV-installations. As diatoms are the dominant species in the reference water column (table 2), the reduction of their concentration allows for a growth of the other phytoplankton species. Indeed, the behavior of the other species (picophytoplankton and dinoflagallates) is very similar to the one of flagellates (results not presented).

Primary production (figure 10c), follows mostly the reduction of diatoms. The reduction is mostly driven by ef1 however ef2 contributes as well. The over all reduction of primary production is stronger than the reduction due to ef1. Thus, for the location of Oyster Grounds it cannot be argued that effects ef2, ef3 and ef4 of the PV installations may compensate the impacts of ef1.

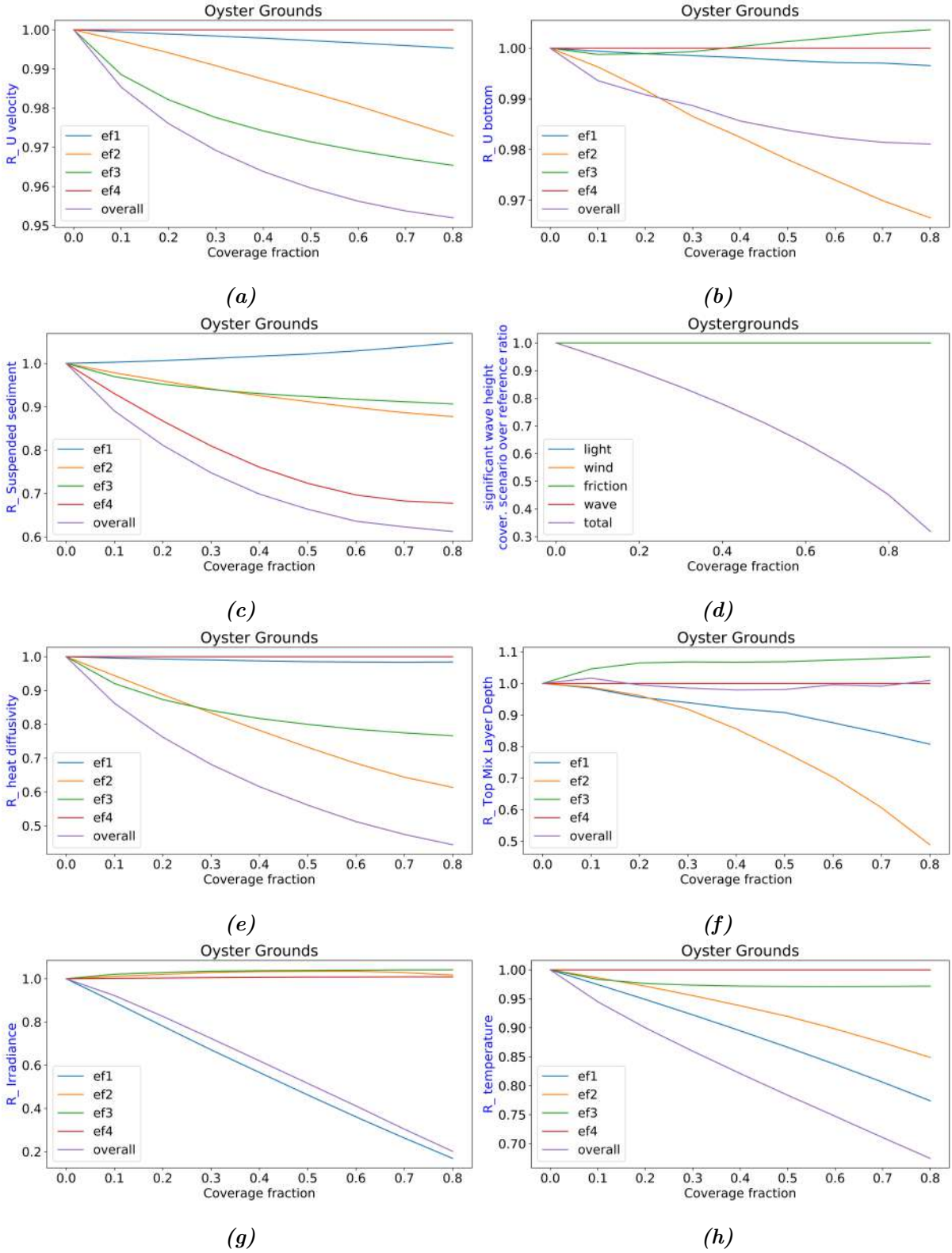

Figure 9: *Oyster Grounds: Relative change (see equation 35) of selected variables of the water column, with coverage. The results are presented for: depth-averaged current velocity (a), bottom current velocity (b), suspended sediment (c), wave height (d), eddy diffusivity(e), top mixed layer depth (f), irradiance (g) and temperature (h). The indication of the legend are: ef1: shadowing effect of the platforms,ef2: reduced wind stress, ef3: surface stress experienced by currents, due to friction with the platforms, ef4: reduced wave height, Overall: the overall effect of ef1, ef2, ef3, 3f4.*

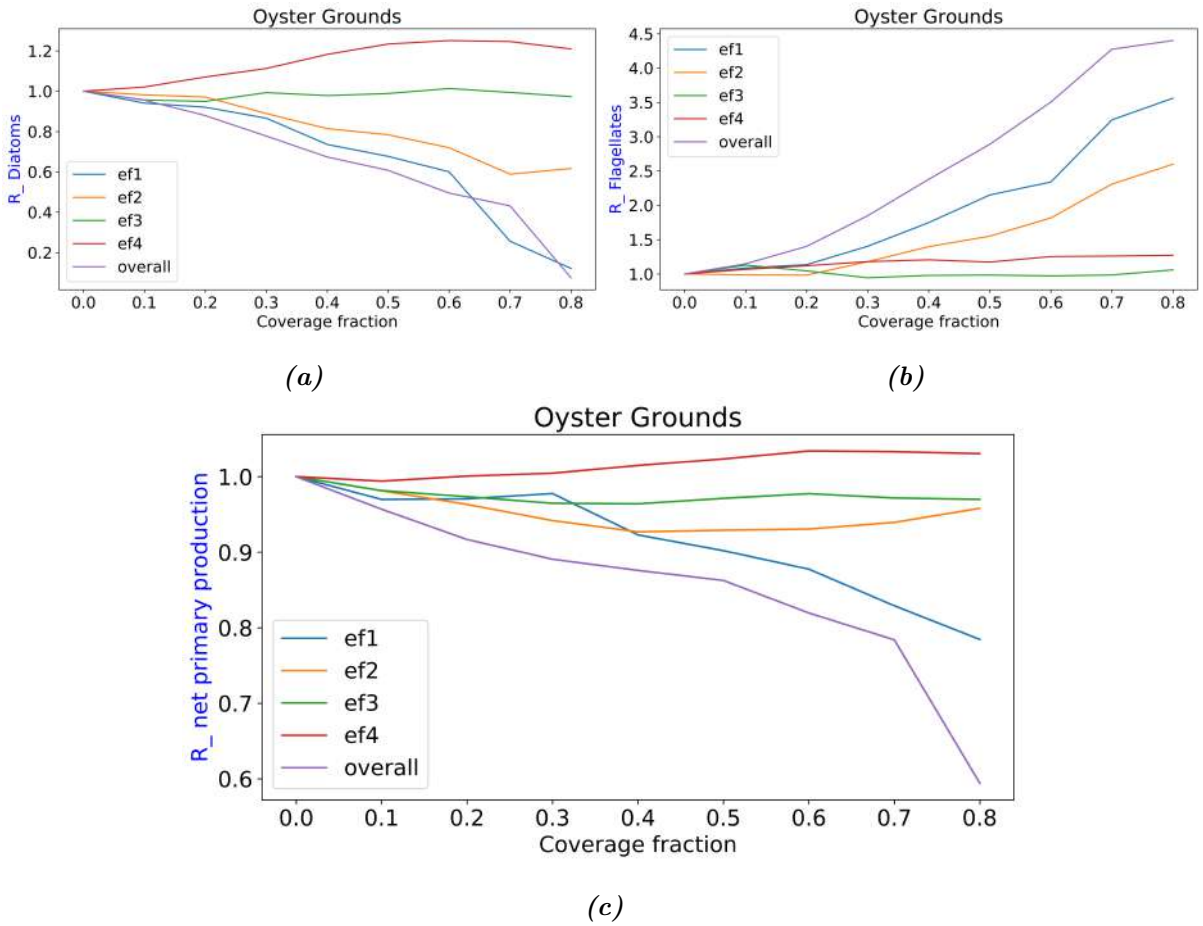

Figure 10: *Oyster Grounds: Relative change (see equation 35) of selected variables of the water column, with coverage. The results are presented for: diatom concentration (a), flagellate concentration (b), net-primary production (c). The indication of the legend are: ef1: shadowing effect of the platforms,ef2: reduced wind stress, ef3: surface stress experienced by currents, due to friction with the platforms, ef4: reduced wave height, Overall: the overall effect of ef1, ef2, ef3, 3f4.*

As mentioned, under ef1 the water column of Oyster Grounds stratifies later in the year. This leads to a shift of the spring bloom towards the summer months (see figure 19a of the appendix). On the other hand ef2 and ef3 result in an earlier stratification and an earlier occurrence of the spring bloom. The overall pattern of $TMLd$ follows ef2 and ef3 and results in an earlier stratification and consequently in an earlier spring bloom (at least for small percentages of coverage) (see figures 27a and 26d of the appendix). The effect of the later stratification that induces a later (during the sunnier summer months) spring bloom, is by its self a compensating effect for the reduced light availability. Thus, ef2 and ef3 that result in earlier stratification and spring bloom, enhances the impact of the PV installations on primary production.

3.2.2 Noordwijk - West Gabbard

Here the effects of the PV installations on the variables of depth-averaged current velocity, bottom current velocity, suspended sediment, significant wave height, eddy diffusivity, top mixed-layer depth , irradiance and temperature are presented only for the location of Noordwijk, as they were nearly identical between this location and West Gabbard. The reader may refer to figure 48 of the appendix for the plots of the above mentioned variables for the location

of West Gabbard. The ecological variables of diatom and flagellate concentration and primary production are presented for both locations in figure 12.

The main difference between the location of Oyster Grounds and Noordwijk relates with the fact that the water column of Oyster Grounds stratifies, while the water column of Noordwijk remains well mixed during the whole year. Due to the large values of the current velocities in the region the changes in the velocity regime are shaped by ef3. As a result, the time-depth averaged value of U is reduced (figure 11a), wile the velocity at the bottom increases due to the suppression of the flow towards larger depths (figure 11b) (see also figure 32a of the appendix).

The suspended sediment of the domain decreases (figure 11c). This is mainly a response to the decreased wave height (ef4) (figure 11d). The ef3 contributes to the reduction as well, especially for small fractions of coverage. The reduction due to ef3 cannot be explained by means of reduced resuspension, as bottom current velocity is increasing. Thus, it is a result of a decreased upward diffusion (see equation 18) due to the decreased value of ${\nu'}_t$ (figure 11e). Even if Noordwijk is a location that remains well mixed during the whole year, the model captures a small surface mixed layer ($\sim$ 0.5m) that forms during summer. Possibly as a response to increased turbulence near the surface, $TMLd$ under ef3 experiences a prominent increase of its depth for small percentages of coverage (figure 11f). The mechanisms behind the formation of this $TMLd$ and its enhancement mostly for the small percentages of coverage should not be considered as completely understood. As in the case of Oyster Grounds, the shadowing effects of the platforms (ef1) is the main driver for the changes on irradiance (I) (figure 11g). This leads to the decrease in temperature observed in figure 11h as well. The contribution of decreased suspended sediment on I is important only for the first percentages of coverage and under ef3 where an increase of I is observed (the decreased suspended sediment of ef4 occurs mainly at the bottom and thus does not result in any increase of I, see also 34b and c of the appendix). The reason for the decrease of I after 10% of coverage with ef3 relates to an increase of suspended sediment in the first meters of the water column (see figures 32c of the appendix). The minimum of SSC at surface for 10% of coverage (and maximum of I) coincides with a minimum of ${\nu'}_t$ for $cover$ =10% in the first $\sim$5 m of the water column (see figure 32f of the appendix).

For the location of Noordwijk similarly to the case of Oyster Grounds the concentration of diatoms reduces strongly due to ef1 (figures 12a). The ef2 and ef3 result in minor changes for diatoms, however ef4 results in a prominent increase of their concentration. In contrast to the case of Oyster Grounds, the shadowing effect of the platforms (ef1) results in a decrease of the flagellate concentration (figure 12b). A possible reason for this different behavior between the locations is the vertical distribution of the two species. In the case of Oyster Grounds diatoms are more abandoned in large depths (see figure 19a of the appendix). This way, the reduction of diatoms results in higher fluxes of nutrients towards the surface and thus towards flagellates. On the other hand, for the case of Noordwijk the two species are well mixed within the water column. This means that the effect of reduced irradiance would be more or less the same for both.

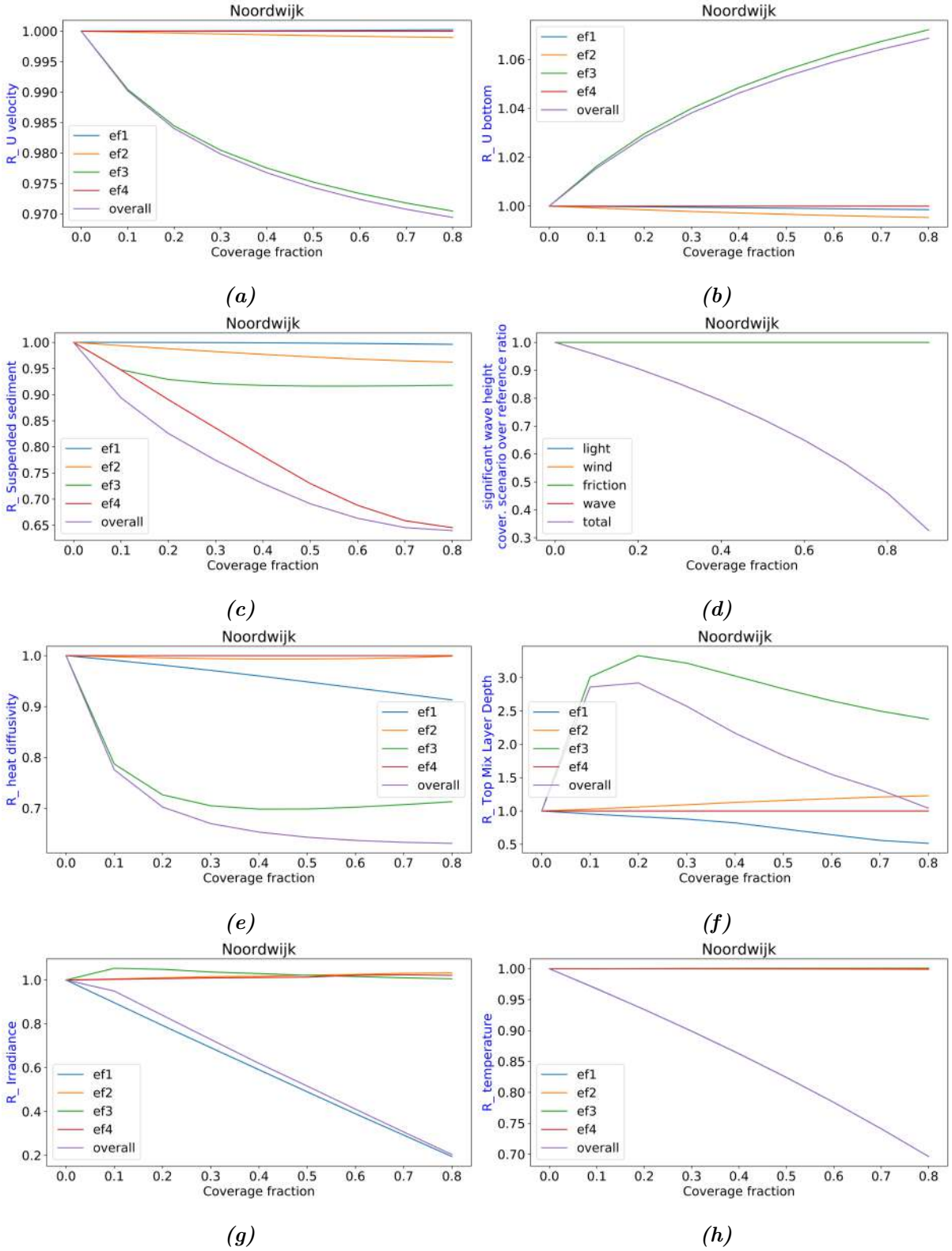

Figure 11: *Noordwijk: Relative change (see equation 35) of selected variables of the water column, with coverage. The results are presented for: depth-averaged current velocity (a), bottom current velocity (b), suspended sediment (c), wave height (d), eddy diffusivity(e), top mixed layer depth (f), irradiance (g) and temperature (h). The indication of the legend are: ef1: shadowing effect of the platforms,ef2: reduced wind stress, ef3: surface stress experienced by currents, due to friction with the platforms, ef4: reduced wave height, Overall: the overall effect of ef1, ef2, ef3, 3f4.*

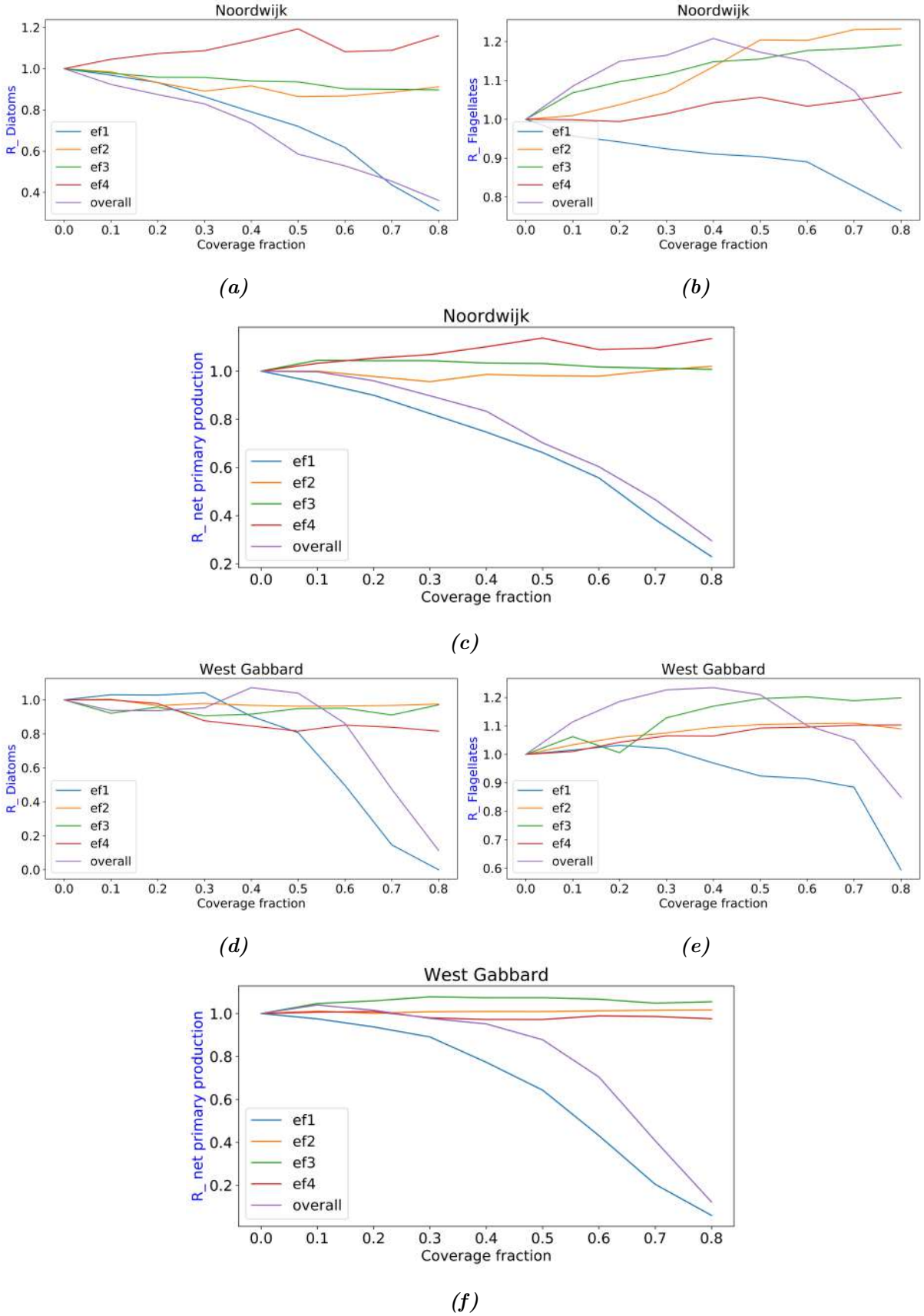

Figure 12: *Noordwijk (NW) and West Gabbard (WG): Relative change (see equation 35) of selected variables of the water column, with coverage. The results are presented for: diatom concentration at NW (a), flagellate concentration at NW (b), net-primary production at NW (c), diatom concentration at WG (d), flagellate concentration at WG (e), net-primary production at WG (f). The indication of the legend are: ef1: shadowing effect of the platforms,ef2: reduced wind stress, ef3: surface stress experienced by currents, due to friction with the platforms, ef4: reduced wave height, Overall: the overall effect of ef1, ef2, ef3, 3f4.*

Primary production follows mainly the patterns of diatoms (figure 12c). Again the shadowing effect (ef1) is the most important. However, for the case of Noordwijk ef1 is partly compensated by ef2, ef3 and ef4 as the overall effect is smaller than the ef1.

Similar to the case of Noordwijk, the water column of West Gabbard remains well mixed during the whole year. Moreover, the relative change of important hydrodynamic variables, as those presented in figure 11, are nearly identical between the two locations (see figure 48 of the appendix). Still, prominent differences are observed for their ecological variables.

Similarly to the other locations, the concentration of diatoms reduces due to the shadowing effect of the platforms (ef1) (figure 12d). However, this occurs only for *cover* >30%, revealing a resilience of the variable on ef1. In West Gabbard as in Noordwijk ef2 and ef3 result in minor changes for diatoms. Surprisingly, the effect of decreased wave height results in a decrease of diatom concentration. Waves in GOTM-ERSEM-BFM are considered only for resuspension purposes. As mentioned, the model accounts for the resuspension of detritus with a coupling between the variable and suspended sediment. Detritus then can be transformed to nutrients from the pelagic bacteria. The reduction of wave height that results in the reduction of suspended sediment, should lead to a decrease in the resuspension of detritus and thus decreased concentrations of nutrients within the pelagic ecosystem. Consequently, under certain condition the reduction of wave height could lead in a reduction of primary production, however this remains an assumption as it has not been tested explicitly. Similarly to the case of Noordwijk ef1 eventually leads in a decrease of the flagellate concentration (figure 12e), while ef3 results in a small increase. For primary production the shadowing effect (ef1) is again the dominant one 12f), however in this case it is strongly compensated by the effects of ef2, ef3 and ef4 and for small percentages of coverage even reversed.

The differences between the effects of the PV installations on the ecosystem of Noordwijk and West Gabbard, with more exceptional the resilience of the West Gabbard ecosystem to ef1, cannot be explained through the relative changes of the hydrographic variables as those are similar for both locations. Thus, the differences should relate to the great deviations between the reference states of the locations, from ecological as well as from hydrological perspective (table 2).

4 Discussion

4.1 Potential impacts of a solar power plant

In order to examine the potential impacts of a solar power plant with a 1D model, firstly it is necessary to define the percentage of coverage that the power plant would occupy. This is an arbitrary approach for a 1D model and thus should be interpreted accordingly. According to the plans of OOE individual solar power plants would cover an area of 100 m × 100 m (10^4 m^2). Assuming that the 1D model is approximately resolving a domain with the size of 1 km × 1 km (∼ size of 1 greed cell for a local fine-resolution 3D model), an area of 10^4 m^2 would translates to 1% of the 1D domain. Hence the scenario of 10% coverage is indicative of a case where a number of PV power plants are installed at close distances. Thus, RQ3 is addressed taking in to account the relative change of primary production under the scenario of *cov* =10% (figure 13c). In order to understand better the response of primary production the relative change under *cov* =10% is given for the variables of suspended sediment and irradiance as well (figures 13a 13b).

Overall, for *cover* =10% the depth-averaged suspended sediment (SSC) of the three locations is reduced by ∼-10% (figure 13a). This is mostly due to ef3 and ef4, however ef2 contributes as well. A small increase of SSC is observed for the location of Oystergrounds under ef1. This is due to the reduced duration of stratification that allows for more sediment to penetrate near the surface. The depth-averaged irradiance is reduced by ∼-0.5% (figure 13b). The effect of shadow (ef1) is compensated mostly by ef3 which decreases SSC near the surface, while ef4 results in a decrease of SSC only in larger depths not affecting this way the light availability of the domain. Moreover, the increase due to ef3 is larger when the value of the ratio of equation 32 is smaller (∼0.3 for West Gabbard, ∼0.55 for Noordwijk, ∼1.5 for Oyster Grounds). The ratio of equation 32 indicates the importance of suspended sediment for the extinction of light and is proportional to $1/SSC$. This means that locations with larger concentrations of suspended sediment experience a larger increase of irradiance due to decreased turbidity, partly compensating this way the effect of shadow (ef1).

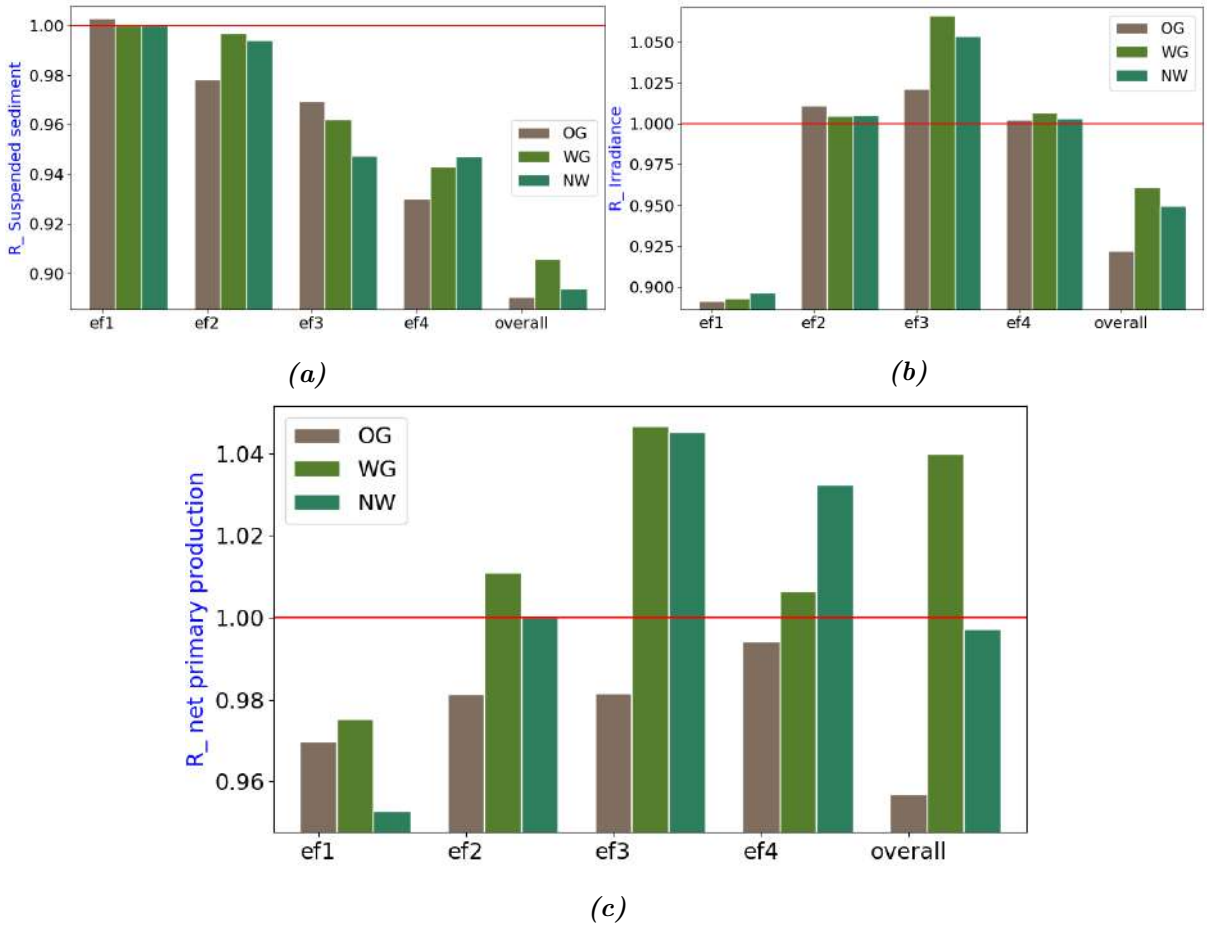

Figure 13: *Relative change (see equation 35) of suspended sediment (a), irradiance (b) and primary production (c), at the different locations of the North Sea, for 10% of coverage under the different effects of the PV installations. The indication are: ef1: shadowing effect of the platforms,ef2: reduced wind stress, ef3: surface stress experienced by currents, due to friction with the platforms, ef4: reduced wave height, Overall: the overall effect of ef1, ef2, ef3, ef4. With OG, WG and NW the locations of Oyster Grounds, West Gabbard and Noordwijk are mentioned. The red line indicates no relative change*

The overall behavior of primary production is different for each location. For the location of Oyster Grounds (figure 13c) it decreases by -4.5%. In this case, all individual effects add

to the reduction of primary production. The reduction due to ef2 and ef3 should relate with the earlier stratification of the location, while the reduction due to ef4 could relate with a reduced resuspension of detritus (not tested explicitly). For the location of Noordwijk primary production remains fairly constant -0.3%. This is due to the compensating effects of ef3 and ef4 to the shadowing effect of the platforms. The increase of primary production for the location of West Gabbard, for 10% of coverage with PV installations is a striking result and should be treated carefully. The limitations of the present approach (see section 4.4) do not allow for conclusions in terms of exact numbers and results should only be treated qualitatively. This increase is attributed to two factors. Firstly, as it has been mentioned the ecosystem variables of West Gabbard are characterized by a resilience on ef1. This is shown by the small reduction, comparing to Noordwijk, of primary production under the effect. This cannot be explained by the present study and more research is essential. Secondly, primary production in West Gabbard (as in Noordwijk) responds to the increase of irradiance, observed for small values of coverage under ef3.

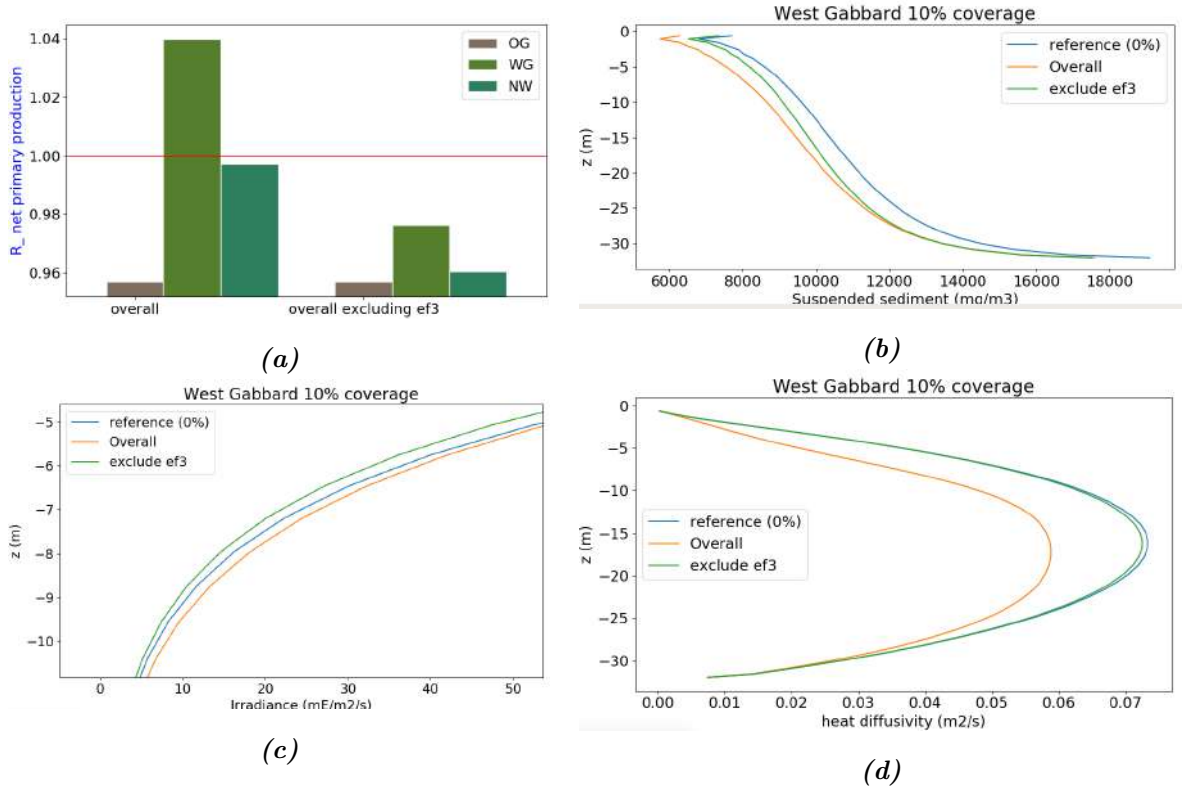

Figure 14: *Panel a. Relative change (see equation 35) of primary production for cover =10% under the overall effect and the overall excluding ef3 for the three locations. Panel b,c and d. Location of West Gabbard, comparison of the overall run and the overall excluding ef3 with reference, for the: b) Time averaged vertical profiles of suspended sediment, c) time averaged vertical profiles of irradiance (middle of the water column), d) time averaged vertical profiles of eddy diffusivity, for the cover =10% scenario.*

In order to further investigate the contribution of ef3, the overall effect excluding ef3 is presented. The comparison between the relative change of the two scenarios for *cover* =10% is shown in figure 14a. The figure shows much lower values of primary production for the case where ef3 is not taken in to account, indicating that ef3 is the most important compensating effect for small percentages of coverage. This is because ef3 results in a decrease of suspended sediment near the surface (figure 14b) which leads to an increase of irradiance at middle

depths of the water column (figure 14c) and eventually to an increase of primary production. The decrease concentration of suspended sediment is related with the strong decrease of eddy diffusivity (ν'_t) that results from ef3 (figure 14d).

Thus, for RQ3, it is concluded that a favorable location for the installation of a solar power plant would be characterized by high current velocities and high concentration of suspended sediment (SSC) near the surface. This is due to the compensating effect of decreased near surface SSC that follows the reduced current velocities, on the shadowing effect of the platforms. It is stressed that the above statement is restricted from the assumption that a solar power plant will not cover more than 20% of the domain. This is shown by the relative change of primary production with coverage for the three locations (figure 15a). Here, it is clear that for larger percentages of coverage other processes seem to interfere, enhancing the impact of the PV installations on primary production for locations like Noordwijk and West Gabbard. Thus, more research is needed on the topic.

4.2 Comparison with existing literature

As discussed in section 1, the effects of the platforms on aquatic ecosystem have been discussed mainly for inshore environments (Santafe et al. [2014] ; Sahu et al. [2016] ; da Silva and Branco [2018]), denoting the decrease of evaporation and limitation of algal growth due to the shadowing effect of the platforms. Still, no specific numbers are given for the latter effect. However, the shadowing effect of the PV installations should be similar to the one of the artificial floating islands (AFI) presented in Nakamura and Mueller [2008]. In figure 3 the results of this work are presented, for an experimental test cell with surface 24 m^2 and depth: 2 m. The results take in to account the overall effect of AFIs (shadow and nutrient uptake). However, the importance of the individual effects was explicitly tested and the effect of shadow was the dominant one (see figure 17a of the appendix). Figure 15b shows the results of GOTM-ERSEM-BFM for the relative change of chlorophyll a at the locations of Oyster Grounds, West Gabbard and Noordwijk. A comparison with figure 3 suggests that the effect of the PV-installations on the ecosystem of offshore locations is completely different, resulting to less significant changes compering to those presented by Nakamura and Mueller [2008].

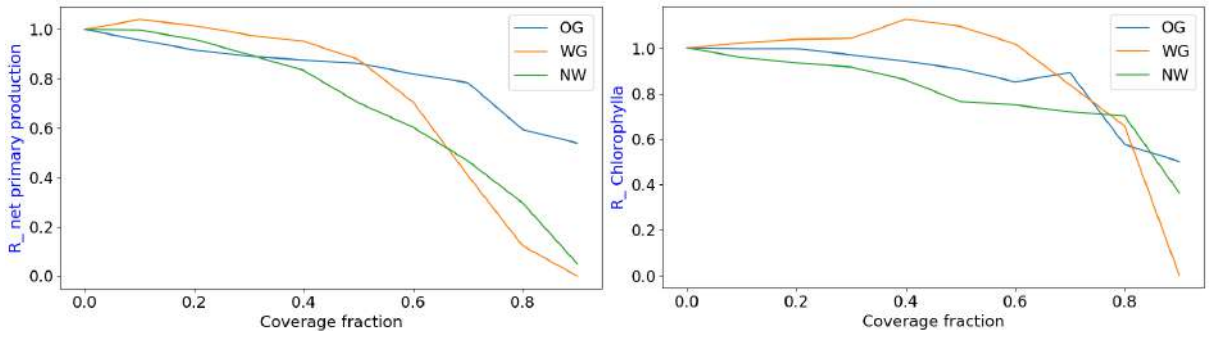

(a) *(b)*

Figure 15: *Relative change (see equation 35) of primary production (a) and chlorophyll a (b) with increasing coverage under the overall effect of the PV installations for the three locations.*

Here the differences between the experiments need to be taken in to account. Firstly, for figure 3 even if the effect of shadow is the dominant one, the effect of nutrient uptake should

enhance the decrease of chlorophyll a. Secondly, an experimental approach with test cells (see figure 17b of the appendix) like the one used from Nakamura and Mueller [2008] is completely different from a modeling approach for real marine environments. A difference should relate with the absence of suspended sediment within the cells. Moreover, the small depth (2 m) of the test cells could be an important reason for the strong decrease of chlorophyll a observed in figure 3. Due to the conical shape of a platforms shade in three dimensions, the percentage of water volume remaining permanently under shadow due to the presence of a platform increases with decreasing total depth. Thus, the impact due to the shadow of floating platforms on the ecosystem is expected larger for small values of the total depth.

4.3 Expectations for the near future

Current IPCC estimates infer an accelerated sea level rise for the near future (IPCC [2018]). The increased sea level will induce substantial alterations to the tidal characteristics of the European continental shelf, with prominent tidal amplitude increases and decreases for different locations (Pickering et al. [2012]). Moreover, changes in future North Atlantic weather systems will induce a reduction ($\sim$0.2 m) of mean significant wave height for the region. According to Holt et al. [2018] "a shutdown of the exchange between the Atlantic and the North Sea and a substantial decrease in the circulation of the North Sea in the second half of the 21st century" is expected. Subsequently, the sea will become more estuarine with increased risk of coastal eutrophication (Holt et al. [2018]). Concluding, the effects of solar power plants on the ecosystem of the North Sea could be completely different in the near future. Thus, today's ideal locations for the installations are not the ideal locations of tomorrow.

4.4 Limitations of the approach

The limitations of a 1D model approach related with the potential importance of advection for real marine environments have been addressed in section 1. Additionally to that, a 1D model approach requires assumptions as the linear dependence of certain variables on coverage (see equations 25, 26 28, 31), that has been used in the present study. This approach neglects phenomena as the non linear interactions between waves (de León et al. [2011]) and do not allow for a realistic representation of the structure of a solar power plant, the characteristics of which (eg. distance between platforms) could result in significant difference for the response of the ecosystem. The inadequacy of the approach for wave height reduction by means of decreased fetch has been discussed in section 2.2.4. Additionally to that, the implementation of waves in GOTM-ERSEM-BFM poses limitations for a realistic representation of ef4. As discussed, waves in the model are taken in to account only from the ERSEM-BFM for resuspension purposes. GOTM ignores their existence and thus waves do not feed into the calculations of turbulence. So ν_t and ${\nu'}_t$ for the model do not depend on wave height, while in reality this is not the case. It was evident from the study that the reduction of current velocity through the reduction of ${\nu'}_t$ resulted in a decrease of SSC near the surface, thus it is rational to assume that a further reduction of ${\nu'}_t$ due to reduced wave height will result in even less suspended sediment near the surface and further increase of primary production.

As mentioned, the model resulted in unrealistic values for phaeocystis concentrations and thus phaeocystis was excluded from the calculations. Normally phaeocystis blooms occur every several years depending on the availability of nutrients. However, in several locations e.g. the region of Noordwijk the frequency of phaeocystis blooming is enhanced due to the constant input of nutrients from the river Rhine Riegmann et al. [1991]. Advection of nutrients or of any other tracer is a process not resolved by a 1D column model. The model runs resulted in an interanual

variability of the ecological variables which was not capture by the observations. This variability was related with occasional blooms of phaeocystis present in the model, while in reality phaeocystis may bloom every year for locations with input of nutrients. Thus, the inadequacy of a 1D model to resolve phaeocystis at locations were advection of nutrients is important is an other limitation.

4.5 Further work

The realistic effects of the PV installations on the marine ecosystem should be expected as different from the presented once in several ways. Some of them have been discussed in section 4.4. Additionally, it is mentioned that due to their great amount the results were mainly studied under long time and depth-averaged values. This is a procedure that could disregard important information of more local scale. Moreover, the results addressed the effects of the PV installations at three locations in the North Sea. Even if the response for locations with similar characteristics (Noordwijk, West Gabbard) were comparable, the differences in the response of the ecosystem variables indicate that model runs for new locations could add valuable information. Furthermore, the model runs addressed a limited amount of coverage scenarios. However, the results for low values of coverage indicated interesting effects of the PV installations. As those values are more essential for a scenario of power plant installation, new runs focused on smaller values of coverage could be considered. Finally, the study did consider the sustainability of a marine ecosystem only in terms of primary production. However, from the results disturbances of the balance between species were indicated. The results showed a different response of diatoms and flagellates on the effects of PV installations and even if those differences were not prominent for low values of coverage, still they should be addressed. For those reasons more research is needed on the topic. This could include:

1) Calibration and reference-coverage scenario runs of the 1D model for new location.

2) New runs of the 1D model, focused around lower values of coverage.

3) New coverage scenario runs of the 1D model for varying values of certain variables that have been considered as important (eg: water dept, current velocity, porosity of bed, detritus), in order to quantify how the effects of the PV installations on the ecosystem depend on their value.

4) Examination of the effects of the PV installation with monthly or daily time intervals.

5) Quantification of the effects of the PV installations on the balance between different species.

6) Examination of the effects of the PV installations with a local fine-resolution 3D model that would be nested to a coarser grid model and it would include phaeocystis and a more realistic implementation of waves that would feed in to the calculations of turbulence.

5 Conclusions

The following effects of the PV installations on the hydrodynamics and the ecosystem of the North Sea have been analyzed: **ef1:** decreased light conditions due to the shadowing effect of the platforms, **ef2:** reduced wind stress due to the limitation of the free surface of the water column, **ef3:** introduction of an additional surface stress experienced by currents, due to friction induced by the platforms, **ef4:** Reduced wave height due to the presence of the platforms.

The experiments were conducted for three different locations in the North Sea (Oyster Grounds, West Gabbard, Noordwijk). The location of Oyster Grounds should be representative of the poor in nutrients, open-sea regions with low current velocities and seasonal stratification. The locations of West Gabbard and Noordwijk should be representative of the nutrient enriched, shallow near coast regions, with high current velocities that remain well mixed during the whole year. The following three research questions were addressed.

RQ1) What is the skill of a 1D vertical column model to reproduce observed data of ecological variables (chlorophyll a, nutrients) for different locations of the North Sea?

The 1D model was proved to be efficient in the calculations of basic ecosystem variables as chlorophyll a, nitrate and silicate. The calibration was considered as more efficient in the location of Oyster Grounds, where advection of tracers is of less importance and phaeocystis blooming not prominent. For the case of Noordwijk, where advection and phaeocystis blooming were of greater importance, the agreement between model and observations was less good.

RQ2) What is the overall effect of the PV installations on the hydrography and ecosystem at different locations in the North Sea and what is the relative importance of the individual effects? Under which circumstances can it be argued that the effects ef2, ef3 and ef4 could compensate the impact of ef1 on the ecosystem?

Regarding the effects of the platforms on the ecosystem, the shadowing effect (ef1) was usually the most important. For Oystergrounds, a location characterized by seasonal stratification, ef2, ef3 and ef4 did not result in a compensation of ef1, on the contrary they deteriorate the impact. For the well mixed locations of Noordwijk and West Gabbard, ef2, ef3 and ef4 indeed were compensating ef1 in an extent, while for small percentages of coverage ef3 could be of comparable importance with ef1, resulting in no significant impact of the overall effect.

RQ3) Which location characteristics would be favorable for the implementation of PV power plants in terms of ecosystem response?

Overall, assuming that a PV power plant will not occupy more than 20% of the 1D domain, locations of the second type (Noordwijk, West Gabbard) are more favorable in terms of ecosystem response for the installation of solar power plants. This is mostly because well mixed locations with high current velocities and high concentration of suspended sediment (SSC) experience a decrease of near surface SSC due to decreased upward diffusion. This leads to higher light availability for the subsurface layers and compensates partly the effect of shadow.

Bibliography

J.W. Baretta, Ebenhof W., and Ruardij P. The European regional seas ecosystem model, a complex marine ecosystem model. *Netherlands Journal of Sea Research*, 33(3/4):233–246, 1995. doi: 10.1016/0077-7579(95)90047-0.

M. Blaas and H. de Swart. Vertical structure of residual slope circulation driven by JEBAR and tides: an idealised model. *Continental Shelf Research*, 22(2002):2687–2706, 2002. URL https://doi.org/10.1016/S0278-4343(02)00121-8.

H. Burchard. Recalculation of surface slopes as forcing for numerical water column models of tidal flow. *Applied Mathematical Modeling*, 23:737–755, 1999. URL https://doi.org/10.1016S0307-904X(99)00008-6.

H. Burchard, K. Bolding, M.R. Villarreal, European Commission. Joint Research Centre, and Space Applications Institute. *GOTM, a General Ocean Turbulence Model: Theory, Implementation and Test Cases*. EUR / European Commission. Space Applications Institute, 1999. URL https://books.google.nl/books?id=zsJUHAAACAAJ.

H. Burchard, Strips A., Eifler W., Bolding K., and Villarreal M. Numerical Simulation of Dissipation Measurements in Non-Stratified and Strongly Stratified Estuaries. pages 1–18, 2000.

H. Burchard, Bolding K., Kuhn W., Meister A., Neumann T., and Umlauf L. Description of a flexible and extendable physical–biogeochemical model system for the water column. *Journal of Marine Systems*, 61:180–211, 2006. URL https://doi.org/10.1016/j.jmarsys.2005.04.011.

J.P. Coelingh, Wijk A.J., and Holtslag A.A. Analysis of wind speed observations over the North Sea. *Journal of Wind Engineering and Industrial Aerodynamics*, 61:51–69, 1996. URL https://doi.org/10.1016/0167-6105(96)00043-8.

G.D. da Silva and D.A. Branco. Is floating photovoltaic better than conventional photovoltaic? Assessing environmental impacts. *Impact Assessment and Project Appraisal*, 2018. doi: 10.1080/14615517.2018.1477498.

S.P. de León, Bettencourt J.H., and Kjerstad J. Simulation of irregular waves in an offshore wind farm with a spectral wave model. *Continental Shelf Research*, 31:1541–1557, 2011. doi: https://doi.org/10.1016/j.csr.2011.07.003.

B. Galperin, Kantha L.H., Hassid S., and Rosati A. A Quasi-equilibrium Turbulent Energy Model for Geophysical Flows. 1988. URL https://doi.org/10.1175/1520-0469(1988)045<0055:AQETEM>2.0.CO;2.

R.J. Geider, H.L. MacIntyre, and T.M. Kana. Dynamic model of phytoplankton growth and acclimation: responses of the balanced growth rate and the chlorophyll a:carbon ratio to light, nutrient-limitation and temperature. *Marine Ecology Progress Series*, 148:187–200, 1997. doi: 10.3354/meps148187.

A.E. Hill, Brown J., Fernand L., Holt J., Horsburgh K.J. an Proctor R., Raine R., and Turrell W.R. Thermohaline circulation of shallow tidal seas. *Geophysical Research Letters.*, 35, 2008. URL `https://doi.org/10.1029/2008GL033459`.

J. Holt, J. Polton, J. Huthnance, S. Wakelin, E. ODea, J. Harle, A. Yool, Y. Artioli, J.Blackford, J. Siddorn, and M. Inall. Climate-Driven Change in the North Atlantic and Arctic Oceans Can Greatly Reduce the Circulation of the North Sea. *Geophysical Research Letters*, 45(21): 11,827–11,836, 2018. doi: 10.1029/2018GL078878.

J.R. Hunter and J.H. Simpsons. Fronts in the Irish Sea. *Nature*, 250:404–406, 1974. doi: 10.1038/250404a0. URL `https://doi.org/10.1038/250404a0`.

IMSA. *Ecosystems associated with North Sea oil and gas facilities and the impact of decommissioning options*. IMSA Amsterdam, 2011.

IPCC. *Global Warming of* 1.5^oC. Intergovernmental Panel on Climate Change., 2018.

J. Kondo. Air-sea bulk transfer coefficients in diabatic conditions. *Boundary-Layer Meteorology*, 9:91–112, 1975. doi: 10.1007/BF00232256.

K. Nakamura and G. Mueller. Review of the performance of the artificial floating island as a restoration tool for aquatic environments. *World Environmental and Water Resources Congress*, 2008. doi: 10.1061/40976(316)276.

J. Nauw, de Haas H., and Rehder G. A review of oceanographic and meteorological controls on the North Sea circulation and hydrodynamics with a view to the fate of North Sea methane from well site 22/4b and other seabed sources. *Marine and Petroleum Geology*, 68(2015): 861–882, 2015. URL `http://dx.doi.org/10.1016/j.marpetgeo.2015.08.007`.

P. Nejata, Jomehzadeha F., MahdiTaherib M., Goharic M., Zaimi M., and Majidd A. A global review of energy consumption, CO2 emissions and policy in the residential sector (with an overview of the top ten CO2 emitting countries). *Renewable and Sustainable Energy Reviews*, 43:843–862, 2015. URL `https://doi.org/10.1016/j.rser.2014.11.066`.

N.G.Jerlov. *Marine Optics*. Number 14. Elsevier Oceanography Series, 1976.

L. Otto, Zimmermann J., Furnes G., Mork M., Saetre S., and Becker G. Review of Physical Oceanography of the North Sea. *Netherlands Journal of Sea Research*, 26:161–238, 1990. URL `https://doi.org/10.1016/0077-7579(90)90091-T`.

S.C. Painter, Lapworth D.J., Woodward M.S., Kroeger S., Evanse C.D., Mayor D.J., and Sanders R.J. Terrestrial dissolved organic matter distribution in the North Sea. *Science of the Total Environment*, 630:630–647, 2018. URL `https://doi.org/10.1016/j.scitotenv.2018.02.237`.

C. Paulson and J. Simpson. Irradiance measurements in upper ocean. *Journal of Physical Oceanography*, 7:952–956, 1977. URL `https://doi.org/10.1175/1520-0485(1977)007<0952:IMITUO>2.0.CO;2`.

M.D. Pickering, Wells N.C., Horsburgh K.J., and Green J.A.M. The impact of future sea-level rise on the European Shelf tides. *Continental Shelf Research*, 35:1–15, 2012. URL https://doi.org/10.1016/j.csr.2011.11.011.

R.D. Pingree, Holligan P.M., and Mardell G.T. The effects of vertical stability on phytoplankton distributions in the summer on the northwest European Shelf. *Deep-Sea Research*, 25:111–128, 1978. URL https://doi.org/10.1016/0146-6291(78)90584-2.

P.C. Reid, Lancelot C., Gieskes W.W., Hagmeier E., and Weichart G. Phytoplankton of the North Sea and its Dynamics: A review. *Netherlands Journal of Sea Research.*, 26:295–331, 2016. URL https://doi.org10.1016/0077-7579(90)90094-W.

R. Riegmann, Noordeloos A., and Cadee G. Phaeocystis blooms and eutrophication of the continental coastal zones of the North Sea. *Marine Biology*, 112:479–484, 1991. URL https://doi.org/10.1007/BF00356293.

A. Rosati and K. Miyakoda. A General Circulation Model for Upper Ocean Simulation. *Journal of Physical Oceanography*, 18:1601–1626, 1988. doi: 10.1175/1520-0485(1988)018<1601:AGCMFU>2.0.CO;2.

A. Sahu, Yadavb N., and Sudhakarc K. Floating photovoltaic power plant: A review. *Renewable and Sustainable Energy Reviews*, 66:815–824, 2016. doi: https://doi.org/10.1016/j.rser.2016.08.051.

M.R. Santafe, Bautista J. Soler T., Javier F. Romero S., Pablo S. Gisbert F., Javier J., Gozálvez F., and Carlos M. Gisbert F. Theoretical and experimental analysis of a floating photovoltaic cover for water irrigation reservoirs. *Energy*, 67:246–255, 2014. URL https://doi.org/10.1016/j.energy.2014.01.083.

J. Sundermann and T. Pohlmann. A brief analysis of North Sea physics. *Oceanologia*, 53(3):663–689, 2011. URL https://doi.org/10.5697/oc.53-3.663.

H.U. Sverdrup. On Conditions for the Vernal Blooming of Phytoplankton. *Journal of Marine Science*, 18(3):287–295, 1953. URL https://doi.org/10.1093/icesjms/18.3.287.

P. Tett, Gowen R., Mills D, Fernandes T., Gilpin L., Huxham M., Kennington K., Read P., Servise P., Wilkinson M., and Malcom M. Defining and detecting undesirable disturbance in the context of marine eutrophication. *Marine Pollution Bulletin*, 55:282–297, 2007. URL https://doi.org/10.1016/j.marpolbul.2006.08.028.

S.B. Tijssen and F.J. Wetsteyn. Hydrographic observations near a subsurface drifter in the Oyster Ground, North Sea. *Netherlands Journal of Sea Research*, 18:1–12, 1984. URL https://doi.org10.1016/0077-7579(84)90021-8.

L. Umlauf, H. Burchard, and K. Bolding. *GOTM - Scientific Documentation Version 3.2.* Number 63. Institut fur Ostseeforschung Warnemund, 2005.

J. van der Molen and H. de Swart. Holocene wave conditions and wave-induced sand transport in the southern North Sea. *Continental Shelf Research*, 21(2001):1723–1749, 2001. doi: 10.1016/S0278-4343(01)00018-8.

J. van der Molen, Smith H., Lepper P., Limpenny S., and Rees J. Predicting the large-scale consequences of offshore wind array development on a North Sea ecosystem. *Continental shelf research*, 85:60–72, 2014. doi: 10.1016/j.csr.2014.05.018.

J. van der Molen, Ruardij P., and Greenwood N. Potential environmental impact of tidal energy extraction in the Pentland Firth at large spatial scales: results of a biogeochemical model. *Biogeosciences*, 13:2593–2609, 2016. doi: 10.5194/bg-13-2593-2016.

J. van der Molen, Ruardij P., and Greenwood N. A 3D SPM model for biogeochemical modeling with application to the north- west European continental shelf. *Journal of Sea Research*, 127 (2017):63–81, 2017. doi: 10.1016/j.seares.2016.12.003.

M. Vichi, N. Pinardiand, and S. Masina. A generalized model of pelagic biogeochemistry for the global ocean ecosystem. Part I: Theory. *Journal of Marine Systems*, 64(2007):89–109, 2006. URL `https://doi.org/10.1016/j.jmarsys.2006.03.006`.

R.A. Watson, Green B.S., Tracey S.R., Farmery A., and T.J. Pitcher. Provenance of global seafood. *Fish and Fisheries*, 17:585–595, 2016. URL `https://doi.org/10.1111/faf.12129`.

R. Weisse and H. Gunther. Wave climate and long-term changes for the Southern North Sea obtained from a high-resolution hindcast 1958 – 2002. *Ocean Dynamics.*, 57:167–172, 2007. doi: 0.1007/s10236-006-0094-x.

L.P. Wetsteyn and J.C. Kromkamp. Turbidity, nutrients and phytoplankton primary production in the Oosterschelde (The Netherlads) before, during and after a large-scale coastal engineering project (1980-1990). *Hydrobiologia*, 282:61–78, 1994. URL `https://doi.org/10.1007/BF00024622`.

6 Appendix

6.1 Additional figures for the North Sea

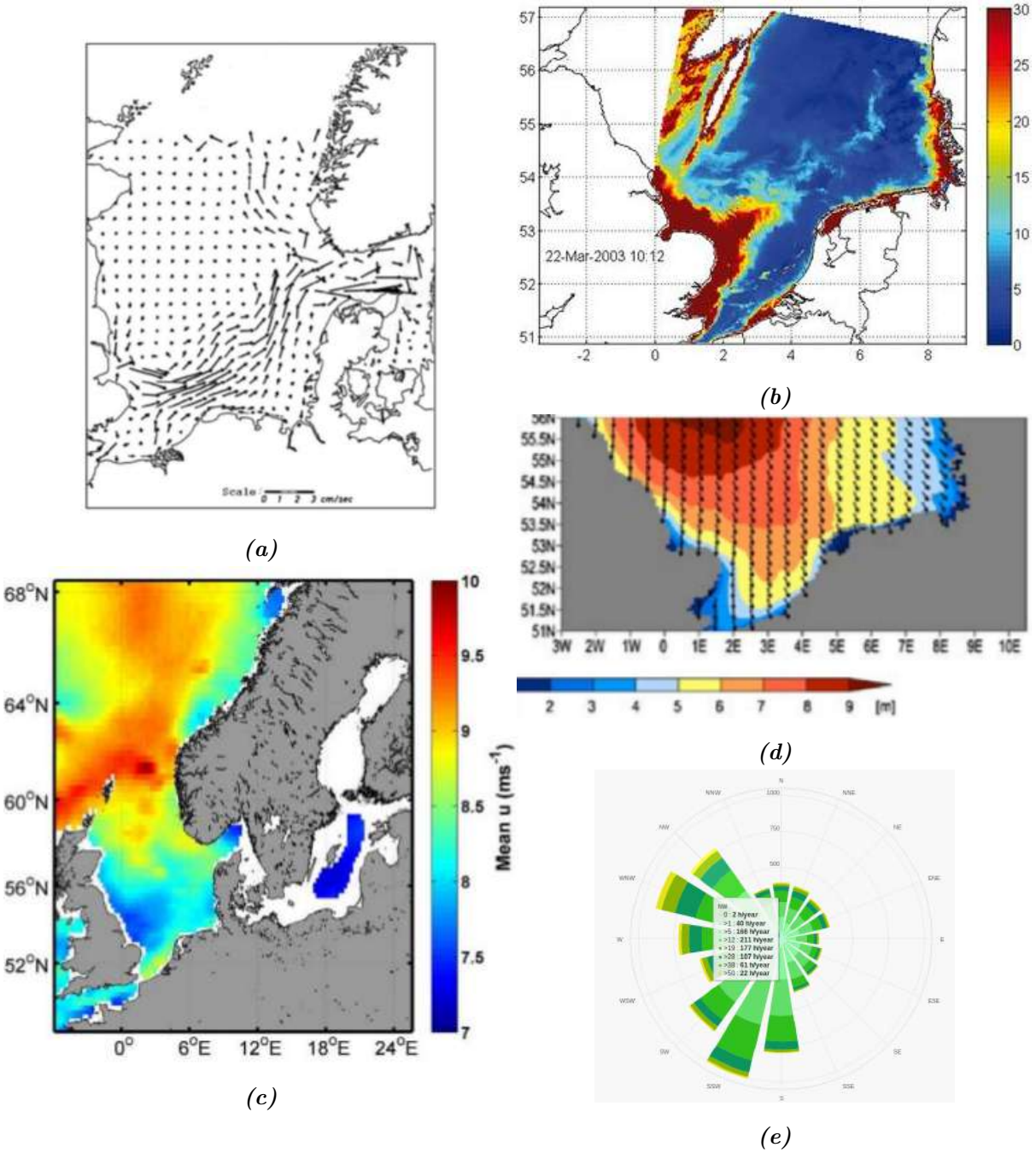

(a)

(b)

(c)

(d)

(e)

Figure 16: *Panel a) Residual circulation induced by the M2 tide (Brettschneider, 1967). Figure reprinted from Nauw et al. [2015]. Panel b) SPM surface concentrations in mg/l, as derived from a MERIS satellite scene, on March 22nd 2003 (?). Panel c) Wind climate (1999-2009) at 10 m for the North Sea from altimetry data (QuiqSCAT). http : //bibliotheek.knmi.nl/knmipubTR/TR342.pdf . Panel d) Significant wave heigth and mean wave direction averaged over 1958-2002. Results from WAM model (Weisse and Gunther [2007]). Panel e) The wind rose for North Sea. Shows how many hours per year the wind blows from the indicated direction https : //www.meteoblue.com/en/weather/forecast/modelclimate/north − sea$_u$nited − states − of − america$_5$129210.*

6.2 Additional figures for artificial floating islands

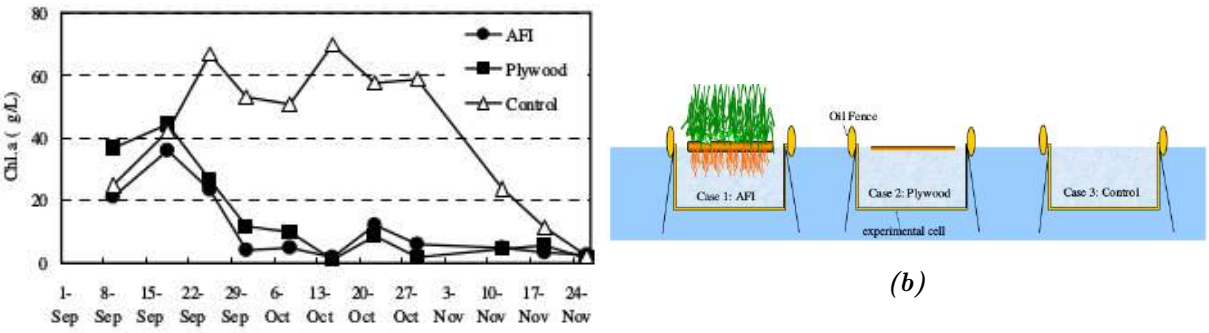

(a) *(b)*

Figure 17: *a) Figure denoting the small differences between chlorophyll under the effect of an artificial floating island (shade and nutrient uptake) and the effect of floating plywood (shade only). b) Representation of the experimental cells from the study of Nakamura and Mueller [2008]*

6.3 Additional figure for Oyster Grounds

Effect of light reduction

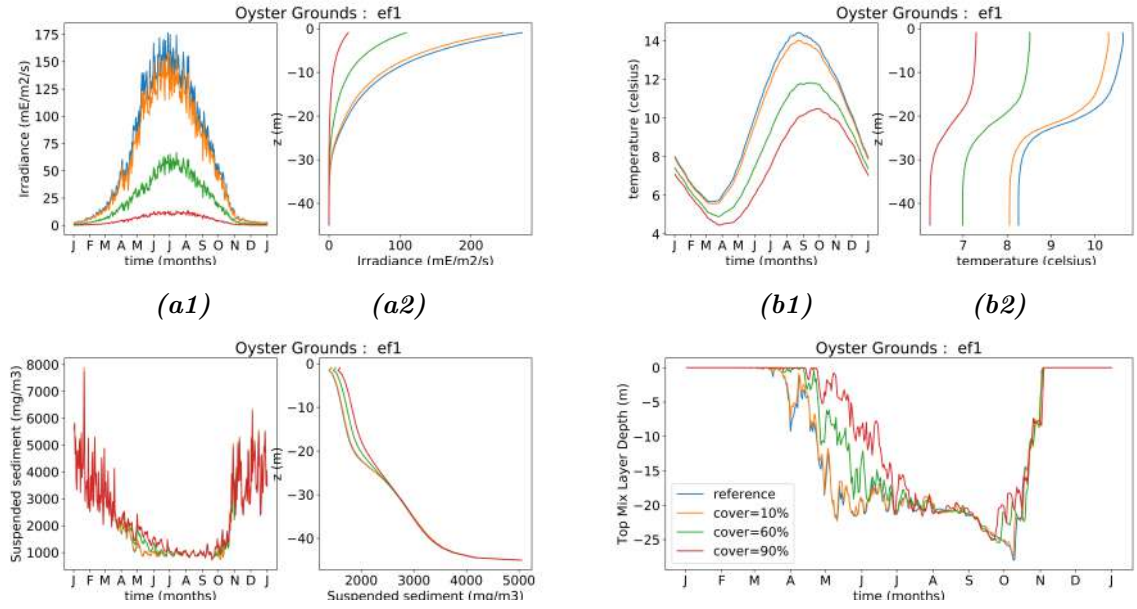

(a1) *(a2)* *(b1)* *(b2)* *(c1)* *(c2)* *(d)*

Figure 18: *Station of Oyster Grounds, effect of light reduction on selected hydrographic variables (averaged over 1980-2008): Yearly time series averaged over depth (a1, b1, c1, d) and time averaged profiles (a2, b2, c2) of, irradiance (a), temperature (b) and suspended sediment (c). In panel (d) the yearly time series of the top mixed layer depth are presented. The results are presented for different scenarios of coverage (reference: 0%, scenario 1: 10%, scenario 2: 60%, scenario 3: 90%)*

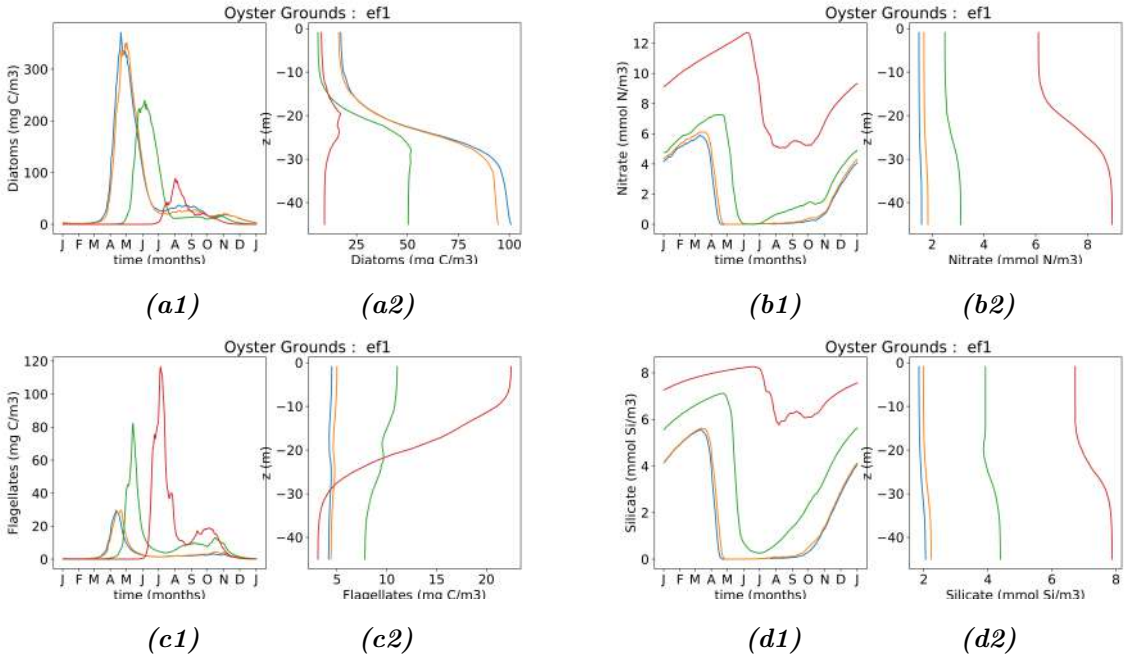

Figure 19: *Station of Oyster Grounds, effect of light reduction on selected ecological variables (averaged over 1980-2008): Yearly time series averaged over depth (a1, b1, c1, d1) and time averaged profiles (a2, b2, c2, d2) of, diatoms (a), nitrate (b), flagellates (c) and silicate (d). The results are presented for different scenarios of coverage (reference: 0%, scenario 1: 10%, scenario 2: 60%, scenario 3: 90%)*

Effect of wind stress

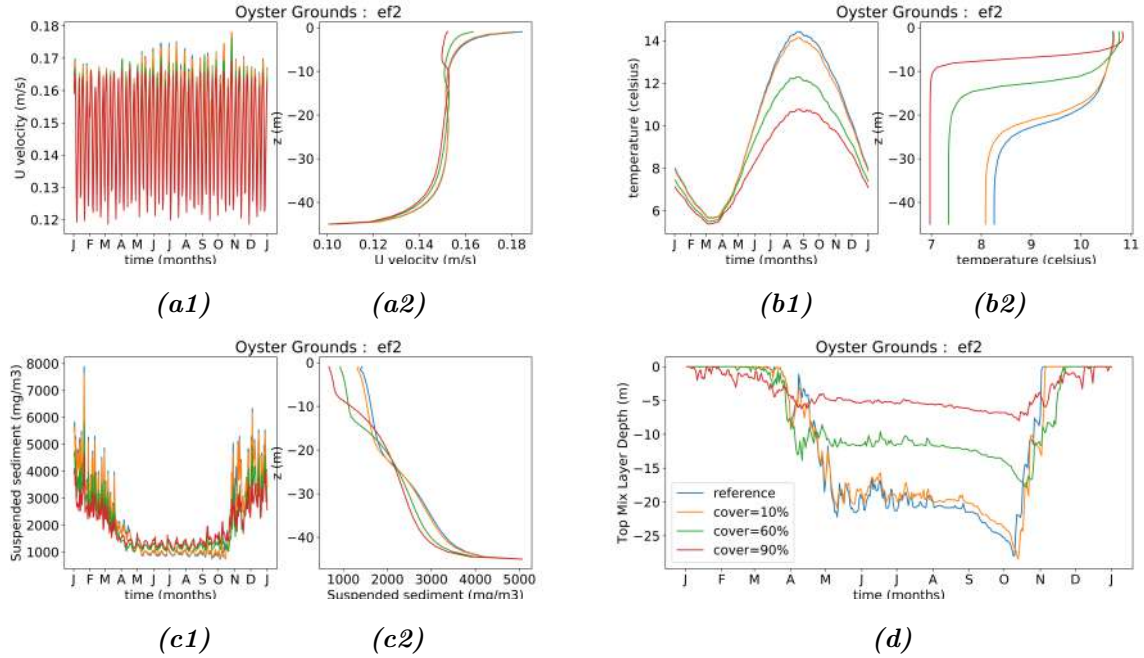

Figure 20: *Station of Oyster Grounds, effect of wind stress reduction on selected hydrographic variables (averaged over 1980-2008): Yearly time series averaged over depth (a1, b1, c1, d) and time averaged profiles (a2, b2, c2) of, current velocities (a), temperature (b) and suspended sediment (c). In panel (d) the yearly time series of the top mixed layer depth are presented. The results are presented for different scenarios of coverage (reference: 0%, scenario 1: 10%, scenario 2: 60%, scenario 3: 90%)*

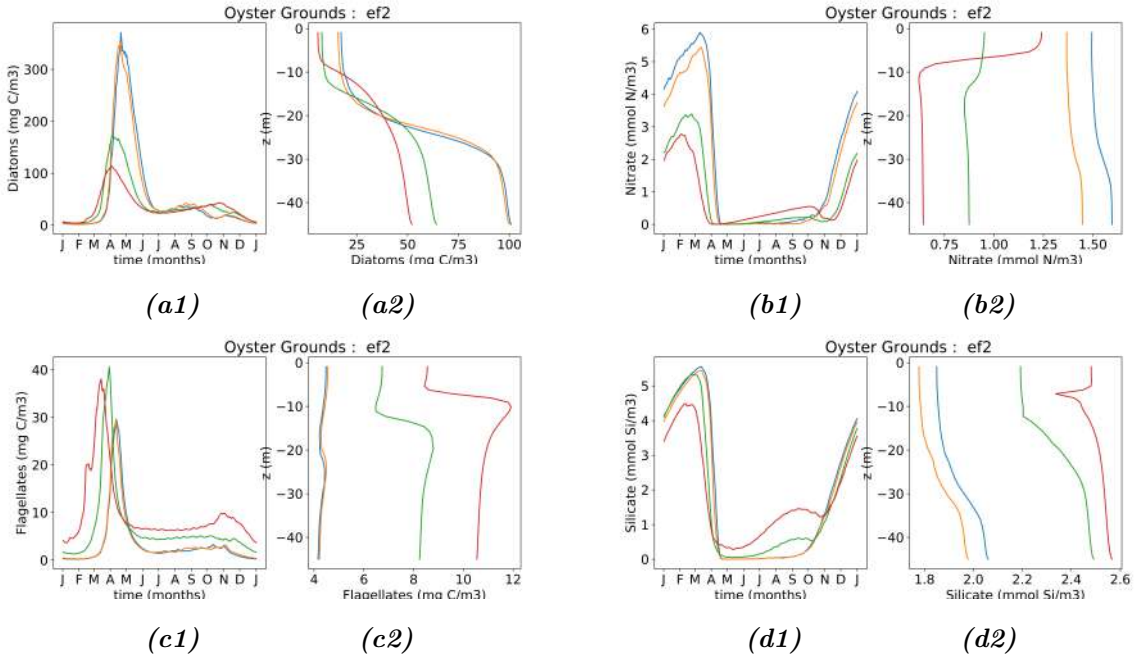

Figure 21: *Station of Oyster Grounds, effect of wind stress reduction on selected ecological variables (averaged over 1980-2008): Yearly time series averaged over depth (a1, b1, c1, d1) and time averaged profiles (a2, b2, c2, d2) of, diatoms (a), nitrate (b), flagellates (c) and silicate (d). The results are presented for different scenarios of coverage (reference: 0%, scenario 1: 10%, scenario 2: 60%, scenario 3: 90%)*

Effect of surface stress due to friction

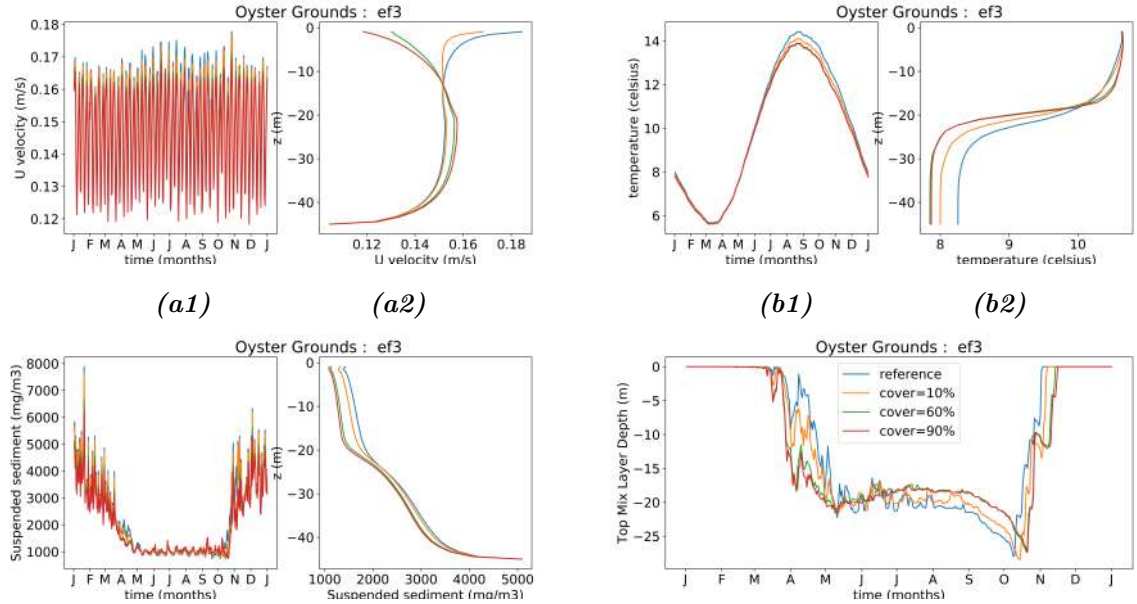

Figure 22: *Station of Oyster Grounds, effect of surface friction on selected hydrographic variables (averaged over 1980-2008): Yearly time series averaged over depth (a1, b1, c1, d) and time averaged profiles (a2, b2, c2) of, current velocities (a), temperature (b) and suspended sediment (c). In panel (d) the yearly time series of the top mixed layer depth are presented. The results are presented for different scenarios of coverage (reference: 0%, scenario 1: 10%, scenario 2: 60%, scenario 3: 90%)*

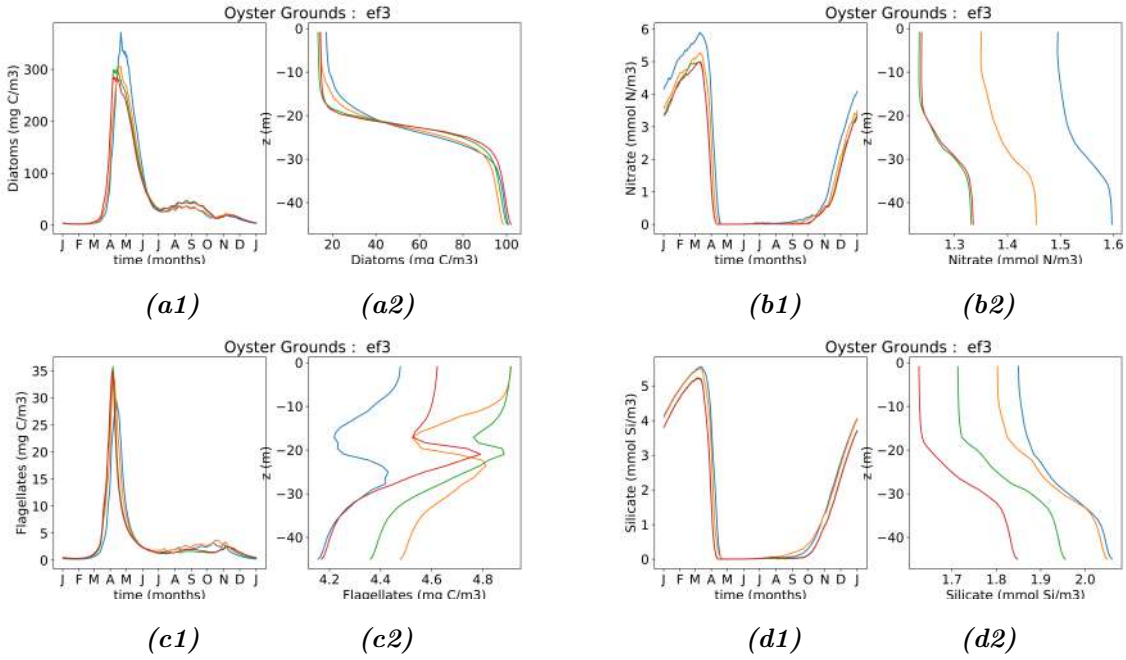

Figure 23: *Station of Oyster Grounds, effect of surface friction on selected ecological variables (averaged over 1980-2008): Yearly time series averaged over depth (a1, b1, c1, d1) and time averaged profiles (a2, b2, c2, d2) of, diatoms (a), nitrate (b), flagellates (c) and silicate (d). The results are presented for different scenarios of coverage (reference: 0%, scenario 1: 10%, scenario 2: 60%, scenario 3: 90%)*

Effect of wave heigth

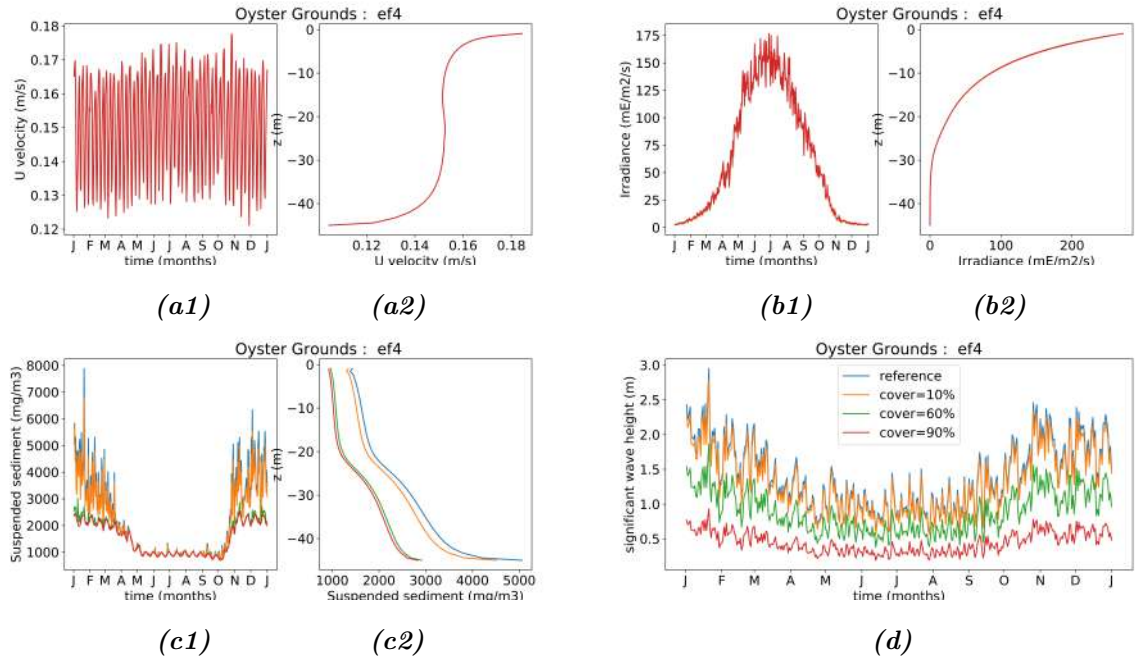

Figure 24: *Station of Oyster Grounds, effect of reduced wave height on selected hydrographic variables (averaged over 1980-2008): Yearly time series averaged over depth (a1, b1, c1, d) and time averaged profiles (a2, b2, c2) of, current velocities (a), irradiance (b) and suspended sediment (c). In panel (d) the yearly averaged time series of the significant wave height are presented. The results are presented for different scenarios of coverage (reference: 0%, scenario 1: 10%, scenario 2: 60%, scenario 3: 90%)*

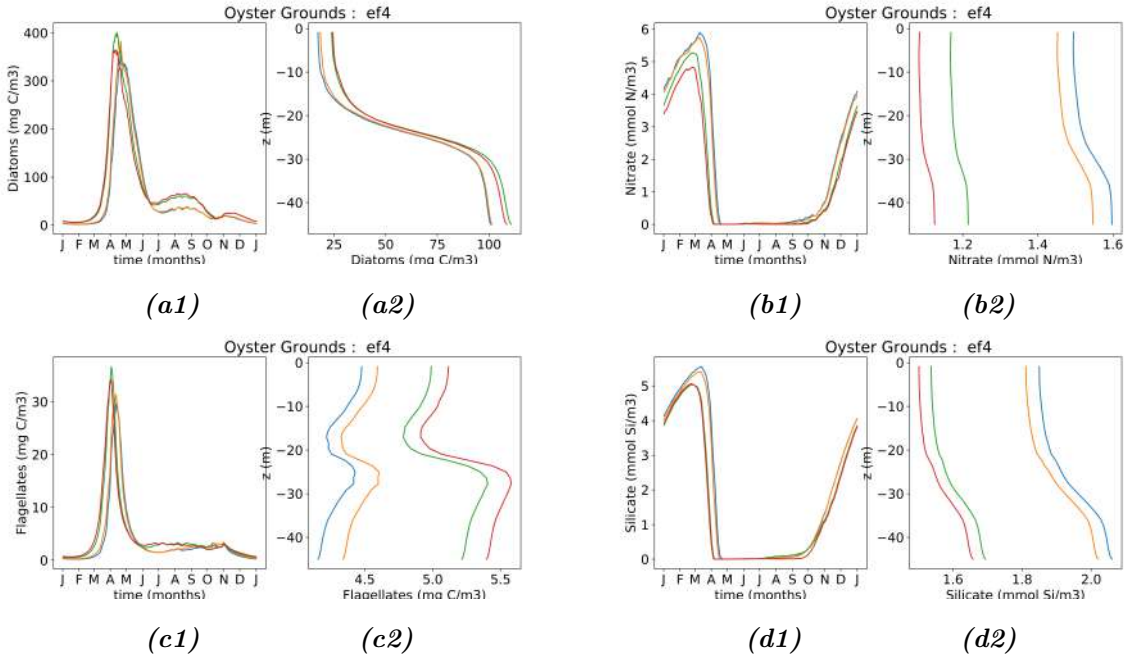

Figure 25: *Station of Oyster Grounds, effect of reduced wave height on selected ecological variables (averaged over 1980-2008): Yearly time series averaged over depth (a1, b1, c1, d1) and time averaged profiles (a2, b2, c2, d2) of, diatoms (a), nitrate (b), flagellates (c) and silicate (d). The results are presented for different scenarios of coverage (reference: 0%, scenario 1: 10%, scenario 2: 60%, scenario 3: 90%)*

Overall effect of PV Installations

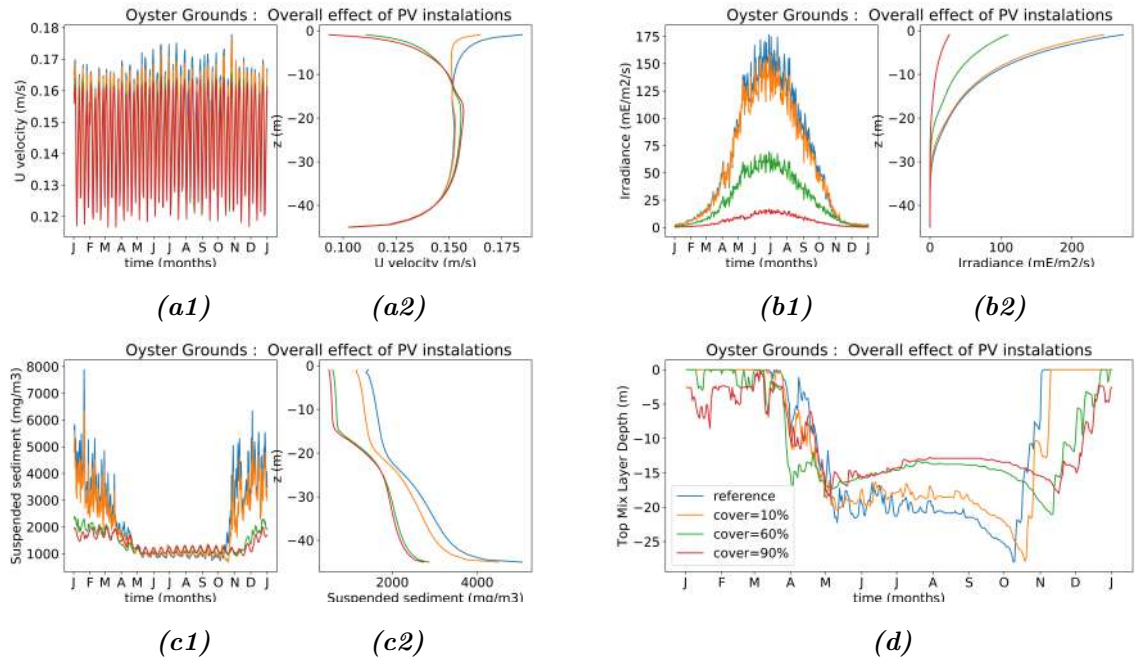

Figure 26: *Station of Oyster Grounds, total effect of PV installations on selected hydrographic variables (averaged over 1980-2008): Yearly time series averaged over depth (a1, b1, c1, d) and time averaged profiles (a2, b2, c2) of, current velocities (a), irradiance (b) and suspended sediment (c). In panel (d) the yearly time series of the top mixed layer depth are presented. The results are presented for different scenarios of coverage (reference: 0%, scenario 1: 10%, scenario 2: 60%, scenario 3: 90%)*

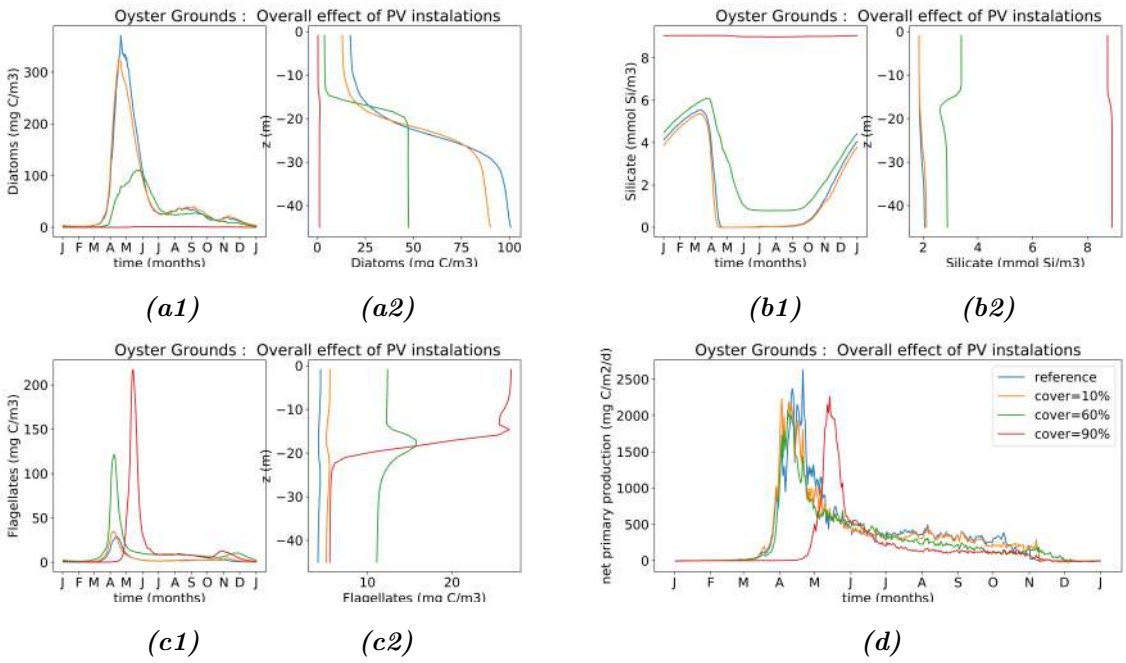

Figure 27: *Station of Oyster Grounds, total effect of PV installations on selected ecological variables (averaged over 1980-2008): Yearly time series averaged over depth (a1, b1, c1) and time averaged profiles (a2, b2, c2) of, diatoms (a), silicate (b) and flagellates(c). In panel (d) the depth-averaged primary production of the domain is presented. The results are presented for different scenarios of coverage (reference: 0%, scenario 1: 10%, scenario 2: 60%, scenario 3: 90%)*

6.4 Additional figures for Noordwijk

Effect of light reduction

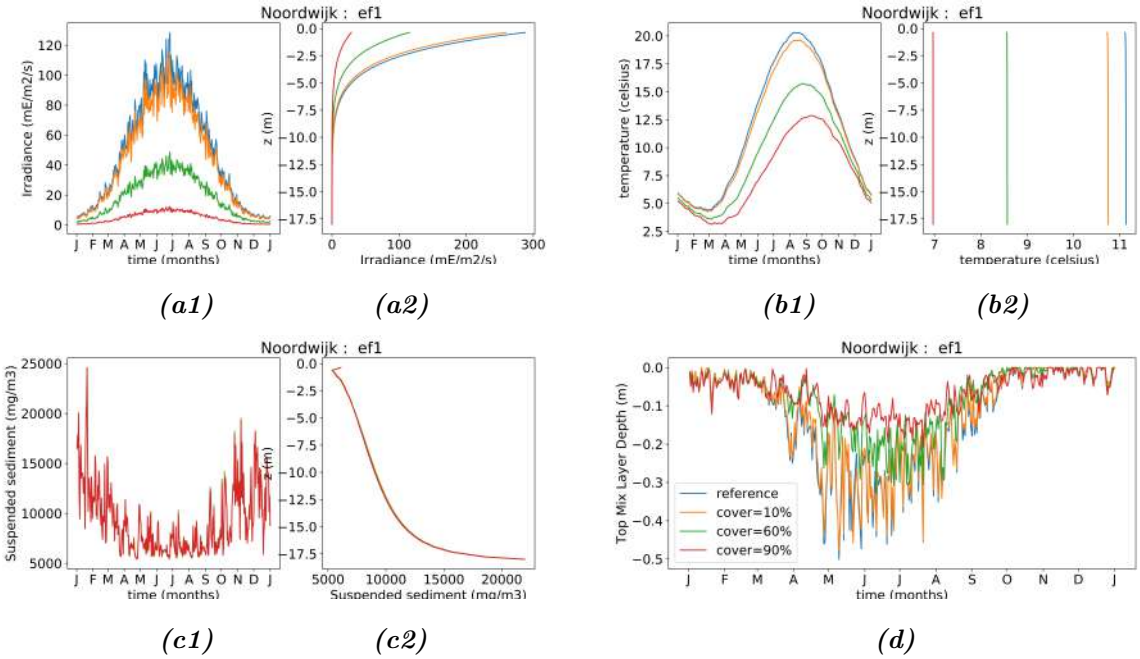

Figure 28: *Station of Noordwijk, effect of light reduction on selected hydrographic variables (averaged over 1980-2008): Yearly time series averaged over depth (a1, b1, c1, d) and time averaged profiles (a2, b2, c2) of, irradiance (a), temperature (b) and suspended sediment (c). In panel (d) the yearly time series of the top mixed layer depth are presented. The results are presented for different scenarios of coverage (reference: 0%, scenario 1: 10%, scenario 2: 60%, scenario 3: 90%)*

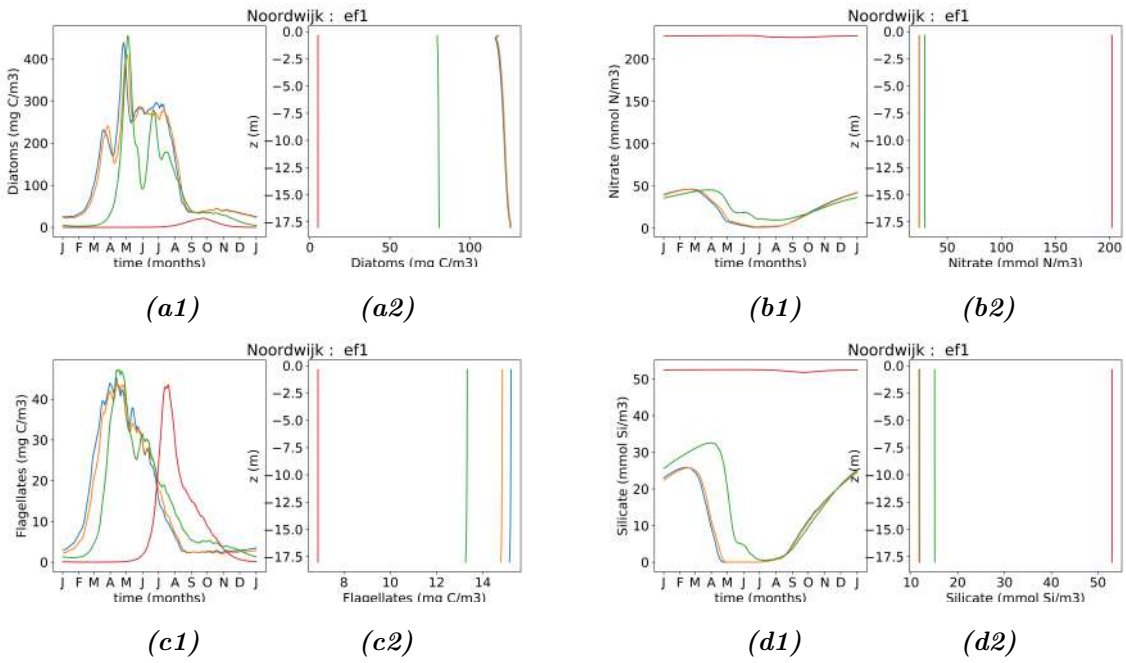

(a1) ***(a2)*** ***(b1)*** ***(b2)***

(c1) ***(c2)*** ***(d1)*** ***(d2)***

Figure 29: *Station of Noordwijk, effect of light reduction on selected ecological variables (averaged over 1980-2008): Yearly time series averaged over depth (a1, b1, c1, d1) and time averaged profiles (a2, b2, c2, d2) of, diatoms (a), nitrate (b), flagellates (c) and silicate (d). The results are presented for different scenarios of coverage (reference: 0%, scenario 1: 10%, scenario 2: 60%, scenario 3: 90%)*

Effect of wind stress

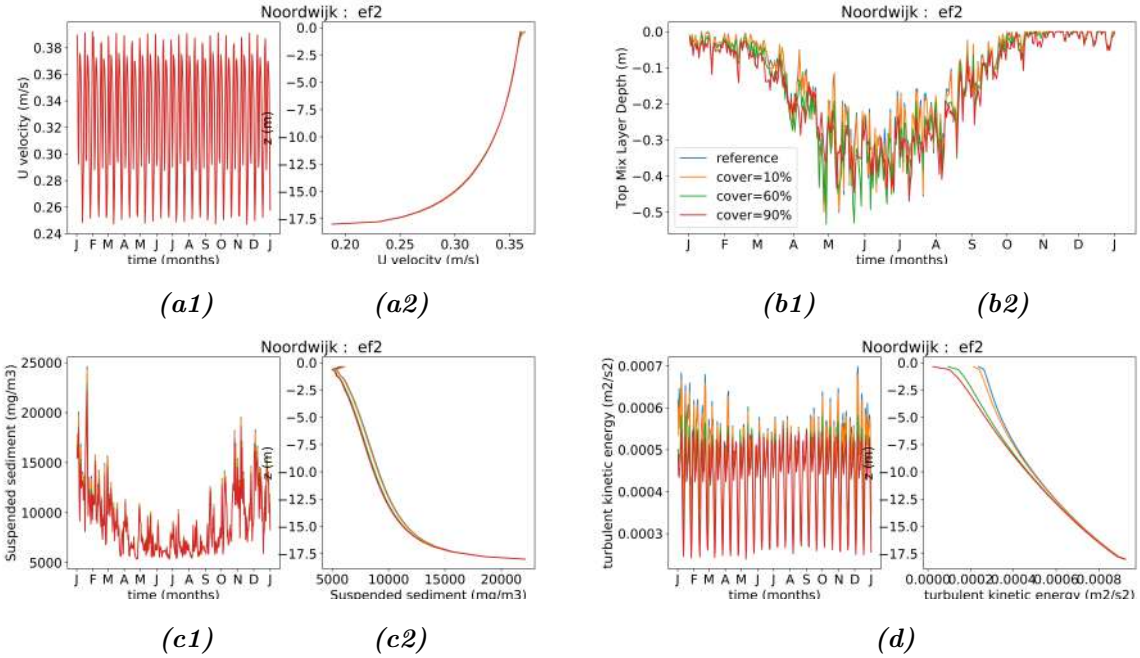

Figure 30: *Station of Noordwijk, effect of wind stress reduction on selected hydrographic variables (averaged over 1980-2008): Yearly time series averaged over depth (a1, b1, c1, d) and time averaged profiles (a2, b2, c2) of, current velocities (a), top mixed layer (b) and suspended sediment (c). In panel (d) the time averaged vertical profiles of turbulent kinetic energy are presented. The results are presented for different scenarios of coverage (reference: 0%, scenario 1: 10%, scenario 2: 60%, scenario 3: 90%)*

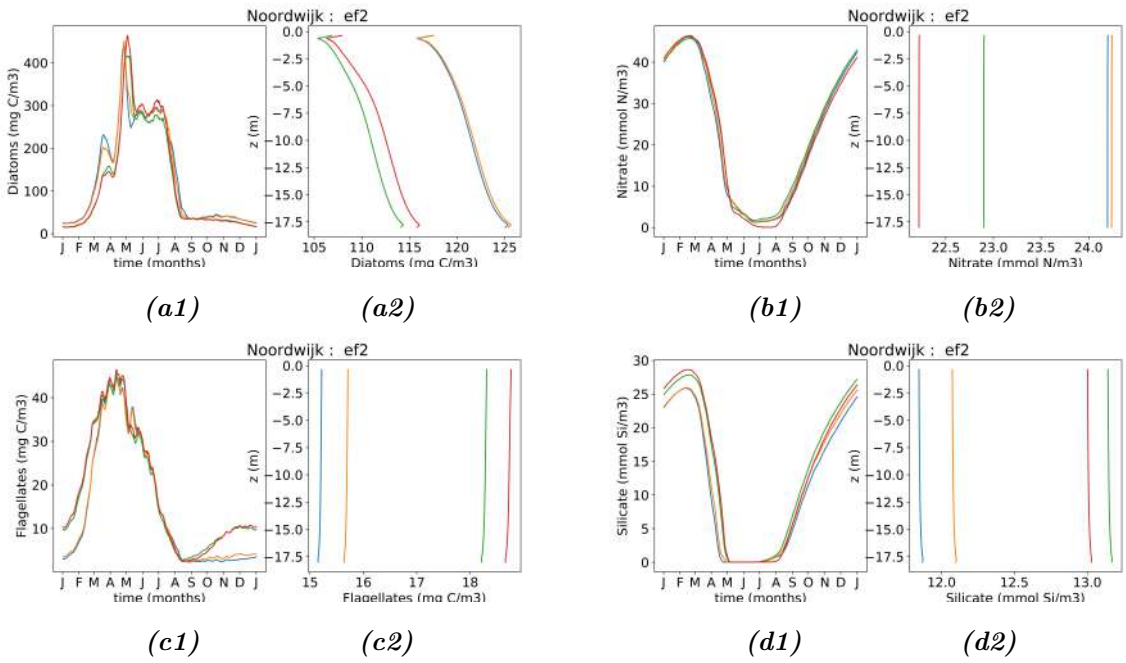

Figure 31: *Station of Noordwijk, effect of wind stress reduction on selected ecological variables (averaged over 1980-2008): Yearly time series averaged over depth (a1, b1, c1, d1) and time averaged profiles (a2, b2, c2, d2) of, diatoms (a), nitrate (b), flagellates (c) and silicate (d). The results are presented for different scenarios of coverage (reference: 0%, scenario 1: 10%, scenario 2: 60%, scenario 3: 90%)*

Effect of surface stress due to friction

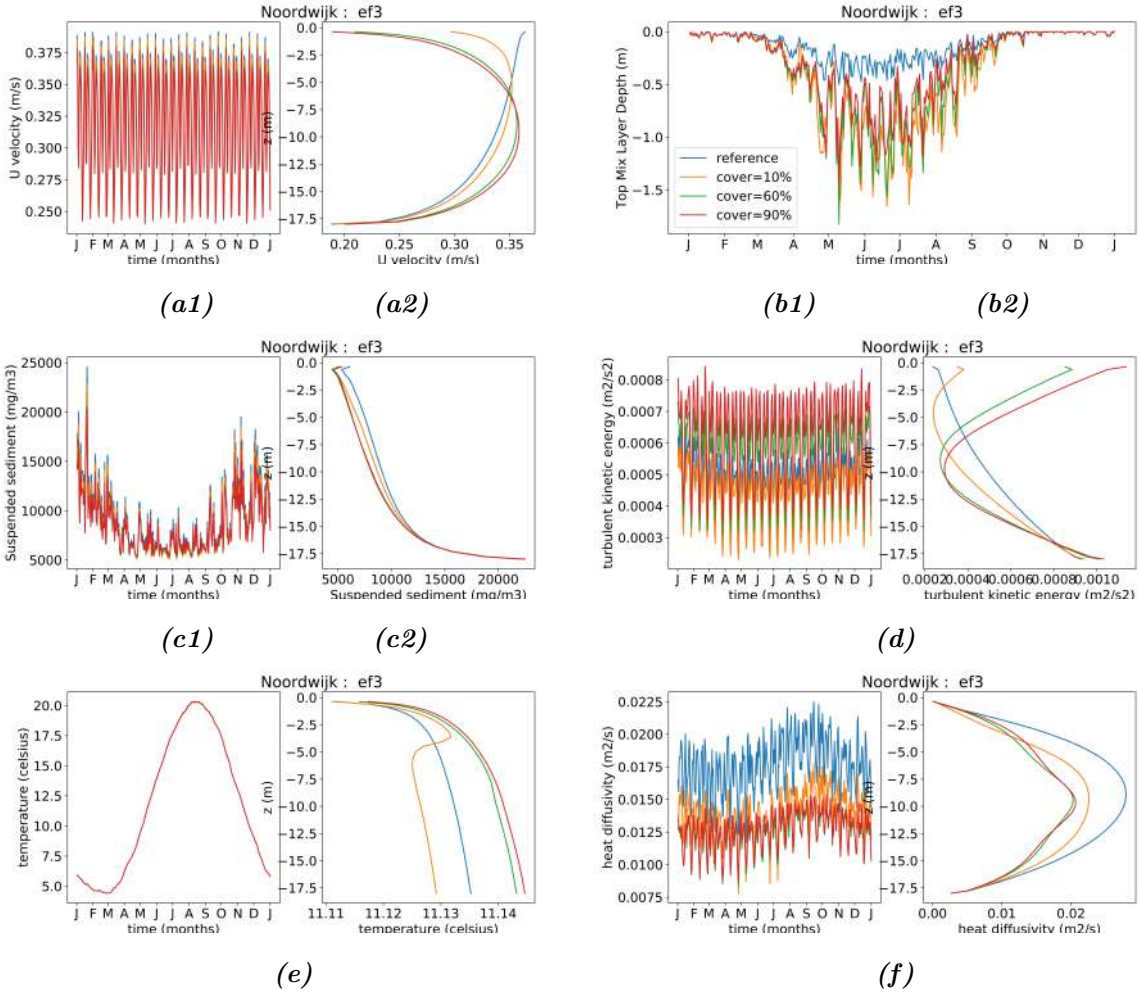

Figure 32: *Station of Noordwijk, effect of surface friction on selected hydrographic variables (averaged over 1980-2008): Yearly time series averaged over depth (a1, b, c1, d1, e1,f1) and time averaged profiles (a2, c2, d2, f2) of, current velocities (a), top mixed layer (b), suspended sediment (c), turbulent kinetic energy (d), temperature (e), diffusion coeficient (f). The results are presented for different scenarios of coverage (reference: 0%, scenario 1: 10%, scenario 2: 60%, scenario 3: 90%)*

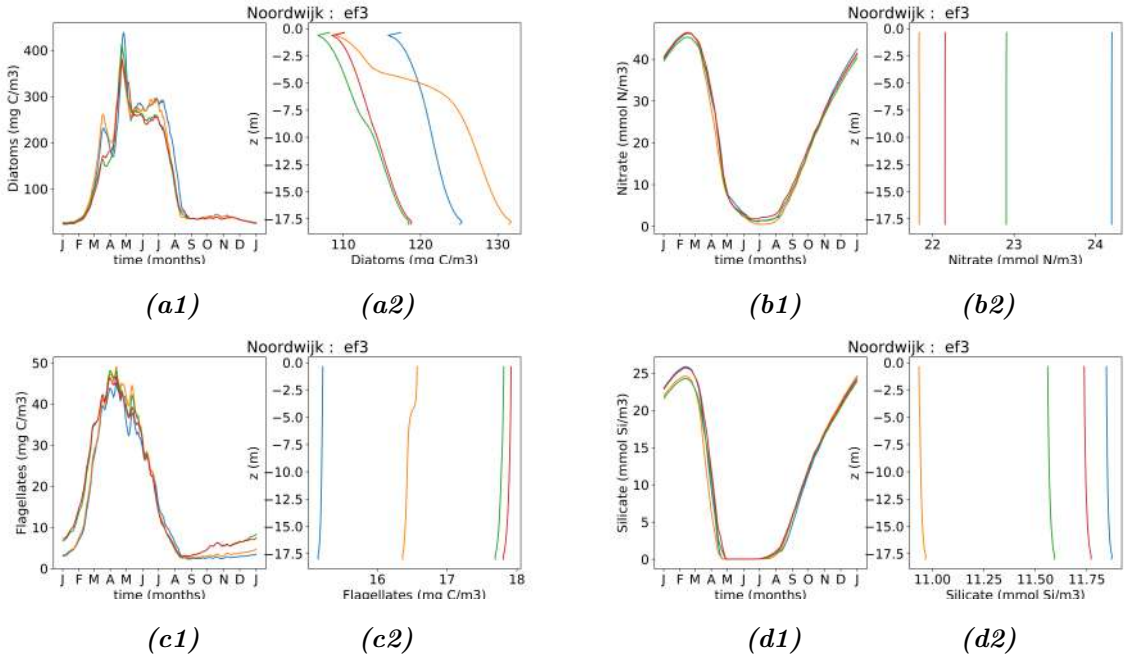

Figure 33: *Station of Noordwijk, effect of surface friction on selected ecological variables (averaged over 1980-2008): Yearly time series averaged over depth (a1, b1, c1, d1) and time averaged profiles (a2, b2, c2, d2) of, diatoms (a), nitrate (b), flagellates (c) and silicate (d). The results are presented for different scenarios of coverage (reference: 0%, scenario 1: 10%, scenario 2: 60%, scenario 3: 90%)*

Effect of wave height

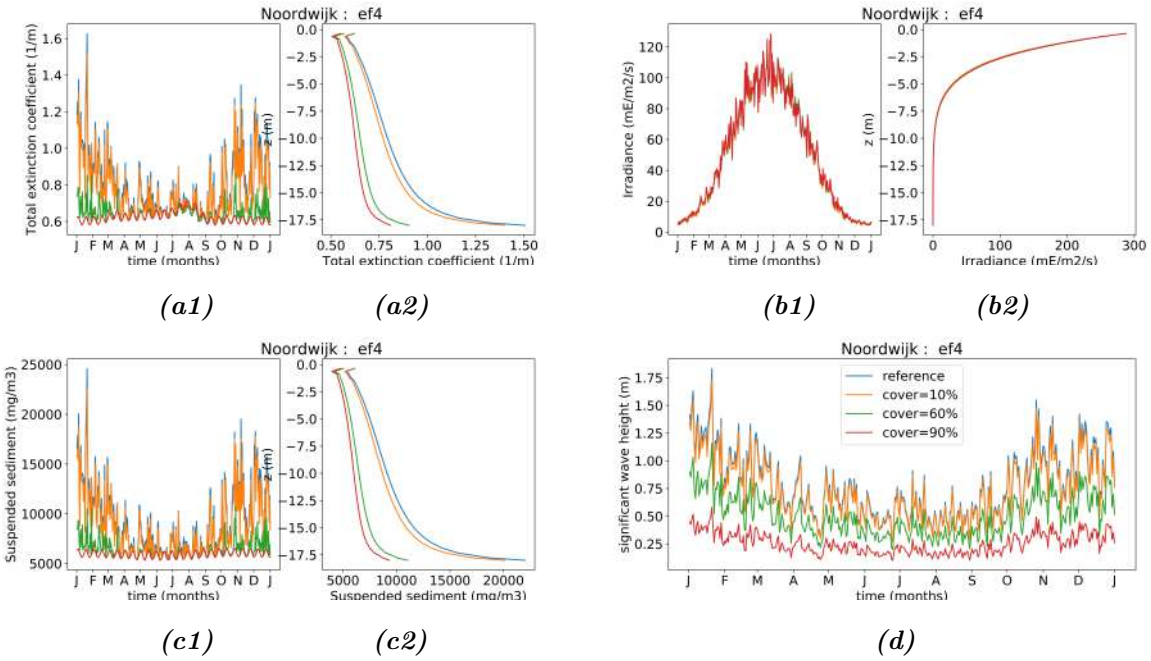

Figure 34: *Station of Noordwijk, effect of reduced wave height on selected hydrographic variables (averaged over 1980-2008): Yearly time series averaged over depth (a1, b1, c1, d) and time averaged profiles (a2, b2, c2) of, light extinction coefficient (a), irradiance (b) and suspended sediment (c). In panel (d) the yearly averaged time series of the significant wave height are presented. The results are presented for different scenarios of coverage (reference: 0%, scenario 1: 10%, scenario 2: 60%, scenario 3: 90%)*

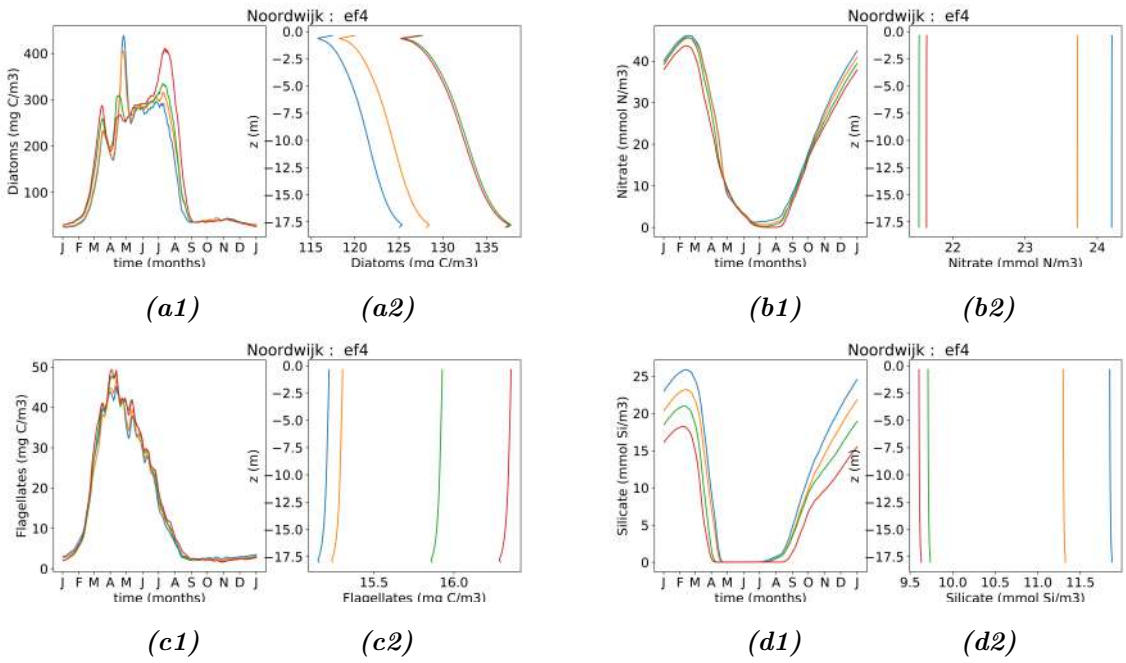

Figure 35: *Station of Noordwijk, effect of reduced wave height on selected ecological variables (averaged over 1980-2008): Yearly time series averaged over depth (a1, b1, c1, d1) and time averaged profiles (a2, b2, c2, d2) of, diatoms (a), nitrate (b), flagellates (c) and silicate (d). The results are presented for different scenarios of coverage (reference: 0%, scenario 1: 10%, scenario 2: 60%, scenario 3: 90%)*

Overall effect of PV installations

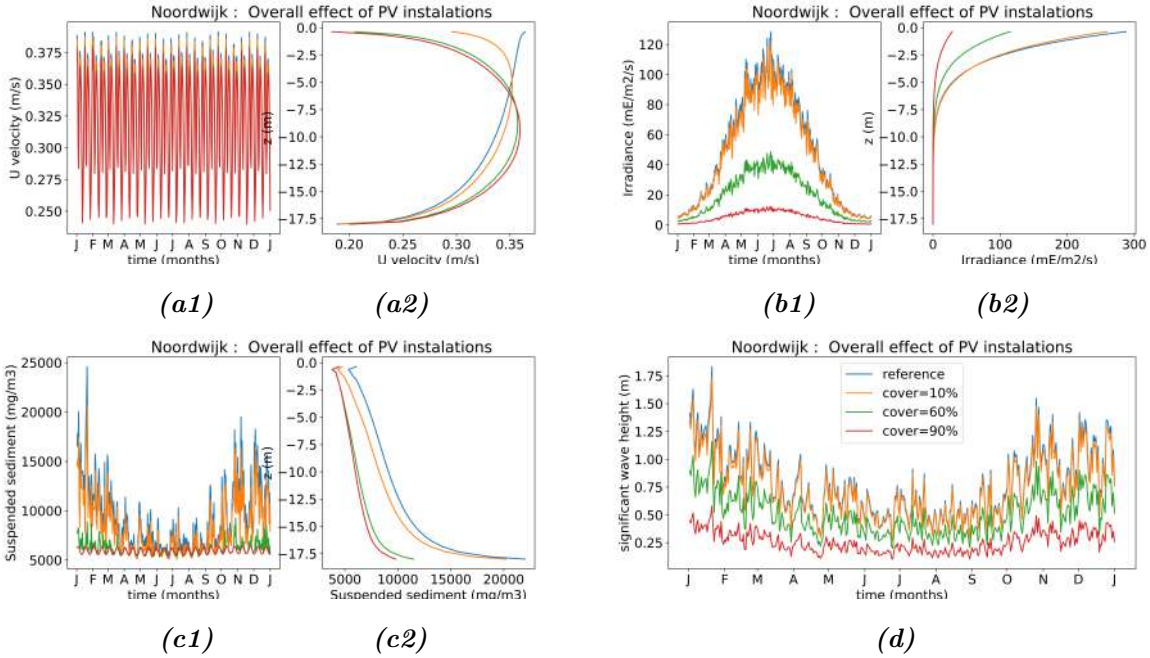

Figure 36: *Station of Noordwijk, total effect of PV installations on selected hydrographic variables (averaged over 1980-2008): Yearly time series averaged over depth (a1, b1, c1, d) and time averaged profiles (a2, b2, c2) of, current velocities (a), irradiance (b) and suspended sediment (c). In panel (d) the yearly time series of the significant wave height are presented. The results are presented for different scenarios of coverage (reference: 0%, scenario 1: 10%, scenario 2: 60%, scenario 3: 90%)*

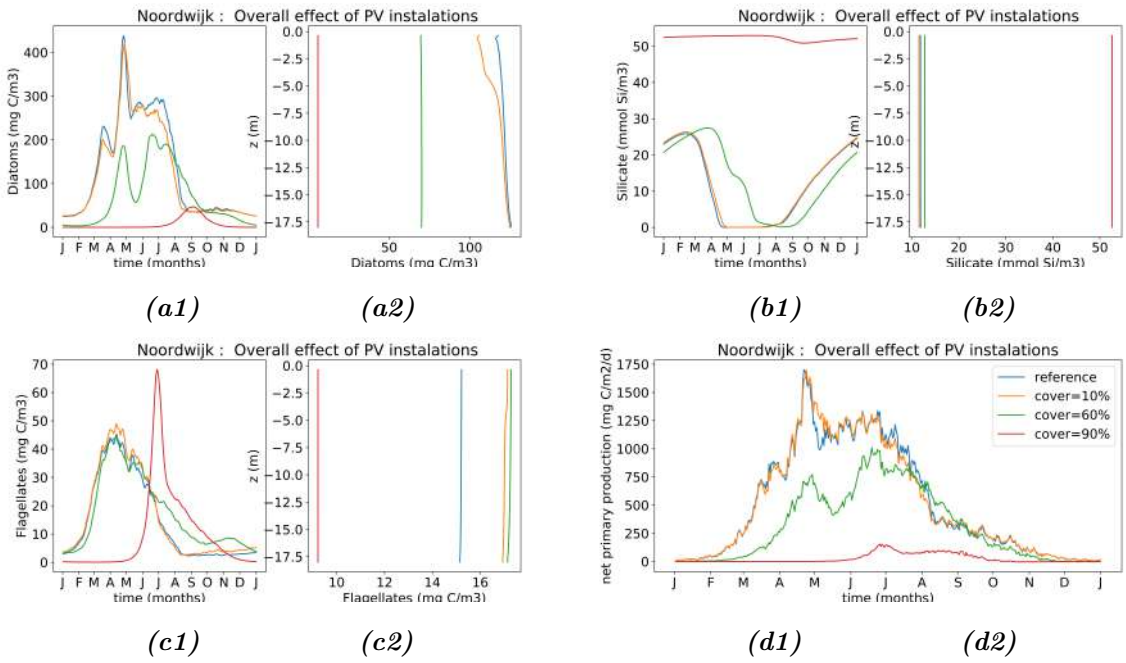

Figure 37: *Station of Noordwijk, total effect of PV installations on selected ecological variables (averaged over 1980-2008): Yearly time series averaged over depth (a1, c1) and time averaged profiles (a2, c2) of, diatoms (a) and flagellates(c). In panel (b) the relative concentration of the two phytoplankton species is considered, as a measure of the biodiversity of the domain. In panel (d) the depth-averaged primary production of the domain is presented. The results are presented for different scenarios of coverage (reference: 0%, scenario 1: 10%, scenario 2: 60%, scenario 3: 90%)*

6.5 Additional figure for West Gabbard

Effect of light reduction

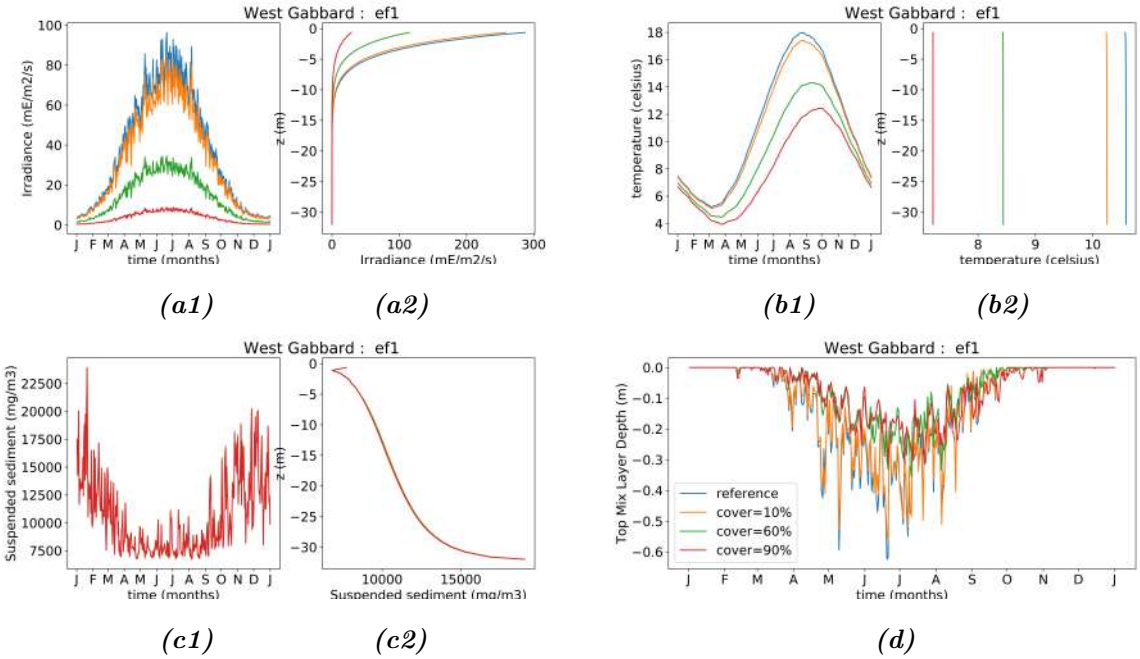

Figure 38: *Station of West Gabbard, effect of light reduction on selected hydrographic variables (averaged over 1980-2008): Yearly time series averaged over depth (a1, b1, c1, d) and time averaged profiles (a2, b2, c2) of, irradiance (a), temperature (b) and suspended sediment (c). In panel (d) the yearly time series of the top mixed layer depth are presented. The results are presented for different scenarios of coverage (reference: 0%, scenario 1: 10%, scenario 2: 60%, scenario 3: 90%)*

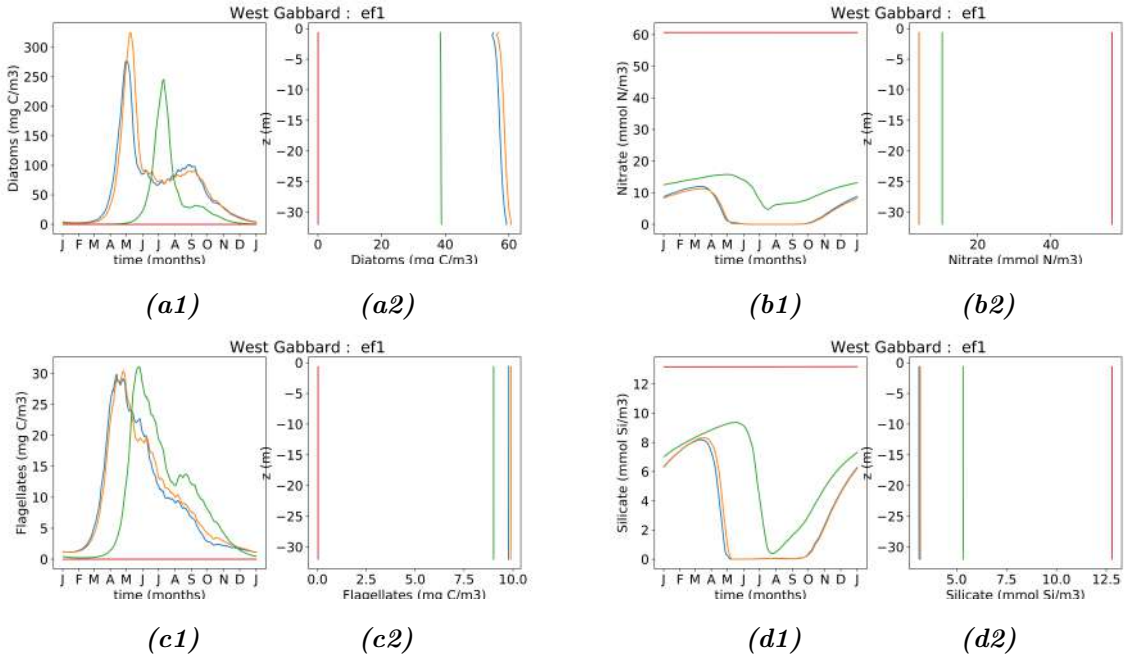

Figure 39: *Station of West Gabbard, effect of light reduction on selected ecological variables (averaged over 1980-2008): Yearly time series averaged over depth (a1, b1, c1, d1) and time averaged profiles (a2, b2, c2, d2) of, diatoms (a), nitrate (b), flagellates (c) and silicate (d). The results are presented for different scenarios of coverage (reference: 0%, scenario 1: 10%, scenario 2: 60%, scenario 3: 90%)*

Effect of wind stress

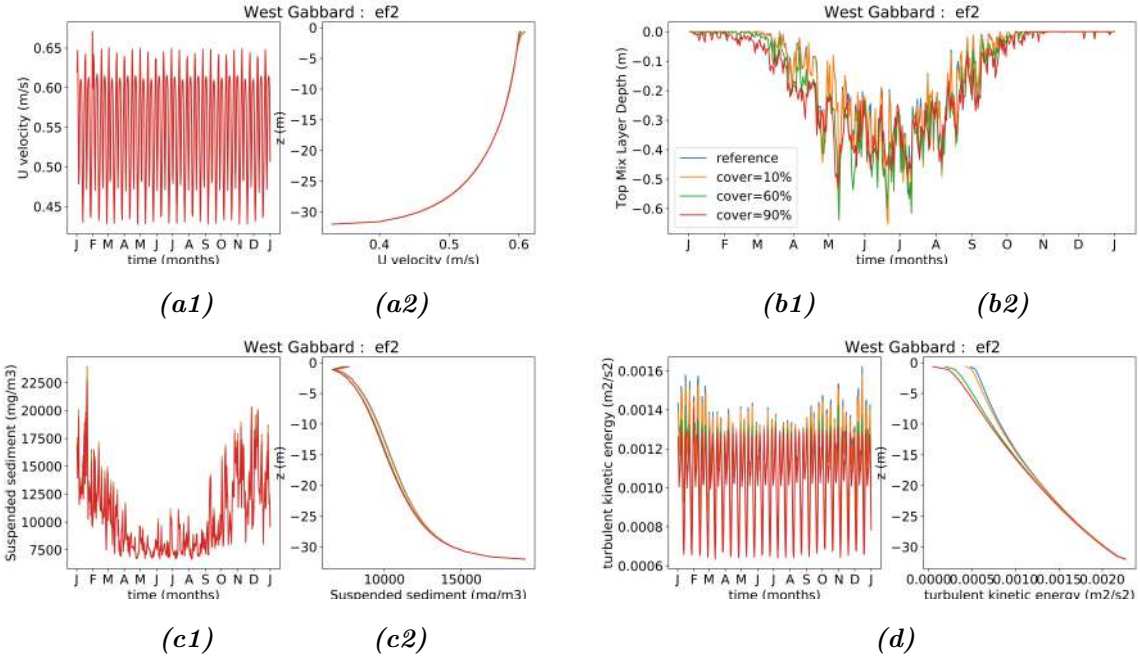

Figure 40: *Station of West Gabbard, effect of wind stress reduction on selected hydrographic variables (averaged over 1980-2008): Yearly time series averaged over depth (a1, b1, c1, d) and time averaged profiles (a2, b2, c2) of, current velocities (a), top mixed layer (b) and suspended sediment (c). In panel (d) the time averaged vertical profiles of turbulent kinetic energy are presented. The results are presented for different scenarios of coverage (reference: 0%, scenario 1: 10%, scenario 2: 60%, scenario 3: 90%)*

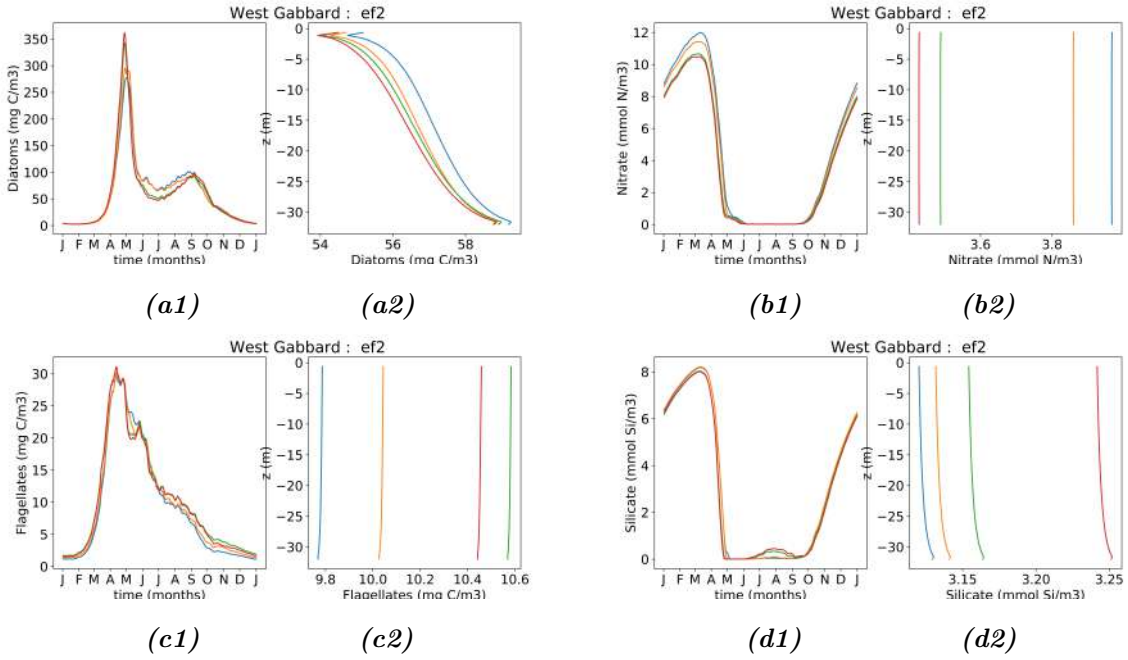

Figure 41: *Station of West Gabbard, effect of wind stress reduction on selected ecological variables (averaged over 1980-2008): Yearly time series averaged over depth (a1, b1, c1, d1) and time averaged profiles (a2, b2, c2, d2) of, diatoms (a), nitrate (b), flagellates (c) and silicate (d). The results are presented for different scenarios of coverage (reference: 0%, scenario 1: 10%, scenario 2: 60%, scenario 3: 90%)*

Effect of surface stress due to friction

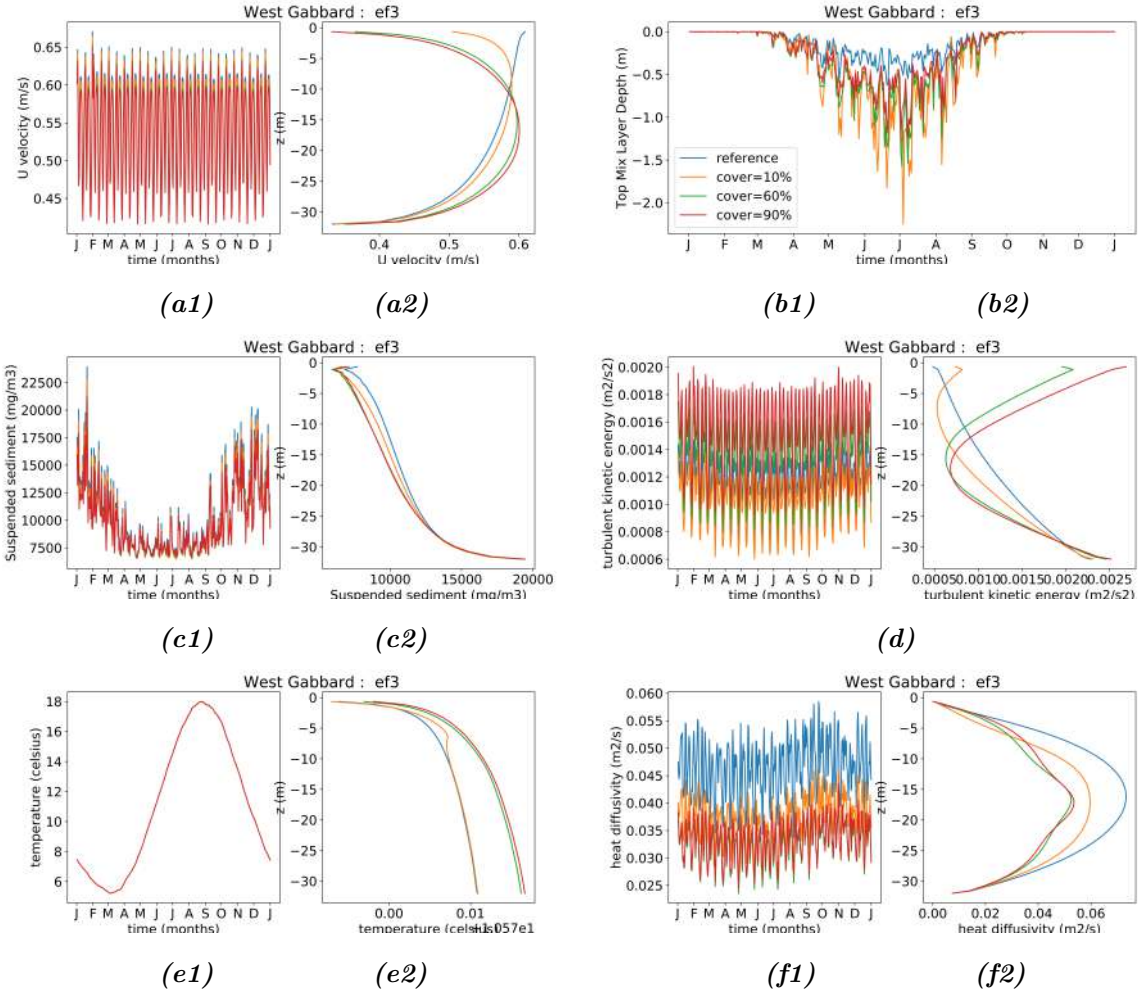

Figure 42: *Station of West Gabbard, effect of surface friction on selected hydrographic variables (averaged over 1980-2008): Yearly time series averaged over depth (a1, b, c1, d1, e1,f1) and time averaged profiles (a2, c2, d2, f2) of, current velocities (a), top mixed layer (b), suspended sediment (c), turbulent kinetic energy (d), temperature (e), diffusion coeficient (f). The results are presented for different scenarios of coverage (reference: 0%, scenario 1: 10%, scenario 2: 60%, scenario 3: 90%)*

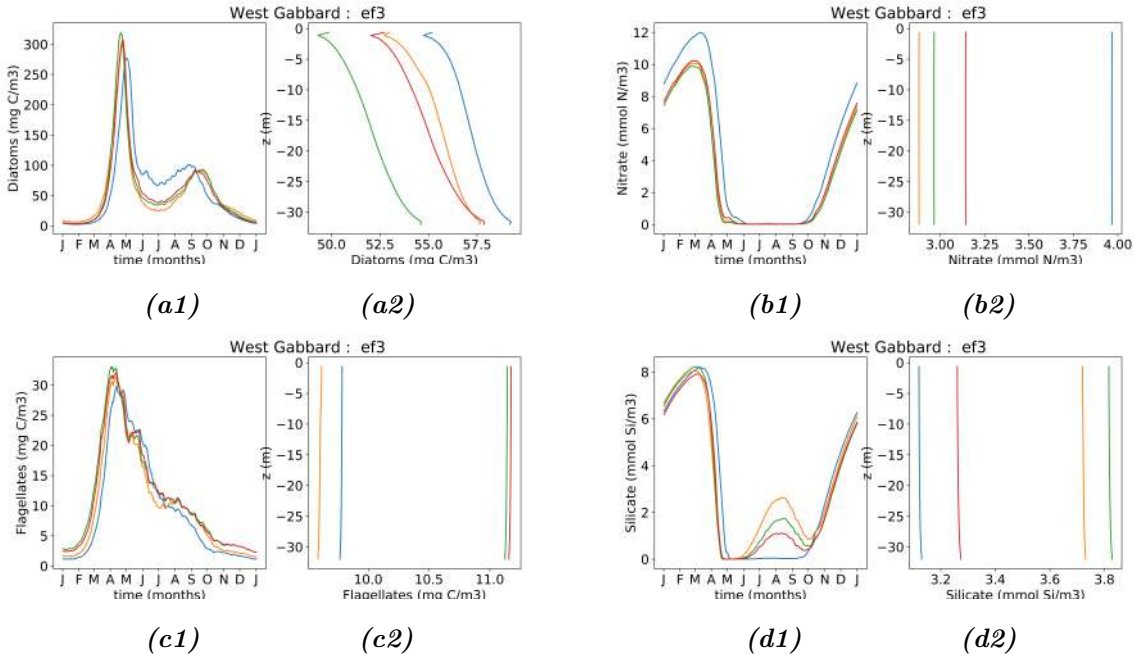

Figure 43: *Station of West Gabbard, effect of surface friction on selected ecological variables (averaged over 1980-2008): Yearly time series averaged over depth (a1, b1, c1, d1) and time averaged profiles (a2, b2, c2, d2) of, diatoms (a), nitrate (b), flagellates (c) and silicate (d). The results are presented for different scenarios of coverage (reference: 0%, scenario 1: 10%, scenario 2: 60%, scenario 3: 90%)*

Effect of wave height

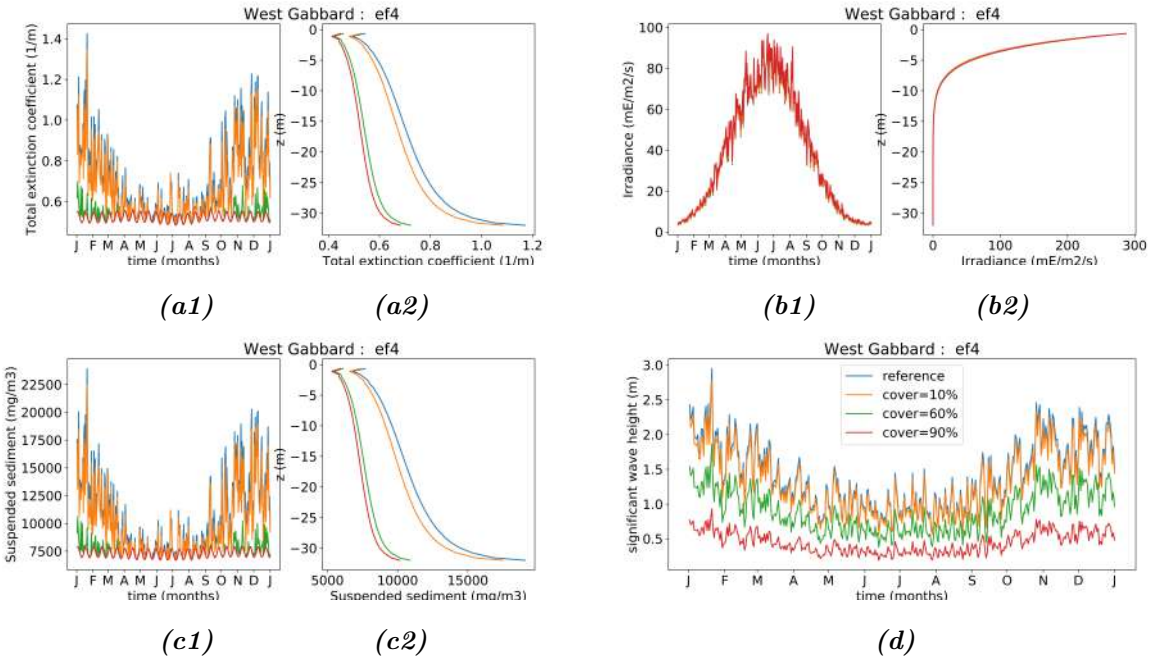

Figure 44: *Station of West Gabbard, effect of reduced wave height on selected hydrographic variables (averaged over 1980-2008): Yearly time series averaged over depth (a1, b1, c1, d) and time averaged profiles (a2, b2, c2) of, light extinction coefficient (a), irradiance (b) and suspended sediment (c). In panel (d) the yearly averaged time series of the significant wave height are presented. The results are presented for different scenarios of coverage (reference: 0%, scenario 1: 10%, scenario 2: 60%, scenario 3: 90%)*

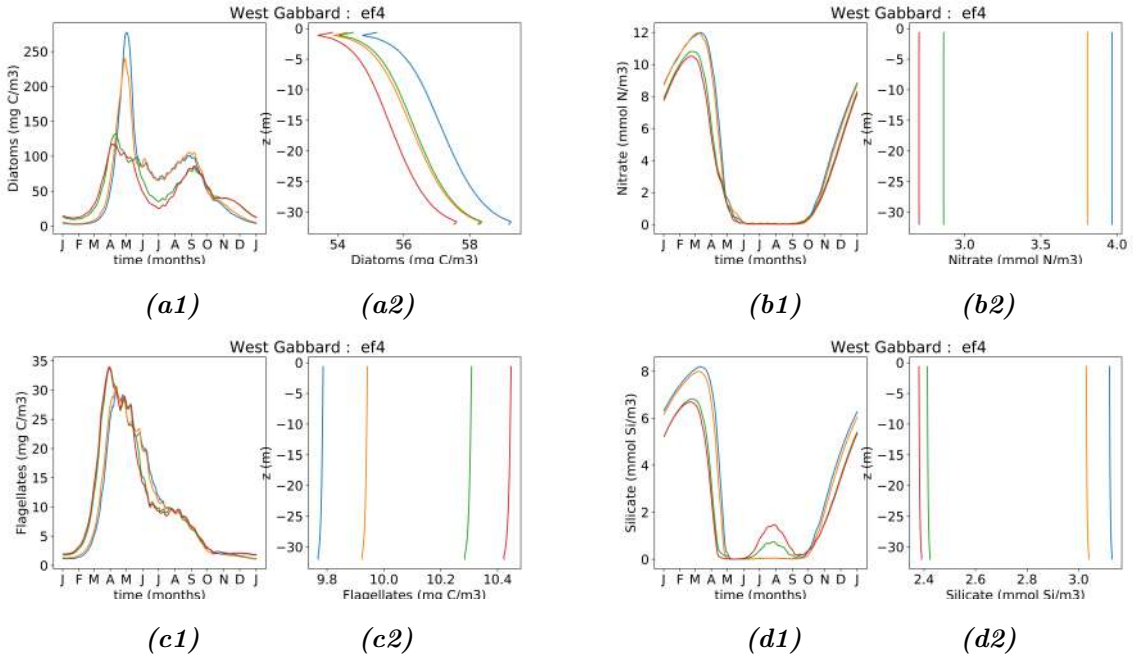

Figure 45: *Station of West Gabbard, effect of reduced wave height on selected ecological variables (averaged over 1980-2008): Yearly time series averaged over depth (a1, b1, c1, d1) and time averaged profiles (a2, b2, c2, d2) of, diatoms (a), nitrate (b), flagellates (c) and silicate (d). The results are presented for different scenarios of coverage (reference: 0%, scenario 1: 10%, scenario 2: 60%, scenario 3: 90%)*

Overall effect of PV installations

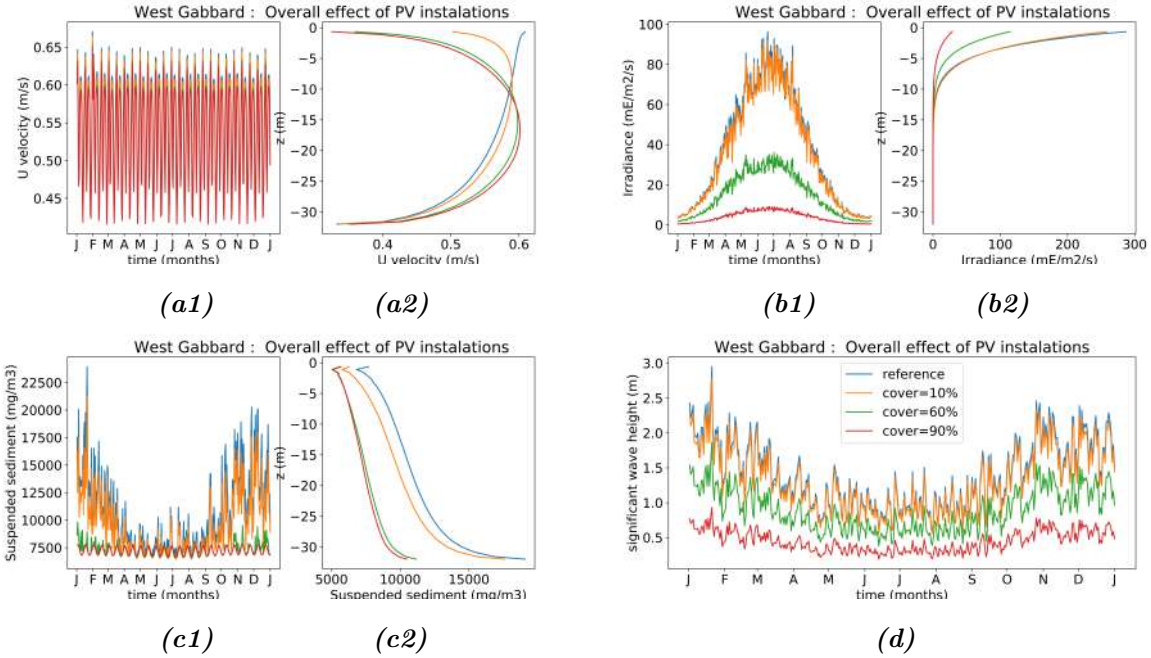

Figure 46: *Station of West Gabbard, total effect of PV installations on selected hydrographic variables (averaged over 1980-2008): Yearly time series averaged over depth (a1, b1, c1, d) and time averaged profiles (a2, b2, c2) of, current velocities (a), irradiance (b) and suspended sediment (c). In panel (d) the yearly time series of the significant wave height are presented. The results are presented for different scenarios of coverage (reference: 0%, scenario 1: 10%, scenario 2: 60%, scenario 3: 90%)*

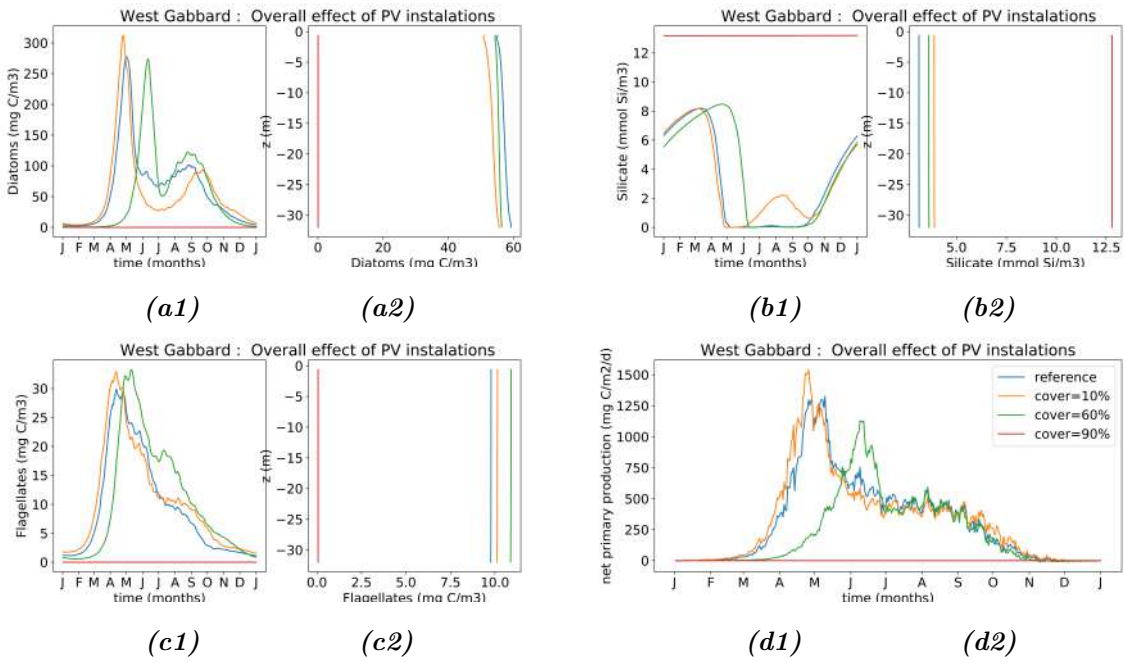

Figure 47: *Station of West Gabbard, total effect of PV installations on selected ecological variables (averaged over 1980-2008): Yearly time series averaged over depth (a1, b1, c1) and time averaged profiles (a2, b2, c2) of, diatoms (a), silicateand (b) flagellates(c). In panel (d) the depth-averaged primary production of the domain is presented. The results are presented for different scenarios of coverage (reference: 0%, scenario 1: 10%, scenario 2: 60%, scenario 3: 90%)*

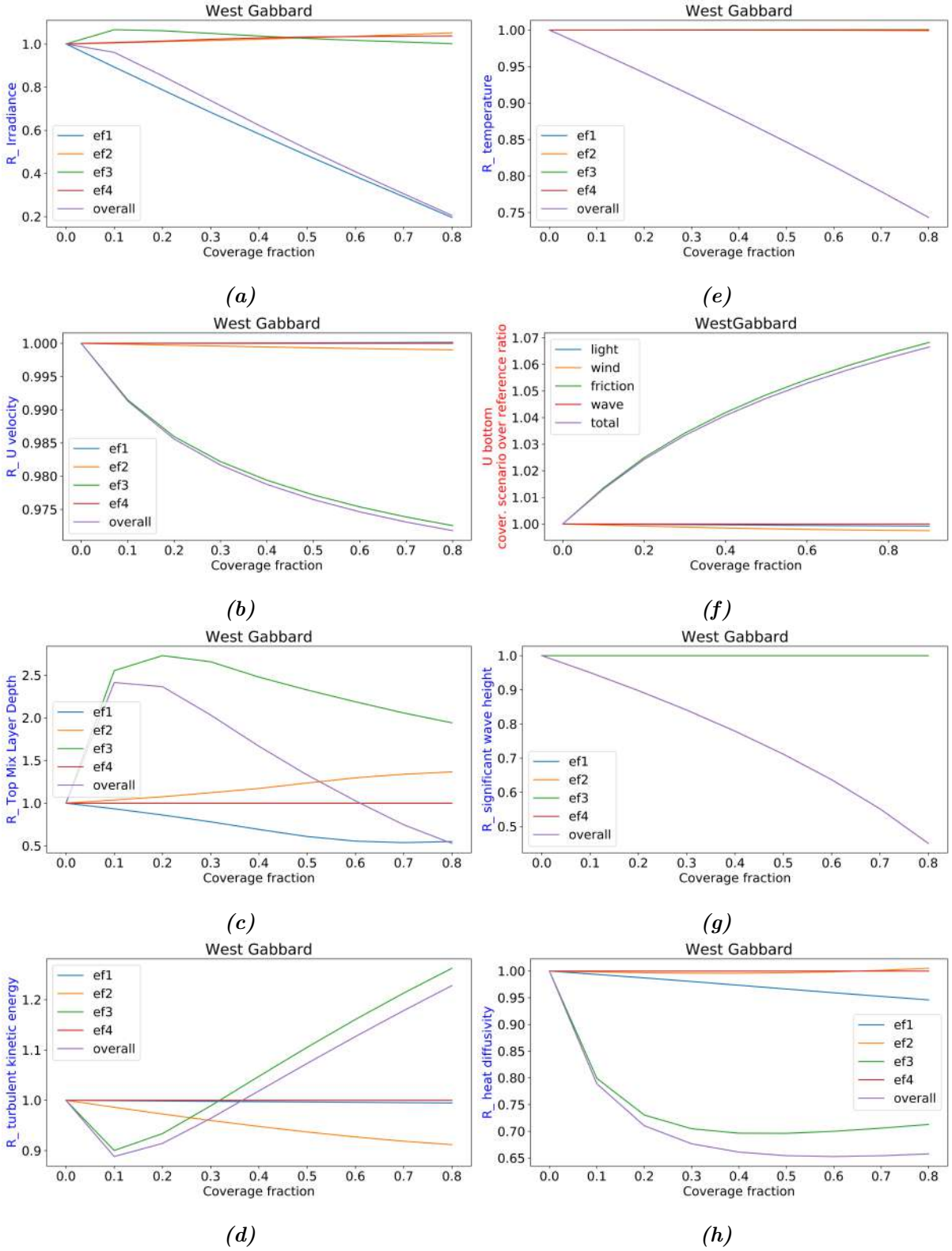

Figure 48: *West Gabbard: Relative change (see equation 35) of selected variables of the water column, with coverage. The results are presented for: irradiace (a), depth-averaged current velocity (b), top mixed layer depth (c), turbulent kinetic energy (d), temperature (e), bottom current velocity (f), wave height (g) and heat diffusivity (h). ef1: shadowing effect of the platforms,ef2: reduced wind stress, ef3: surface stress experienced by currents, due to friction induced by the platforms, ef4: reduced wave height.*